Study of Phase Transition in Astrophysics and Heavy-ion Collisions

THESIS SUBMITTED FOR THE DEGREE OF DOCTOR OF PHILOSOPHY (SCIENCE)

JADAVPUR UNIVERSITY

2013

SARBANI MAJUMDER
PHYSICS DEPARTMENT
BOSE INSTITUTE
KOLKATA

CERTIFICATE FROM THE SUPERVISOR

This is to certify that the thesis entitled "Study of Phase Transition in Astrophysics and Heavy-ion Collisions " submitted by Smt. Sarbani Majumder, who got her name registered on 12.05.2008 for the award of Ph.D. (Science) degree of Jadavpur University, is absolutely based upon her own work under the supervision of Prof. Sanjay K. Ghosh and that neither this thesis nor any part of it has been submitted for either any degree/diploma or any other academic award anywhere before.

(Signature of the Supervisor & date with official seal.)

To my parents

Acknowledgements

I would like to use this space to express my sincere gratitude to the persons whose constant support has helped me to complete the work in five and half years.

First of all I would like to thank the Council of Scientific and Industrial Research (CSIR), India, for providing the funding and facilities to carry out my research throught out the five years. I am also grateful to my own institute, Bose Institute , Kolkata, for giving me an extension of 6 months to carry out the final part of my work.

I am indebted to my supervisor, Prof. Sanjay K. Ghosh for his patient guidence and teaching. Despite of having a great responsibility of development of our centre at Saltlake, he was always approachable and supportive for a open discussion with our academic as well as non-academic problems. I would like to thank Prof. Sibaji Raha, the director of our institute, also one of the members of our research group. Despite a busy schedule, he was always willing to help in every possible way.

It was not absolutely possible for me to complete my thesis without the enormous help and support of my collaborator Dr. Rajarshi Ray of Bose Institute. His insights to understand physics from different points of view is second to none. Besides, he is an example to follow for his rigor and passion on research and also being very cool and calm in any kind of problematic situations. He has helped me a lot to overcome my primary inconvenience and discomfort about numerical computations.

No words of thanks are enough to express my gratitude to my freind and collaborator Anirban Lahiri of Bose Institute for his constant support and encouragement to continue my research work.

I would like to use this opportunity to thank Dr. Partha S. Joarder of our institute for his valuable suggestions and inspiration.

I would also like to express my sincere gratitude to all my collaborators, Prof. Munshi Golam Mustafa of SINP, Kolkata, Dr. Jan e Alam of VECC, Kolkata, Dr. Bedanga Das Mohanty of NISER, Bhubaneswar and Dr. Abhijit Bhattacharyya of University of Calcutta, for their help and valuable suggestions.

I want to convey my gratitude towards my seniors Dr. Tamal K. Mukherjee and Dr. Ritam Mallick and all the other seniors and juniors of the main campus and Saltlake campus of our institute. I would like to thank all of my freinds in Jadavpur University, SINP and VECC.

No words of thanks will be sufficient to express my gratitude to my parents and my family members for their inspiration.

Contents

CHAPTER 1

Introduction

1.1 Overview

The concept of strong interaction came about with the discovery of proton by Rutherford experiment and that of neutron by Chadwick. In classical picture of ordinary matter, positively charged nucleus and negatively charged electrons are held together inside the atom by electrical force. The stability of nucleus in normal nuclear matter implies the existence of some other force, stronger than the electrical repulsion between the positively charged protons. Later this was understood as 'Strong Force' after the discovery of meson, mediator of strong interaction by Yukawa in 1934. Strongly interacting particles were divided into two families namely baryons and mesons. The members of each family was distinguished accordingly by their charge, strangeness and mass. In 1964 Gell-Mann introduced the idea of eightfold way, i.e. the baryons and mesons were found to fit into patterns of octet or decuplet according to their charge, strangeness and mass. It was not still well understood why the hadrons fit into these peculiar pattern? In 1964, Gell-mann and Zweig independently postulated the existence of quarks, the elementary particles by which the hadrons are composed. According to their quark model every baryon is composed of three quarks and every meson is composed of a quark and an anti quark. The explanation of the eightfold way became quite straightforward after the proposition of quark model.

At present six different types of quarks are observed in nature, the up(u),

charm(c) and top(t) with charge $+2e/3$, and down(d), strange(s), and beauty(b) quarks having charge $-e/3$. The quarks being spin half particles must obey the Pauli exclusion principle. However, the Δ^{++}, is composed of three identical u quarks in the same state, inconsistent with the Pauli principle. The problem was resolved when Greenberg proposed the idea of color quantum number, i.e. the quarks not only come with different flavors but also with three different colors (red, green, blue). Although Δ^{++} is composed of three u quarks, they are not indistinguishable because the color quantum numbers are different for each quarks. To study the strong interaction between the quarks, the mediator 'gluon' was proposed and it's existence was confirmed in the electron-positron collision experiment at DESY. There are theoretically nine possible types of gluons belonging to a color singlet state in the U(1) group and color octet state in SU(3) group. The existence of the color singlet gluon has been ruled out because of the fact that the color singlet gluon will lead to a long range color interaction between the hadrons which is absent in nature. So there are only eight gluons as members of the color octet, all of these carry color charge like quarks. The nice aspect of the color terminology is that the all the particles in nature are colorless. Isolated colored quarks has never been seen in nature or identified in experiments.

1.2 Color Confinement and Chiral Symmetry Breaking

In Standard Model, theory of strong interaction between the quarks is described by Quantum Chromo Dynamics (QCD) in which color plays the role of electric charge in QED. Since gluon carry color charge, it interacts with quarks as well as with gluons unlike QED. In QCD, the coupling constant depends on the energy scale of the theory, thus it is running coupling. The running coupling of QCD to one loop order can be written as:

$$\alpha_s(P^2) = \frac{4\pi}{(11N_c - \frac{2}{3}N_f)ln(\frac{P^2}{\Lambda^2_{QCD}})} \tag{1.1}$$

where, Λ_{QCD} is the scale of QCD. Now, in infrared region (low energy), α_s becomes large and diverges at $P^2 = \Lambda^2_{QCD}$. Due to this behavior of running coupling the theory cannot be explored in the low energy regions with the perturbative methods that have been enormously successful at high momenta.

At high energies the coupling is small, and doing standard perturbative renormalization one can obtain

$$\frac{d\alpha_s(\epsilon)}{dln\epsilon} = \beta_0\alpha_s^3 + \beta_1\alpha_s^5 + ... \tag{1.2}$$

where,

$$\beta_0 = -\frac{1}{16\pi^2}(11 - \frac{2}{3}n_f); \qquad \beta_1 = (\frac{1}{16\pi^2})^2(102 - \frac{38}{3}n_f) \tag{1.3}$$

where, ϵ is the energy, n_f is the number of flavors. We notice that, when $n_f \leq 16$ (In reality, $n_f = 6$), the coupling α_s decreases to zero as the energy scale increases to infinity. It predicts the interaction between quarks becomes weaker as two quarks get closer. In the limit of $r \to 0$, the quarks are noninteracting. This is the so-called asymptotic freedom [1].

On the contrary, the behavior at large r is quite different and can be realized from the interaction potential between a $q\bar{q}$ pair:

$$V(r) = -\frac{A(r)}{r} + Kr \tag{1.4}$$

where, $A(r) \propto \frac{1}{ln(r^{-1})}$. It is clear that at large r, the second term is dominating, and $V(r)$ becomes linear. So it is difficult to separate two color sources as the energy cost grows proportionally with the distance. This is the basic idea of 'color confinement'.

Apart from color confinement, the another most important aspect of low energy QCD is Chiral symmetry breaking. Chiral symmetry is the symmetry of QCD Lagrangian under which the left-handed and right-handed quark fields transform independently. This symmetry is perfect in the limit of vanishing quark masses. When the quarks acquire mass the left handed and right handed chirality is mixed up and this symmetry is broken explicitly. By adding and subtracting the generators of the symmetry groups of left handed and right handed quarks one can obtain new generators of vector symmetry group and axial vector symmetry group respectively. The QCD symmetry groups at the vanishing quark masses can be written as: $SU(3)_c \times U(N_f)_L \times U(N_f)_R \equiv SU(3)_c \times SU(N_f)_L \times U(1)_L \times SU(N_f)_R \times U(1)_R$, which is equivalently $SU(3)_c \times SU(N_f)_V \times SU(N_f)_A \times U(1)_A \times U(1)_V$. $SU(N_f)_V$ and $SU(N_f)_A$ are exact symmetry of the QCD Lagrangian of mass less quarks.

This can be understood in the following way [2]. Consider the Lagrangian

of two flavor massless fermions.

$$\mathcal{L} = i\bar{\psi}_i \partial\!\!\!/ \psi_i \tag{1.5}$$

Now, in two flavor case under vector transformation $SU(2)_A$ the quark field ψ transforms as:

$$\psi \to e^{-i\frac{\vec{\tau}}{2}\cdot\vec{\theta}}\psi$$

where, $\vec{\tau}$ is the Pauli matrix and θ is the rotation angle in isospin space. Considering infinitesimal transformation, one gets

$$\psi \to (1 - i\frac{\vec{\tau}}{2}\cdot\vec{\theta})\psi$$

Similarly,

$$\bar{\psi} \to (1 + i\frac{\vec{\tau}}{2}\cdot\vec{\theta})\psi$$

After a trivial algebra we get that the Lagrangian in Eq.(1.5) is invariant under vector transformation with a conserved vector current:

$$V^a_\mu = \bar{\psi}\gamma_\mu\frac{\tau^a}{2}\psi$$

Now, let us consider the axial vector transformation $SU(2)_A$ on Eq.(1.5). Here,

$$\psi \to e^{-i\gamma_5\frac{\vec{\tau}}{2}\cdot\vec{\theta}}\psi$$

Proceeding in the similar way for the vector transformation, we get the Lagrangian is now also symmetric under $SU(2)_A$ with a conserved axial vector current:

$$A^a_\mu = \bar{\psi}\gamma_\mu\gamma_5\frac{\tau^a}{2}\psi \tag{1.6}$$

So the massless 2 flavor QCD Lagrangian is invariant under the chiral symmetry $SU(2)_V \times SU(2)_A$.

It can be shown that the axial vector transformation $SU(2)_A$ is broken and the vector transformation $SU(2)_V$ remains unbroken when we introduce a mass term in $m\bar{\psi}\psi$ in the Lagrangian. Since the light quark masses are very small compared to the scale of QCD, one expects that $SU(2)_A$ is an approximate symmetry and the axial current should be partially conserved which is known as Partial Conserved Axial Current (PCAC) hypothesis .

Now, if we apply the vector and axial vector transformation on the mesonic states, we find that the vector transformation simply gives an isospin rotation,

whereas the other one gives some non trivial relations resulting in a mass shift in the mesonic states which is not expected if axial vector current is conserved. On the contrary, the Goldberger-Treiman relation and the weak decay of pion provides evidence for the axial vector current to be conserved. Again, if axial vector current is really conserved, the chiral partners with opposite parity of each hadrons should exist in nature, which we do not find. So, we may conclude that $SU(2)_A$ is broken by spontaneous chiral symmetry breaking which is manifested by the existence of a non-vanishing quark condensate $\langle q\bar{q}\rangle$, the order parameter for the chiral symmetry breaking transition. Another hint for the spontaneously broken chiral symmetry is the low mass of the pion which comes about quite naturally if the pions are interpreted as the corresponding Goldstone bosons in the two-flavor case. If chiral symmetry was exact on the Lagrangian level ("chiral limit") they would be massless, while the small but finite pion mass reflects the explicit symmetry breaking through the quark masses.

In the remaining part of this chapter a brief summary of the current understanding of the QCD phase transition along with the various signatures that can be used to study the phase transition is discussed.

1.3 Phase Structure of QCD

The physics in the low-energy region of QCD is subject of ongoing intensive research activities. Exploring the phase structure of quantum chromodynamics (QCD) is certainly one of the most exciting topics in the field of strong interaction physics. At very low energies QCD shows a large variety of bound states which are color singlet hadrons. Low energies are identified with low temperatures, where the system is in the hadronic phase we are living in. Hadrons become deconfined at high temperature and/or high density when they strongly overlap and loose their individuality. The system is then expected to be in the form of quark-gluon-plasma (QGP). So there is clearly two distinct phases of QCD, the hadronic phase and the quark gluon plasma phase. In general, the study of hadron-quark phase transition involves two different kind of phase transitions. These two phase transitions are defined for two extreme limits of the current quark masses and are related to two distinct symmetries of the QCD Lagrangian. The deconfinement phase transition, resulting from Z_3 (for $N_c = 3$) global center symmetry breaking, takes place in the limit of infinite quark masses. The order parameter of this transition is the Polyakov Loop

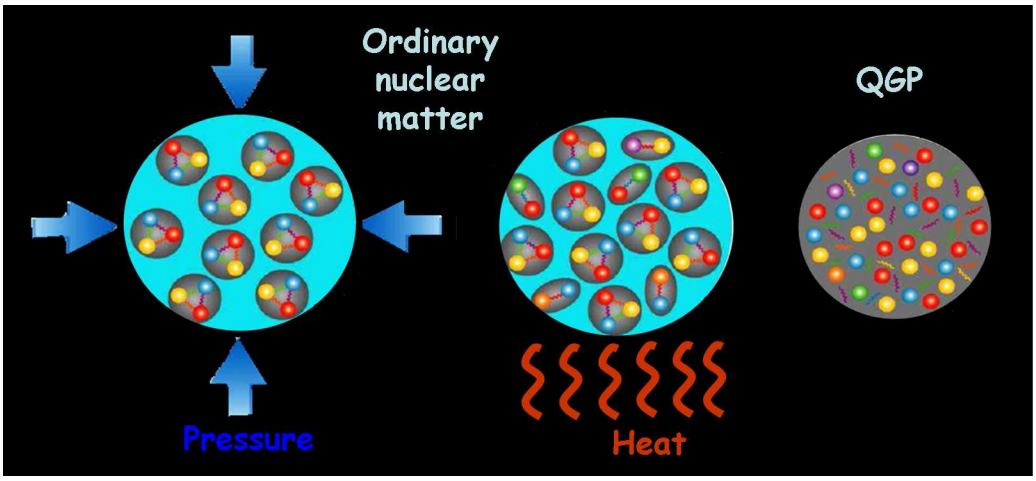

Figure 1.1: QGP formation at extreme condition

[3]. On the other hand, in the massless limit we have chiral phase transition with the chiral condensate as an order parameter. At intermediate masses there is no known exact symmetry. The dynamics of the system may give hints for further symmetries. Numerical simulations show that, in QCD with fundamental fermions, deconfinement and chiral symmetry restoration take place at very close or coincident temperatures [4]. The question whether there is a true phase transition or simply a rapid change (crossover) is fundamental. The presence or absence of a true phase transition is essential to understand whether we can really interpret confinement/deconfinement in terms of some exact symmetry of QCD. Whether confinement is an absolute property of Nature or a fine tuned suppression of color charge, is also crucial for understanding.

The phase diagram is a convenient pictorial way to describe various possible phases in terms of intensive thermodynamic quantities. The schematic phase diagram in temperature-baryon density plane is shown in 1.2. The two different regime of the phase diagram correspond to two different physical scenarios. In the limit of high temperature ($\sim$ 1 GeV) and low chemical potential (almost $\mu = 0$ axis) we have early universe scenario. On the other hand in the limit of high chemical potential ($\gg$ 200 MeV) and low temperature we have situation similar to the one that may exist inside neutron stars. This phase diagram remained the standard picture for a quite long time. Later there was a great progress in the understanding of quark matter at sufficiently high densities [5, 6, 7, 8]. At high density and low temperature quark matter is expected to be a color superconductor, which is a degenerate Fermi gas of quarks with

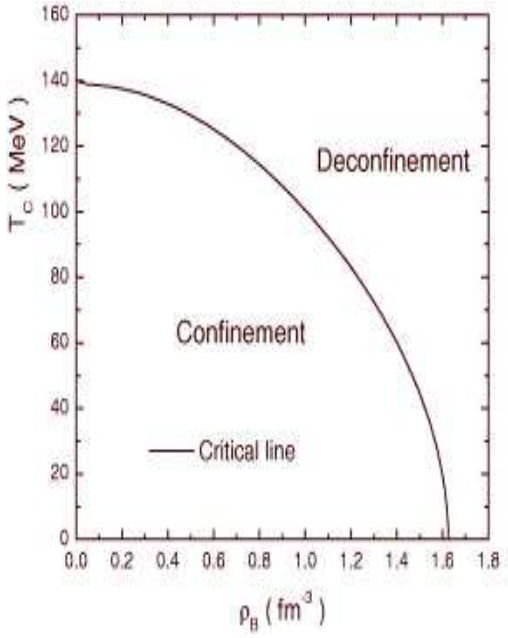

Figure 1.2: Schematic phase diagram for confinement- deconfinement transition.

a condensate of Cooper pairs near the Fermi surface. Color superconductivity comes as a result of the Cooper instability driven by an attractive interaction between quarks. This gives rise to a new phase in the QCD phase diagram, known as color superconducting phase. The possibility of having more than one deconfined phase was not taken into account although the existence of color superconductivity at very large densities and low temperature has become an established consequence of QCD [9]. Since pair of colored quarks cannot be color singlet, the condensate of the two quarks breaks the local color gauge symmetry. Due to the spontaneous breaking of this symmetry the gauge bosons (here gluons) become massive giving rise of 'color Meissner effect'. For two flavor quark matter five gluons out of eight become massive.

Since quarks have color, flavor as well as spin degrees of freedom a variety of quark pairing is possible unlike electrons. At the highest possible densities strange quarks also participate in such pairing and gives rise to a color flavor locked (CFL) phase. The CFL phase is a superfluid, an electromagnetic insulator, and breaks chiral symmetry.

Thus, in addition to the two standard phases, there is a non-negligible region at high density in the QCD phase diagram where strongly interacting matter can be in a color superconducting as well as in a Color Flavor Locked phase. The corresponding phase diagram is depicted in Fig.1.3.

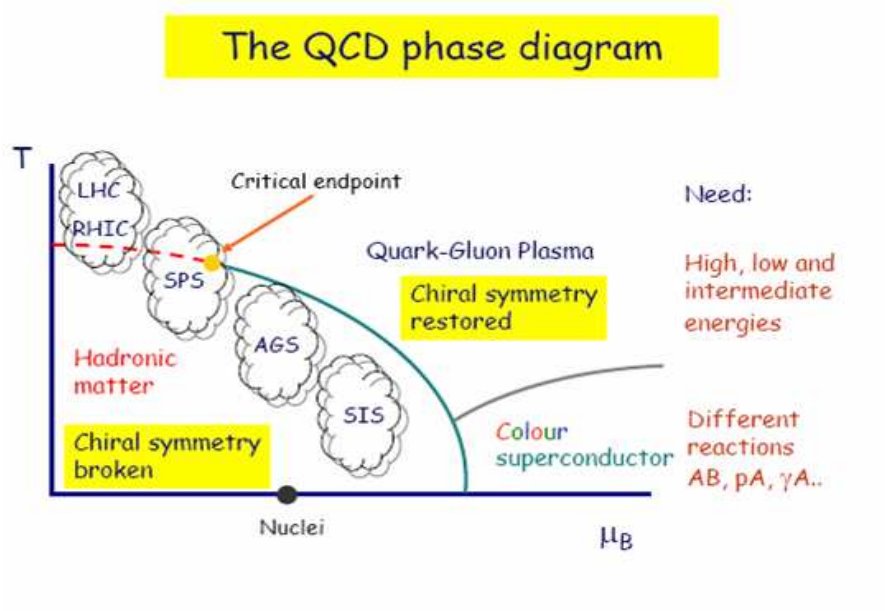

Figure 1.3: QCD phase diagram with color super conducting phase.

The QCD phase transition at finite temperature with zero chemical potential has been studied extensively in the numerical simulation on the lattice [10, 11, 12, 13]. Results depend on the number of colors and flavors. In pure gauge theory for $N_c = 2$ lattice study indicates that the deconfinement transition is of second order [14, 15]. For $N_c = 4$ the transition is first order as claimed in [16] though there are questions about the strength of the first order phase transition. Further increase in the number of colors does not change the transition and it remains a first order transition. In the limit of infinite number of colors there is a strong first order phase transition [17] . But for three colors there exists some controversy about the order of transition. Some results indicate that the transition is first order [18] but others suggest that it is weakly first order or nearly a second order transition [19]. However, it was argued in Ref. [20] that since $N_c = 3$ is more close to two colors than infinity, the order of the phase transition is likely to be a nearly second order phase transition.

The situation is different in the presence of dynamical quarks. For two flavor massless quarks there is a chiral phase transition from broken phase to a chirally restored phase at some critical temperature T_c. For nonzero chemical potential there are various QCD inspired models which indicate that at low temperatures there is a possibility of first order phase transition for a large baryon chemical potential μ_{B_c} . This μ_{B_c} is supposed to decrease with

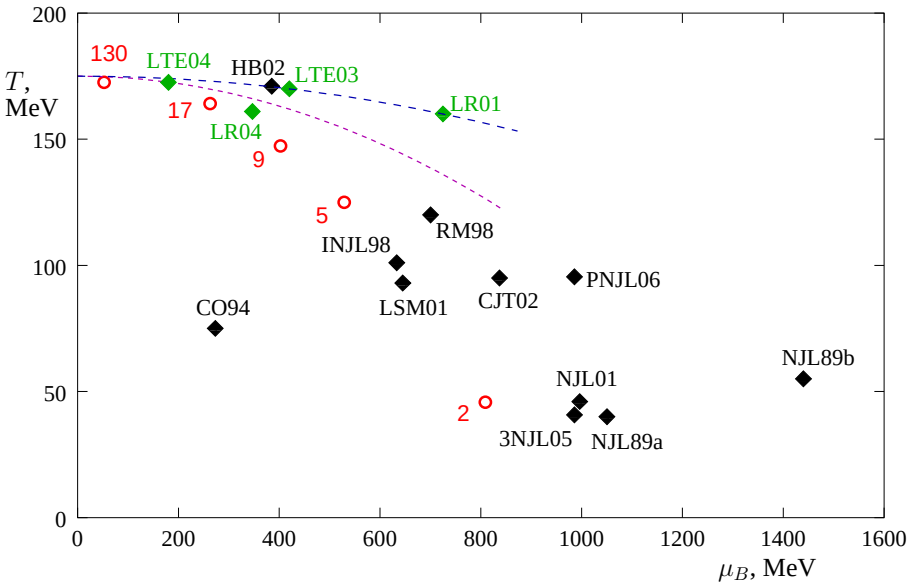

Figure 1.4: Prediction for Critical End Point from different theoretical frameworks. Black points are different model predictions. Green points are from different Lattice calculations and the open red circles are freeze-out points at different center of mass energies per nucleon. The figure is taken from [22].

increasing temperature. Thus there is a first order phase transition line starting from ($T = 0, \mu_B = \mu_{B_c}$) on the μ_B axis in the (T, μ_B) phase diagram which steadily bends towards the ($T = T_c, \mu_B = 0$) point and may actually terminate at a critical end point (CEP) characterized by ($T = T_E$, $\mu_B = \mu_{B_E}$), which can be detected via enhanced critical fluctuations in heavy ion reactions [21]. The existence and location of the CEP has become a topic of intensive research. Various phenomenological models and lattice results predict a wide range of coordinates (T, μ_B) for the critical end point and they seem to be in no agreement with each other as can be seen from the figure 1.4 . But it is interesting to note, as pointed out in [22], that each of these models agree at $T = \mu_B = 0$ to reproduce the vacuum.

1.4 Phase Transition in Early Universe and Compact Stars

From the recent observational evidence, cosmologists came to the conclusion that our Universe is expanding and cooling. The Cosmic Microwave Background Radiation (CMBR) provides information that the temperature and den-

sities were infinitely large at the very beginning and there was an initial singularity called Big Bang. As the Universe began to expand its temperature and densities started to cool and disperse. At present this ambient temperature of the universe is about 2.7K. At that time Universe was a plasma of relativistic particles. A number of spontaneous symmetry breaking phase transitions

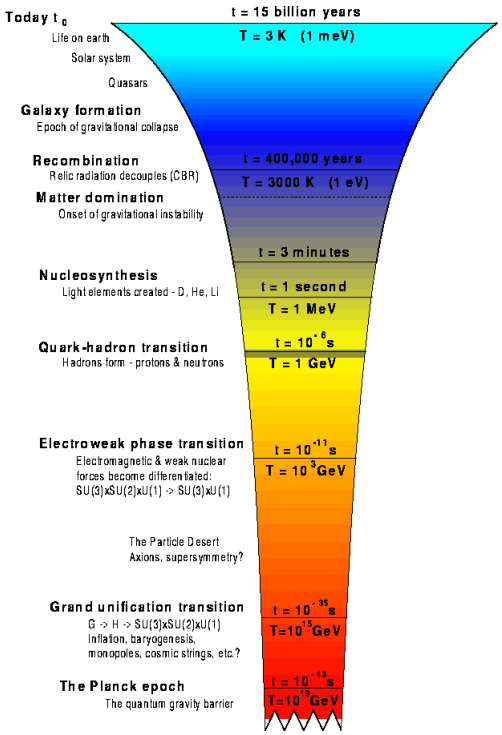

Figure 1.5: Phase transitions at early universe.

took place throughout the earlier stages of the universe. At a temperature of 10^{14} to 10^{16} GeV, the Grand Unification phase transition occurred resulting the separation of strong force from the electromagnetic and weak force. The decoupling of electromagnetic and weak force occurred during electroweak phase transition at a temperature of about 300 GeV. After that, the Universe cools further more, until temperature reaches about 100 to 300 Mev (t $\sim 10^5 s$), where it was undergone through the phase transition associated with chiral symmetry breaking and color confinement. The quarks and gluons combined to form the color singlet baryons and mesons. The cosmic phase transitions have considerable significance in the evolutionary history of the universe. The relics of that era, if found, might have the imprints of the phase transitions. For example, if there was quark-hadron phase transition in the early universe then it must have influenced the process of nucleosynthesis and the measurement

of abundance of various light elements can be used to learn about the quark-hadron transition in the universe. There are also speculation of formation of baryon rich quark nuggets [23, 24] in the cosmic quark-hadron transition. As data from cosmological QCD phase transition proves to be unattainable, there are efforts to recreate and detect the high temperature quark-gluon plasma in laboratories. The heavy ion experiments at RHIC, LHC and FAIR are designed to study strongly interacting matter under extreme conditions of high temperature and/or high baryon density. The knowledge is of key importance for understanding the physics of early universe and its evolution till date, compact stars and other astrophysical phenomena.

The high density in the cores of massive astrophysical objects called neutron stars (NS), inhibits the matter inside it, to stay in the hadronic form, resulting a hadron quark phase transition. Neutron stars are dead stars formed in the after math of a supernovae explosion. The production of thermonuclear energy in the center of the normal stars helps them to counter the inward pressure due to gravity. If the mass of the star goes beyond Chandrasekhar limit [25], it keeps on contracting and becoming denser. At some stage the density becomes so high that protons and electrons are forced to combine to form neutrons, and the whole star then becomes an ocean of neutrons. These stars are called the Neutron Stars. After the supernova explosion during the first tens of seconds, the newly formed proto-neutron star with a radius of about 50 km stays very hot with temperatures of the order of $10^{11} - 10^{12}$ K. Later the star becomes transparent to neutrinos generated in its interior via URCA processes. The proto-neutron star thus rapidly cools down by powerful neutrino emission and shrinks into an ordinary neutron star after 10 to 20 seconds. The central density may be as high as approx. 10 times nuclear matter saturation density. NSs have mass between 1.5 to 2.2 times the solar mass and the radius is of the order of 10 kilometers. The gravitational field is as high as 2×10^{11} times than earth's gravitational pull. NSs are born with very high rotational speed and they gradually slow down. Due to their large central densities, they serve as a natural laboratory to study the properties of the strongly interacting matter at high densities and small temperature. Normal nuclear matter at high enough density and/or temperature, would be unstable against conversion to two-flavor quark matter. Moreover, Witten's conjecture says that strange quark matter, consisting of almost equal numbers of u, d and s quarks, may be the true ground state of strongly interacting matter [26, 27] at high density and/or temperature. This was also supported by Bag model calculations [28]

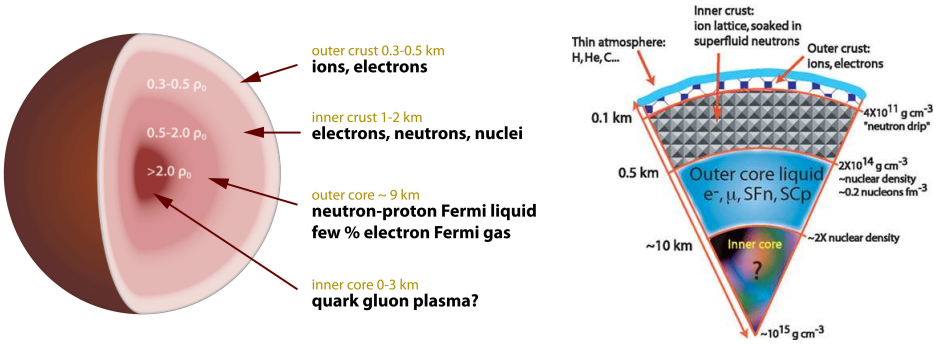

(a) (b)

Figure 1.6: Composition of neutron star from core to surface.

for certain range of values for the strange quark mass and the strong coupling constant. By considering realistic values for the strange quark mass (150 - 200 MeV) [29], it may be shown that the strangeness fraction in a chemically equilibrated quark matter is close to unity for large baryon densities. The above hypothesis may lead to important consequences both for laboratory experiments as well as for astrophysical observations. The two-flavor quark matter would be metastable and would eventually decay to Strange Quark Matter in a weak interaction time scale, releasing a finite amount of energy in the process. If this is true then there is a possibility of conversion of neutron stars to strange stars or at least hybrid stars (HS). Hadron to quark phase transition inside a compact star may yield observable signatures in the form of quasi-periodic oscillations (QPOs) [30] and Gamma-ray bursts (GRBs) [31].

1.5 QCD Phase Transition in Relativistic Heavy Ion Collision

A promising way to produce the strongly interacting matter at high temperature or high density is nucleus-nucleus collision in the laboratory [32, 33, 34, 35, 36]. The evidence for the new state of matter came from the combined data from the experiments in the heavy-ion programme at CERN. The aim was to collide very high-energy lead ions from the Super Proton Synchrotron (SPS) in the experiments, so as to create immensely high concentrations of energy and break down the forces that normally confine quarks inside hadrons. The collisions created temperature is approximately over 10^5 times as hot as the centre of the Sun, and energy densities 20 times that of ordinary nuclear mat-

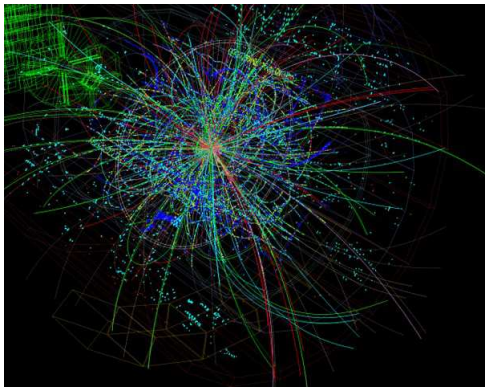

Figure 1.7: Particle showers produced at heavy ion collision.

ter densities that have never been reached in laboratory experiments before. The data provided compelling evidence that a new state of matter had been created, featuring many of the characteristics of the theoretically predicted quark-gluon plasma. It is believed that definite observation of the elusive QGP would be found at higher collision energies with the Relativistic Heavy Ion Collider (RHIC) at the Brookhaven National Laboratory, USA and Large Hadron Collider (LHC) at CERN, Switzerland. There are several experimental evidences which might show that the Quark Gluon Plasma (QGP) could have been formed during the heavy ion collision at RHIC energy. RHIC have provided Au+Au, d+Au and p+p collisions at $\sqrt{s_{NN}}$ = 200 GeV. The RHIC experiments have measured the charged particle multiplicity as a function of collision energy and centrality (impact parameter). The measurements were found to be consistent with a temperature of about 176 MeV at the chemical freeze-out. Currently most of the activities at CERN are based on the experiments at Large Hadron Collider (LHC) and analyzing the data coming out of them. Six experiments namely CMS, ATLAS, LHCb, TOTEM, LHCf and ALICE are built to study heavy ion collision from a different point of view with different technologies. Pb-Pb nuclei collisions will be studied at ALICE at a centre of mass energy of 5.5 TeV per nucleon. The resulting temperature will be enough to generate a quark-gluon plasma at temperature much higher than RHIC energy (200 GeV per nucleon).

In the nucleus-nucleus collisions at ultra-relativistic energies, the energy density is sufficiently high, leading to the formation of a system of quarks and gluons- the QGP. The plasma initially may not be in thermal equilibrium, but subsequent equilibration brings it to local equilibrium. The system then evolves in space and time according to the law of hydrodynamics, expands

and eventually cools down from an initial high temperature. When the particular temperature T_c, *i.e* the transition temperature is reached the quarks and gluons condense to form hadrons. With further expansion, the hadronic system cools. Finally, at a temperature, usually referred to as the freeze-out temperature, the hadrons cease to interact with each other and fly away to the detectors. Thus, a space-time integrated history of the entire evolution is detected through the hadrons. During the time when the matter is in QGP phase the particles which emerges due to the interactions of the constituent of the plasma will actually provide us the information concerning the state of plasma. In the next section various QGP diagnostics mainly strangeness enhancement, J/Ψ suppression, direct photons and dileptons will be discussed. The advantage of considering dileptons as a good probe over the others will be narrated as well. In addition, all the possible sources of dileptons in Heavy Ion Collision will be discussed elaborately in section. In section 1.8 the space time evolution of thermally generated dilepton pairs will be discussed.

1.6 Possible QGP Signatures

1.6.1 Strangeness enhancement

Strangeness enhancement [37] can be thought as a good signature of the QGP. In normal hadronic matter it is energetically favorable to produce up and down quarks rather than strange quarks in heavy ion collisions because the masses of the up and down quarks are considerably less than the strange quarks. In fact, the colliding ions consist not of s quarks, but of u and d quarks. The mass of the strange quark goes down as temperature increases. Therefore it is expected that there should be an increase in the number of strange quarks and anti-quarks in the QGP phase where the temperature is high enough for strangeness production. In fact, at $\mu_u = \mu_d = \mu_s = 0$; when the temperature of the plasma is of the order of strange quark mass, the density of all quarks and anti quarks are almost same [38]. In such a plasma the strangeness content is much larger than that in a equilibrated hadron gas or in colliding nuclear matter. These strange quarks and anti quarks subsequently combine with the neighboring quarks and anti-quarks to form strange particles mainly strange mesons. It has been suggested that the enhancement of strange quarks leads to the enhancement of the strange mesons production and this can be used as a signal of QGP. However, it is hard to argue that strangeness alone suffices

to show the formation of the QGP phase. The CERN experiment WA97, which studies strange particle production at central rapidity in Pb-Pb, p-Pb, p-Be collisions at 158 A GeV/c, has already reported a pronounced enhancement of hyperon production and these results have been supported by the STAR experiment in RHIC which is capable of a wide variety of measurements of the production of Λ and Λ^- particles in nuclear collisions. The particles studied in these experiments are Λ, Ξ and Ω hyperons and K^0 and K^+ mesons. The experimental observation suggested that the ratios of K^+/π^+ , $\bar{\Lambda}/\Lambda$ and $\bar{\Xi}/\Xi$ increase [39].

1.6.2 J/Ψ suppression in Quark Gluon Plasma

The suppression of J/Ψ particle production can be used as a signature of the formation of Quark Gluon Plasma as suggested first by Matsui and Satz [40]. The J/Ψ particle is basically a bound state of charm and anti-charm quark. In Quark Gluon Plasma the interaction between the c and $\bar{c}$ is weakened due to Debye screening. At high temperature the range of attractive interaction becomes so small that it is impossible for the $c\bar{c}$ pair to form a bound state. So effectively the existence of the plasma makes the J/Ψ particle unbound. Therefore the final yield of J/Ψ particle will be suppressed as compared to the case where there is no quark gluon plasma. In Sulfur–Uranium collisions (NA38), the most weakly bound state Ψ' is already dissociated while the more tightly bound state J/Ψ requires higher energy densities to 'melt'. However, analysis of the data collected by the NA50 collaboration with Pb-Pb collisions at 158 GeV/ nucleon shows that J/Ψ is anomalously suppressed in central collisions and the observed pattern can be considered as a strong indication for QGP production [41].

1.6.3 Photon Production in QGP

Directly produced photons are considered as one of the most prominent probes of the QGP. In the quark Gluon Plasma photons are produced by the quark anti-quark annihilation process $q\bar{q} \to \gamma g$. The analogous electromagnetic process is $q\bar{q} \to \gamma\gamma$, but this process is less probable than the other because $\alpha_e < \alpha_s$. The gluon interacts with a quark or anti quark via Compton process and photons are produced by the reaction $gq \to \gamma q$ and $g\bar{q} \to \gamma\bar{q}$. Usually high-energy photons produced in the interior of the plasma pass through the surrounding matter without interacting, carrying information directly from

wherever they are formed to the detector. The photon production rate and its momentum distribution depend on that of quarks, anti-quarks and gluons which are governed by the thermodynamic condition of the plasma. So photons carry the information of the thermodynamical state of the medium at the moment of their production. Unfortunately, thermally generated photons are not the only source of photons created in heavy ion collisions. They can also be emitted during the hot hadron phase because many hadrons are electrically charged. Pions and ρ mesons are the main constituents of such a phase. The dominant contribution of photons from the hadronic sector are: $\pi\pi \rightarrow \rho\gamma$, $\pi\rho \rightarrow \pi\gamma$, $\pi\pi \rightarrow \eta\gamma$, $\pi\eta \rightarrow \pi\gamma$, $\omega \rightarrow \pi^0\gamma$, $\rho^0 \rightarrow \pi^+\pi^-\gamma$. If the thermally produced photon component can be extracted from these huge background, it will provide an excellent diagnostic of the QGP created in ultra-relativistic nuclear collisions. A measurement of direct photon production in Pb-Pb collisions at 158 A GeV has been carried out in the CERN WA98 experiment. Significant direct photon excess is observed at $p_T > 1.5$ GeV/c in central collisions [42].

1.6.4 Dilepton production and QGP signature

Direct lepton pairs (e^+e^- or $\mu^+\mu^-$) are considered, by Feinberg, to be one of the more reliable probes of hot and dense quark matter [43]. The specific advantage for considering dileptons as a good probe is their nature of interaction. These electromagnetically interacting particles have very small interaction cross section compared to strong interaction, so they have large mean free path and can leave the system without any distortion of their energy-momentum. They thus carry the information from the reaction zone quite effectively, as they do not get masked by the details of the evolution process. The situation is clearly very different for the hadrons coming from the reaction zone. Because hadrons interact strongly with the rest of the system during the entire evolution, thus losing the initial information.

However, like photons here also difficulties arise because the dileptons originating from the QGP phase is masked by those produced from the initial hard processes and hadronic decays. One has to subtract these background contributions from the total yield of dileptons for getting an idea of the quark matter created. In 1996, the CERES/NA45 collaboration reported an excess of dileptons in the low invariant mass region approximately 0.2 to 0.6 GeV/c^2 which can be explained by the presence of a QGP phase. Measurements at SPS (center of mass energy, $\sqrt{s_{NN}}$ = 17.3 GeV) [44, 45] and RHIC ($\sqrt{s_{NN}}$ =

200 GeV) [46] have provided results for e^+e^- and $\mu^+\mu^-$ dilepton pairs. Other interacting dilepton data that have demonstrated an enhanced yield over that measured in proton–nucleus reactions are the dimuon spectra in the intermediate mass region from about 1 GeV to roughly 2.5 GeV, measured by the Helios-3 and NA38/50 collaborations [47]. Hence theoretical calculations have so far concentrated on e^+e^- and $\mu^+\mu^-$ dilepton production. With the starting of the heavy-ion collision program at LHC in November 2010 we have reached $\sqrt{s_{NN}}$ = 2.76 TeV and it is shortly planned to reach $\sqrt{s_{NN}}$ = 5.5 TeV. At the LHC energies we expect significant production of the third generation of leptons the τ-leptons. This opens up the possibility to make similar studies with $\tau^+\tau^-$ pair in addition to e^+e^- and $\mu^+\mu^-$ pairs at LHC energies. This will be discussed in detail in this thesis.

1.7 Sources of dileptons in Heavy Ion Collision

1.7.1 Thermal Dilepton

In a thermally equilibrated Quark Gluon Plasma quark anti quark annihilation gives rise to s virtual photon which subsequently decays into a l^+l^- pair. The

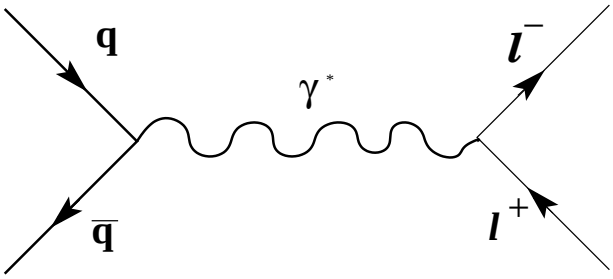

Figure 1.8: Dileptons from $q\bar{q}$ annihilation.

importance of the dileptons for the study of thermodynamic state of the evolving matter was first proposed by Feinberg in 1976 [43]. While, for most of the purposes the dilepton emission rates are calculated in a classical framework, Feinberg showed that the emission rates can be related to the electromagnetic current current correlation function in a thermalized system in a quantum picture and, more importantly, in a non-perturbative manner.

Let us begin our discussions with the dileptons arising from single virtual photon. Following [34] one can write the matrix element S_{HI} for the transition

$|I\rangle$ to $|H; l^+l^-\rangle$ as

$$S_{HI} = e \int \langle H; l^+l^-|J^l_\mu(x)A^\mu(x)|I\rangle d^4x e^{q\cdot x} \tag{1.7}$$

where $|I\rangle$ is the initial state corresponding to the two incoming nuclei, $|H; l^+l^-\rangle$ is the final state which corresponds to a lepton pair plus anything, the parameter 'e 'is the renormalized charge, and $q = (q^0, \vec{q})$ is the four momentum of the lepton pair. We assume that the lepton pair does not interact with the emitting system, we can factorize the matrix element in the following way:

$$\langle H; l^+l^-|J^l_\mu(x)A^\mu(x)|I\rangle = \langle H|A^\mu(x)|I\rangle\langle l^+l^-|J^l_\mu(x)|0\rangle \tag{1.8}$$

where $|0\rangle$ is the vacuum state. Now, thermalization erases all the information about a specific initial state, so we can replace the initial state $|I\rangle$ by the ensemble average of all initial states each weighted by a Boltzman factor. Hence the thermally averaged dilepton multiplicity is:

$$N = \sum_I \sum_H |S_{HI}|^2 \frac{e^{-\beta E_I}}{Z(\beta)} \mathcal{V} \frac{d^3p_1}{(2\pi)^3} \mathcal{V} \frac{d^3p_2}{(2\pi)^3} \tag{1.9}$$

where E_I is the total energy in the initial state, $Z(\beta)$ is the partition function. Using the identity $\sum_I |I\rangle\langle I| = 1$ and $E_H = E_I + q_0$, N can be written in a compact form as:

$$N = e^2 L^{\mu\nu} H_{\mu\nu} \frac{d^3p_1}{(2\pi)^3 E_1} \frac{d^3p_2}{(2\pi)^3 E_2} \tag{1.10}$$

Here, $L^{\mu\nu}$ and $H_{\mu\nu}$ are the lepton and photon tensor respectively and given as:

$$L^{\mu\nu} = \sum_{spins} \bar{u}(p_1)\gamma^\mu v(p_2)\bar{v}(p_2)\gamma^\nu u(p_1) \tag{1.11}$$

and

$$H_{\mu\nu} = \sum_I \sum_H \int d^4x d^4y e^{iq\cdot(x-y)} \langle H|A^\mu(x)|I\rangle \times \langle I|A^\nu(y)|H\rangle \frac{e^{\beta E_I}}{Z(\beta)} \tag{1.12}$$

The photon tensor can be written in terms of photon spectral function $\rho_{\mu\nu}$ [34] and finally we arrive at the dilepton multiplicity per unit space-time volume as:

$$\frac{dN}{d^4x} = 2\pi e_0^2 L^{\mu\nu} \rho_{\mu\nu}(q) e^{-\beta q^0} \frac{d^3p_1}{(2\pi)^3 E_1} \frac{d^3p_2}{(2\pi)^3 E_2} \tag{1.13}$$

The photon spectral function is related with the imaginary part of photon self energy.

For photon self-energies of not more than two-loop order, its imaginary part

reduces to tree level diagrams, in which case it is usually more convenient to find thermal rates using the relativistic kinetic theory. The number of l^+l^- pairs produced per unit space-time volume is :

$$\frac{dN}{d^4x} = N_c N_s^2 \sum_{f=1}^{N_f} (\frac{e_f}{e})^2 \int \frac{d^3p_1}{(2\pi)^3} \frac{d^3p_2}{(2\pi)^3} f(\mathcal{E}_1) f(\mathcal{E}_2) \sigma(M) v_{12} \tag{1.14}$$

$\sigma(M)$ is the bare cross-section of the process $q\bar{q} \rightarrow l^+l^-$. M is the invariant mass of the dilepton pair. $\mathcal{E}_1$ and $\mathcal{E}_2$, $f(\mathcal{E}_1)$ and $f(\mathcal{E}_2)$ are the energies and thermal distribution functions of the quark and anti-quark in the Quark Gluon Plasma respectively. v_{12} is the relative velocity between quark and anti-quark given as[38].

$$v_{12} = \frac{M\sqrt{M^2 - 4m_q^2}}{2\mathcal{E}_1\mathcal{E}_2} \tag{1.15}$$

The perturbative character of this approach thus makes it advantageous over at moderate and high energies and momenta.

1.7.2 Dileptons from Initial Hard Process : Drell-Yan Mechanism

In high energy nucleus-nucleus collision QGP is not the only source of dileptons. Apart from the thermal contribution, an important contribution comes from the Drell-Yan process. In this process a valence quark of a nucleon of one

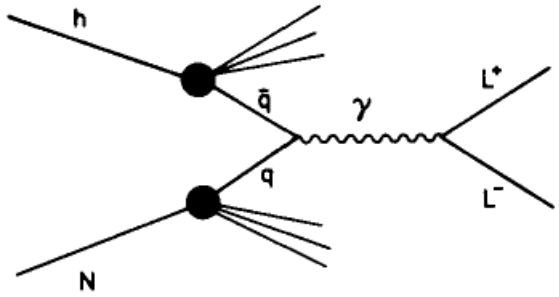

Figure 1.9: Feynmann diagram for the production of dilepton pair via the Drell-Yan process.

of the colliding nuclei interacts with the sea anti-quark of a nucleon of other nucleus. This quark-anti quark annihilation process forms a virtual photon which decay into a dilepton pair. In this process it is assumed that there is no correlation between the nucleons inside the nuclei. So the production of dilep-

ton pairs in this process is the collection of the individual nucleon-nucleon collisions. If σ_q is the basic partonic cross-section of the process $qq \rightarrow \bar{l}^+l^-$ then the differential cross-section in p-p collision can be written according to [38],

$$\frac{d\sigma^{pp}}{dM^2dy} = \frac{1}{N_c}\Sigma_f\sigma_q[q_f^B(x_1,Q^2)\bar{q}_f^A(x_2,Q^2) + \bar{q}_f^B(x_1,Q^2)q_f^A(x_2,Q^2)] \tag{1.16}$$

$q(x_i)$ and $\bar{q}(x_i)$ are the quark and anti-quark distributions in the nucleon. x_i is the parton longitudinal momentum. y is the rapidity and N_c is the number of colors.

The differential cross-section in a nucleus-nucleus collision can be obtained by using the Glauber model[38], which provides a quantitative consideration of the geometric configuration of the two nuclei when they collide.

The DY production in nucleus-nucleus collision is;

$$\frac{dN}{dM^2dy} = \frac{N_{coll}(b)}{\sigma_{\rm in}^{pp}} \times \frac{d\sigma^{pp}}{dM^2dy}$$

where, $N_{coll}(b)$ is the number of binary nucleon nucleon collisions at an impact parameter b calculated using Glauber model and σ_{in} is the inelastic cross section for pp interaction.

1.7.3 Dileptons from Hadronic Interaction

Hadron collisions and hadron resonances are also an important source of dileptons. Hadrons are produced in the initial nucleus-nucleus collision and also in the final state when the quark gluon plasma cools down. The dominant contribution in the hadronic interaction comes from the pion annihilation process, i.e. $\pi^+\pi^- \rightarrow l^+l^-$. l^+l^- pair also comes from the decay of hadron res-

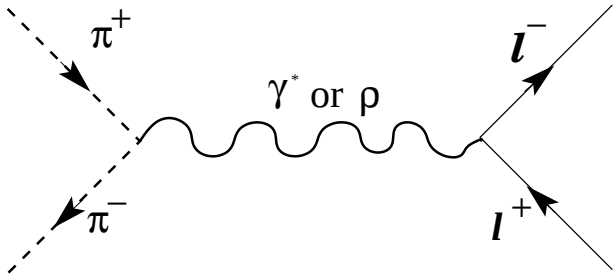

Figure 1.10: Dileptons from hadronic decay.

onances like ρ, ω, ϕ and J/ψ. These resonances may come through the initial collisions as well as from the collision of pions in the dense pion gas during the time of thermalization of hadron gas. The sharp peaks in the invariant mass spectra of the dilepton pairs indicate the decay of such hadron resonances.

1.7.4 Heavy flavor decay and dileptons

Heavy quark production will be substantial at high energy. Both charm and bottom quarks can be produced at high energies and fragmented into heavy mesons which subsequently decay to lepton pairs [48]. Charm and anti-charm pair is produced when a quark anti-quark pair annihilates to produce virtual gluon. This gluon decays into a $c\bar{c}$ pair, i.e. $q + \bar{q} \rightarrow g^* \rightarrow c + \bar{c}$. The $c\bar{c}$ pair

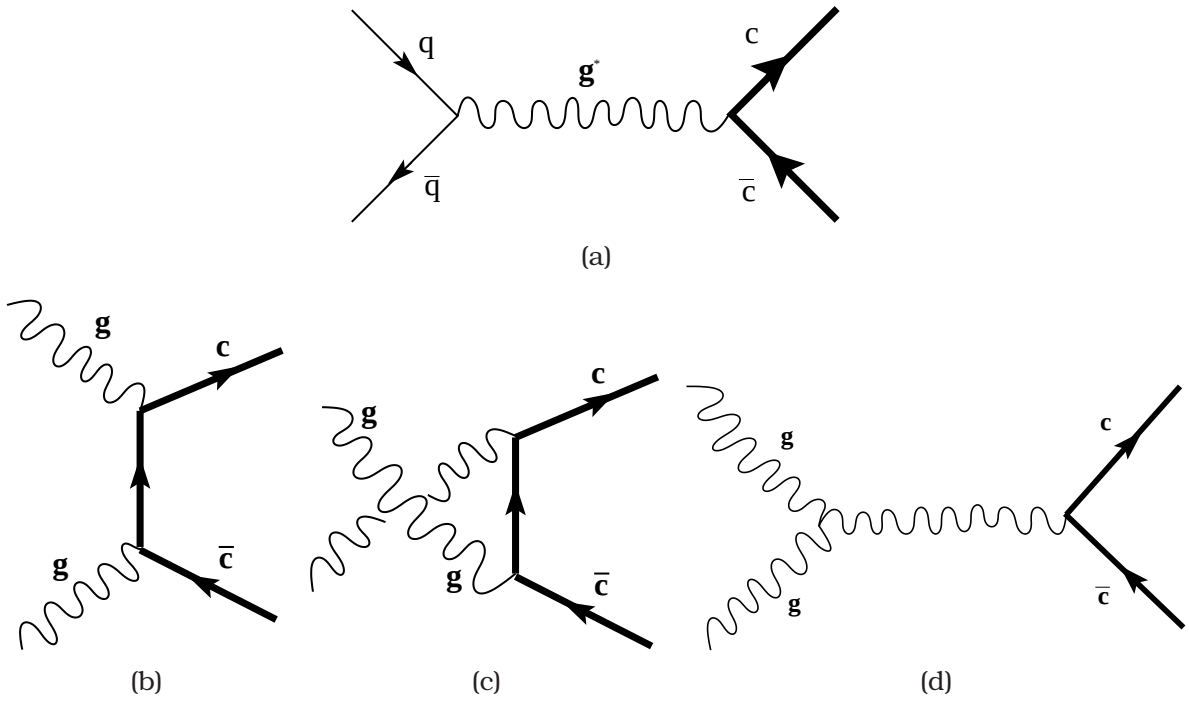

Figure 1.11: Production of heavy flavors in quark gluon plasma.

can also be produced via the interaction of two gluons, i.e $g + g \rightarrow c + \bar{c}$. The produced c and $\bar{c}$ are then fragmented into D^+ and D^- mesons respectively resulting the formation of D^+D^- pair. Dilepton pairs are produced via the subsequent decay of this D^+D^- pair, i.e.,

$$D^+ \rightarrow l^+ + X \;\; ; D^- \rightarrow l^- + X \tag{1.17}$$

1.8 Space-Time Evolution : Bjorken Hydrodynamical Model

In relativistic heavy ion collision the produced matter will either be a hot hadronic gas or a quark gluon plasma. In the earlier section we have discussed about the rate of dilepton emission per unit time from unit volume of a thermal system made up of quark matter at a fixed temperature T. Our next goal is to consider its evolution in space and time. The space-time evolution constitutes the most important aspect of quark-gluon plasma studies. Hydrodynamics, although classical in concept and formulation, provides a manageable computational tool to understand at least the gross features of nucleus-nucleus collisions. This is so because the fundamental conservation laws of energy momentum are built into a proper formulation of hydrodynamics and one expects that the basic features of the space-time evolution are governed largely by these conservation laws alone. Furthermore, the large spatial sizes of the colliding nuclei provide a scenario where the mean free path of the constituent particles could be significantly smaller than the size of the system. These arguments have succeeded in making the use of classical concepts of hydrodynamics in studying the space-time evolution in energetic nucleus-nucleus collisions acceptable [49].

We will restrict ourselves to the central rapidity regime only. The created matter is treated as an ideal fluid. The complete dynamics of the system is described by the pressure (p), energy density (ϵ), temperature (T) and the four velocity of the fluid (u_μ) at different space-time points. The equation of state of the system connects ϵ, p and T, i.e. $\epsilon = \epsilon(p, T)$. Before solving the hydrodynamic equation, the boundary conditions and the initial conditions suitable for the system under consideration should be specified. The boundary conditions at the two edges of the fluid is such that it expands against vacuum, that is the pressure $P = 0$ outside. By the initial condition we mean here the state of the matter when the thermalization has taken place and the hydrodynamic evolution can start. As it was observed experimentally that the particle spectra for the secondaries in nucleon-nucleon collisions exhibit a central plateau in rapidity space, Bjorken assumed that the same kind of plateau will also be observed in the nucleus-nucleus collisions, which implies that the rapidity density is constant over a large range of rapidity variable [50]. This constancy leads to a state of Lorentz invariance in the longitudinal direction [51, 52]. In other words this means that the energy density, and all the thermodynamic

quantities are functions of the initial thermalization (proper) time τ_0 only and do not depend on the space-time rapidity η. This initial symmetry of the thermodynamic quantities will be preserved throughout the evolution scenario. An immediate consequence of perfect fluid hydrodynamics is the conservation of entropy during the entire flow [35, 36]. Under these circumstances, it is reasonably justified to assume that the entire evolution of the 'fireball'from the initial time τ_0 till the freeze-out time τ_f is strictly adiabatic. Following Ref.[35] one can arrive at $T_0^3\tau_0 = \frac{2\pi^4}{45\zeta(3)\pi R_A^2 4a_k}\frac{dN_\pi}{dy}$; from which the initial temperature can be estimated. a_k is degeneracy factor. $\frac{dN_\pi}{dy}$ is the hadronic multiplicity. The temperature of the plasma drops down to to T_c, at the proper time τ_c given by

$$\tau_c = \Big(\frac{T(\tau_0)}{T_c}\Big)^3 \tau_0 \tag{1.18}$$

After that the transition from QGP phase to hadronic phase takes place.

1.9 Plan of the thesis

In this thesis we concentrate mainly on the properties of strongly interacting matter at finite density as well as finite temperature using Polyakov loop extended Nambu Jona-Lasinio (PNJL) model. Due to the non perturbative nature of the strongly interacting matter at low energy regime it is very difficult to study it from the first principle. Lattice QCD, despite of its short comings at finite chemical potential, has given us a wealth of information about the system [4]. It is now well established that at zero chemical potential the transition from hadronic to quark gluon plasma phase is a crossover and the corresponding transition temperature is $T_c \sim 200$ MeV. The chiral symmetry restoration and deconfinement transition are found to occur simultaneously at this temperature. QCD inspired effective models are very useful tool by which one can predict the properties of strongly interacting matter in a easier way compared to lattice simulation or perturbative calculations. The predictive power of these models is not very strong due to the lack of exact order parameter. But in PNJL model we have Polyakov loop, the thermal average of which can be treated as the order parameter of deconfinement transition. There is a lot of interest in the studies of thermodynamics of strongly interacting matter using the Polyakov loop enhanced Nambu-Jona-Lasinio model[53, 54, 55]. A very sensitive observable–the quark number susceptibility (QNS) and also the higher order coefficients in the Taylor expansion of pressure in quark number

chemical potential were estimated for different systems using this model. For example, the 2 flavor and 2+1 flavor quark matter considering six as well as eight quark interactions has been extensively studied in Ref.[56, 57]. Comparing with the data from Lattice QCD (LQCD) [58] one can see that the QNS in the PNJL model and LQCD agree quite well both qualitatively and quantitatively. In the present thesis we are also going to explore the thermodynamics as well as various other characteristics of quark matter using this model.

The thesis is organized as follows. In the next chapter we will discuss the 2+1 flavor isospin asymmetric quark matter at finite chemical potential. Physical characteristics of relevant thermodynamic observables will be discussed within the framework of PNJL model. The asymmetry arises because of the fact that we have considered beta equilibrium among the flavor chemical potentials which are related through electron chemical potential.

$$\mu_d = \mu_u + \mu_e \quad ; \mu_s = \mu_d \tag{1.19}$$

It should be mentioned that for this study the masses of u and d quarks are taken to be same whereas strange quark mass is quite larger than the other two. We will give a comparative analysis with the corresponding observables in the Nambu-Jona-Lasinio model. We will analyze the QCD phase diagram under the beta equilibrium condition for different electron chemical potential values. The present study is expected to give a better insight of superdense matter inside the core of massive astrophysical objects. As the density of matter changes nontrivially along the radial direction of massive stars, we discussed the variations of all thermodynamic quantities w.r.t. chemical potential rather than temperature, which remains almost constant.

In chapter 3 we will describe the isospin asymmetric 1+1 flavor quark matter at finite temperature as well as finite density scenario, where for this case the asymmetry arises entirely due to the mass difference of u-d quark. We have restricted ourselves by considering zero isospin chemical potential. The equality of u and d flavor quark masses are quite good approximation in nature, however, not exactly true. In chapter 3, we are going to investigate the imprint of this type of flavor asymmetry in the thermodynamical observables of the system.

Analyzing the thermodynamic properties of QGP, we studied the signatures of QGP because the most important objective in current research is to search for the existence of the quark gluon plasma created at high temperature

and/or high density. There is no doubt about the fact that the temperature and density achievable in nucleus-nucleus collisions at ultra-relativistic energies would be favorable for the formation of such a phase. The only thing observed in these experiments is a shower of various particles. Theoretically it should be possible to analyze these signals and gain information about QGP. Different kind of QGP signals have been proposed and studied so far. As mentioned earlier, dileptons created in heavy ion collision are thought to be one of the most promising QGP diagnostics. At LHC energies the production of heavy dileptons is supposed to be non-negligible. Since mass of these leptons are order of magnitude higher than that of low mass dileptons, the background production will be small. Hence we can expect a clear signal of QGP by studying these heavy dileptons. This is the main advantage for studying $\tau^+\tau^-$ pairs in chapter 4. We will discuss the yield of $\tau^+\tau^-$ pairs from various sources in detail. Comparing the results we will be able to say whether these heavy leptons can really help in search of QGP.

Bibliography

[1] Gross, D. J., and F. Wilczek, Phys. Rev. Lett. **30**, 1343 (1973)

[2] V. Koch, arXiv: nucl-th/9706075

[3] L. D. Mclerran and B. Svetitsky, Phys. Rev. D **24**, 450 (1981)

[4] E. Laermann and O. Philipsen, Annu. Rev. Nucl. Part. Sci. **53**, 163 (2003)

[5] D. Bailin and A. Love, Phys. Rep. **107**, 325 (1984)

[6] M. G. Alford, A. Schmitt, K. Rajagopal and T. Schäfer Rev.Mod.Phys. **80**, 1455 (2008)

[7] M. G. Alford, Annu. Rev. Nucl. Part. Sci. **51**, 131 (2001)

[8] D. K. Hong, Acta Phys. Pol. B **32**, 1253 (2001)

[9] J.C. Collins, M.J. Perry, Phys. Rev. Lett. **34**, 1353 (1975)

[10] O. Kaczmarek *et. al.*, Phys. Rev. D **83**, 014504 (2011)

[11] S. Borsányi *et. al.*, JHEP **11**, 077 (2010)

[12] M. Cheng *et. al.*, Phys. Rev. D **77**, 014511 (2008)

[13] M. Cheng *et. al.*, Phys. Rev. D **81**, 054504 (2010)

[14] A. Dumitru and R. D. Pisarski, Phys. Lett. B **504**, 282 (2001)

[15] J. Engels , F. Karsch , K. Redlich , Nucl. Phys. B **435**, 295 (1995); J. Engels , S. Mashkevich , T. Scheideler , and G.Z Inovev, Phys. Lett. B **365**, 219 (1996); J. Engels and T. Scheideler, Phys. Lett. B **394**, 147 (1997); Nucl. Phys. B **539**, 557 (1999)

[16] S. Ohta and M. Wingate, Nucl. Phys. Proc. Suppl. B **73**, 435, (1999); ibid. **83**, 381 (2000); Phys. Rev. D **63**, 094502 (2001)

[17] A. Goksch and F. Neri, Phys. Rev. Lett. **50**, 1099 (1983)

[18] B. Svetitsky and L. G. Yaffe, Nucl. Phys. B **210**, 423 (1982)

[19] O. Kaczmarek, F. Karsch, E. Laermann and M. Lutgemeier, Phys. Rev. D **62**, 034021 (2000)

[20] R. D. Pisarski, proceedings of Strong and Electro-Weak Matter 2000, hep-ph/0101168

[21] M. Stephanov, K. Rajagopal, and E. Shuryak, Phys. Rev. Lett. **81**, 4816 (1998)

[22] M. Stephanov, PoS(LAT2006)024, hep-lat/0701002

[23] J. Madsen, Phys. Rev. D **50**, 3328 (1994)

[24] S. Banerjee, Sanjay K Ghosh and S. Raha, J. Phys. G **25**, L15 (1999)

[25] S. Chandrasekhar, Astrophys. J., **74**, 81 (1931)

[26] E.Witten, Phys. Rev. D, **30**, 272 (1984)

[27] P. Haesel, R. Schaeffer, J. L. Zdunik, Astronomy & Astrophysics, **160**, 121 (1986)

[28] E. Farhi and R. L. Jaffe, Phys. Rev. D **30**, 2379 (1989)

[29] A. Chodos, R. L. Jaffe, K. Jhonson, C. B. Thorn and V. B. Weisskopf, Phys. Rev. D **9**, 3471 (1974)

[30] A. Bhattacharyya and S. K. Ghosh, Mod. Phys. Lett. A **22**, 1019 (2007)

[31] A. Bhattacharyya, S. K. Ghosh and S. Raha, Phys. Lett. B **635**, 195 (2006)

[32] L.D.Mclerran and T.Toimela, Phys. Rev. D **31**, 545 (1985)

[33] C. Gale and J.I Kapusta, Nucl.Phys. B **357**, 65 (1991)

[34] H.A. Weldon, Phys. Rev. D **42**, 2384 (1990)

[35] J. Alam, S. Raha, B. Sinha, Phys. Rept. **273**, 243 (1996)

[36] J. Alam, S. Sarkar, P.Roy, T. Hatsuda and B. Sinha, Ann. of Phys. **286**, 159 (2000)

[37] J. Rafelsky, Phys. Rep. **88**, 331 (1982)

[38] C. Y. Wong, Introduction to High-Energy Heavy- Ion Collisions, World Scientific, Singapore, 1999

[39] F. Antinori *et. al*, Nucl. Phys. A **681**, 165 (2001)

[40] T. Matsui and H. Satz, Phys. Lett. B **178**, 416 (1986)

[41] D. Jounan *et. al*, Nucl. Phys. A **681**, 157 (2001)

[42] M. M. Aggarwal, Phys. Rev. Lett. **85**, 3595 (2000)

[43] E. L. Feinberg, Nuovo Cimento A **34**, 391 (1976)

[44] G. Agakichiev et al., CERES Collaboration, Eur. Phys. J. C **41**, 475 (2005); D. Adamova *et al.*, CERES Collaboration, Phys. Rev. Lett. **91**, 042301 (2003)

[45] R. Arnaldi et al., NA60 Collaboration, Eur. Phys. J. C **59**, 607 (2009); Phys. Rev. Lett. **100**, 022302 (2008)

[46] A. Adare et al., PHENIX Collaboration, Phys. Rev. **81**, 034911 (2010).

[47] I. Tserruya Nucl.Phys. A **681**, 133 (2001)

[48] S. Gavin, P. L. McGaughey, P. V. Ruuskanen, and R. Vogt, Phys. Rev. C **54**, 5 (1996)

[49] H. von Gersdorff, M. Kataja, L. D. McLerran and P. V. Ruskanen, Phys. Rev. D **34**, 794 (1986)

[50] J. D. Bjorken, Phys. Rev. D **27**, 140 (1983)

[51] C.B. Chiu, E.C.G. Sudarshan and K.H. Wang, Phys. Rev. D **12**, 902 (1975)

[52] F. Cooper, G. Frye and E. Schonberg, Phys. Rev. D **11**, 192 (1975)

[53] P. N. Meisinger and M. C. Ogilvie, Phys. Lett. B **379**, 163 (1996); Nucl. Phys. B, Proc. Suppl. 47, 519 (1996)

[54] K. Fukushima, Phys. Lett. B **591**, 277 (2004)

[55] C. Ratti, M. A. Thaler, and W. Weise, Phys. Rev. D **73**, 014019 (2006)

[56] S. K. Ghosh, T. K. Mukherjee, M. G. Mustafa, and R. Ray, Phys. Rev. D **73**, 114007 (2006)

[57] A. Bhattacharyya, P. Deb, A. Lahiri and R. Ray, Phys. Rev. D **82**, 114028 (2010); *ibid* D**83**, 014011 (2011)

[58] C. R. Allton *et al.*, Phys. Rev. D **71**, 054508 (2005)

CHAPTER 2

Strongly Interacting Matter at Finite Density With Beta Equilibrium

2.1 Introduction

In the present chapter we are going to discuss the phase transition of strongly interacting hadronic matter at finite density. The phase diagram of strongly interacting matter has been at the center of attention for quite long time. At very high density we also expect a hadron-quark phase transition and a new state of matter called Quark Gluon Plasma (QGP) may be formed [1]. In nature, the highest densities of matter are reached in central regions of compact stars where the temperature is relatively low. The density might be as large as 10 times normal nulear saturation density. It is possible that baryonic matter is deconfined under such conditions [2, 3, 4]. So an understanding of the physics of strongly interacting matter at such environmental conditions would have important cosmological and astrophysical significance.

In the laboratory such conditions of large temperatures and densities can be created by the collision of heavy ions at high energies. Presently the strongly interacting matter at high temperature and close to zero baryon densities – a scenario relevant for early universe – is being explored at Relativistic Heavy Ion Collider (RHIC) at BNL and the Large Hadron Collider (LHC) at CERN. A wealth of information has been obtained from RHIC, and a lot more is expected from both the future runs there as well as from LHC. More recently

a variety of energy scans at RHIC and the upcoming facility (FAIR) at GSI, are expected to give us a glimpse of matter in the baryon-rich environments - the so-called *compressed baryonic matter* (CBM). These experiments will also be useful in the search for signatures of critical phenomena associated with a second order critical end point (CEP).

At the same time, observational data are being collected by a large number of telescopes and satellites [5] such as the radio telescopes at the Arecibo, Parkes, Jo-drell Bank, and Green Bank Observatories, the Hubble Space Telescope, European Space Agency's International Gamma Ray Astrophysics Laboratory (INTEGRAL) satellite, Very Large Telescope (VLT) of the European Southern Observatory, the X-ray satellites Chandra, XMM-Newton and NASA's Rossi X-ray Timing Explorer and the Swift satellite. Observations from these facilities are supposed to tell us about the properties of strongly interacting matter at high densities relevant for the astrophysics of compact stars.

Thus on one hand the laboratory experiments are expected to scan the phase space temperature and various conserved quantum number densities of strongly interacting matter. On the other hand the astrophysical observations are expected to uncover the physics for high baryon number density region of the phase diagram. It should be noted here that the physical characteristics of the matter under consideration may be quite different in the two cases. The time-scale of the dynamics of heavy-ion experiments is so small that only strong interactions may equilibrate thermodynamically. While the dynamics in the astrophysical scenario is slow enough to allow even weak interactions may equilibrate. Thus a question naturally arises – to what extent can laboratory experiments be used to infer about the compact star interiors? The aim of this chapter is to address this question at a preliminary level from the characteristics of the "$\beta-$equilibrated" phase diagrams.

One should be able to study the properties of systems described above from first principles using Quantum Chromodynamics (QCD), which is *the* theory of strong interactions. However, QCD is highly non-perturbative in the region of temperature and density that we are interested in. The most reliable way to analyze the physics in this region of interest is to perform a numerical computation of the lattice version of QCD (Lattice QCD). The scheme is robust but numerically costly. Moreover, there are problems in applying this scheme for the systems having finite baryon density. Thus it has become a common practice to study the physics of strongly interacting matter under the given conditions using various QCD inspired effective models. Generally

the QCD inspired phenomenological models are much easier to handle compared to Lattice or the perturbative QCD calculations. But in all these models despite their simplicity, the absence of a proper order parameter for deconfinement transition adds to the uncertainties inherent in such studies and hence reduces the predictive power of such models. To investigate the properties of dense quark matter it is natural to start with a model for dense matter which is built from the quark level. Until now various quark models, such as, different versions of the MIT bag model [6, 7], the color-dielectric model [8, 9] and different formulations of the NJL model [10, 11] have been used to study the NS structure. Despite the similarity of the results on the value of the maximum NS mass, the predictions on the NS configurations can differ substantially from model to model. The most striking difference is in the quark matter content of the NS, which can be extremely large in the case of EOS related to the MIT bag model or the color-dielectric model, but it is vanishingly small in the case of the original version of the NJL model [10, 12]. In the case of NJL model it turns out that, as soon as quark matter appears at increasing NS mass, the star becomes unstable, with only the possibility of a small central region with a mixed phase of nucleonic and quark matter. This may be a result of the lack of confinement in NJL model. In fact an indirect relationship between confinement and NS stability has been found in a study using NJL model with density dependent cut-off [13]. Hence it is important to study the EOS from the Polyakov−Nambu−Jona-Lasinio (PNJL) model [14, 15, 16], where a better description of confinement has been incorporated through Polyakov loop mechanism. Moreover, a comparison with NJL model might be helpful in understanding the role of Polyakov loop at high chemical potential.

A detailed study of 2+1 flavor strong interactions has already been done using the PNJL model. The general thermodynamic properties along with the phase diagram [17], as well as details of fluctuation and correlations of various conserved charges [18] have been reported. Here we extend the work by including $\beta-$equilibrium into the picture. In the context of NJL model such a study was done earlier in [19, 20]. In Ref.[21, 22] the properties of pseudoscalar and neutral mesons have been studied in finite density region within the framework of 2+1 flavor NJl model in $\beta-$equilibrium.

We investigate and compare different properties of the NJL and PNJL models in the T-μ_B plane. The specialization of these studies to the possible dynamical evolution of NS and/or CBM created in heavy-ion collisions will be

kept as a future excersize.

2.2 Formalism

The supermassive compact objects like neutron stars are born in the aftermath of supernova explosions. The initial temperature of a new born NS can be as high as $T \sim 100$ MeV. For about one minute following its birth, the star stays in a special proto-neutron star state: hot, opaque to neutrinos, and larger than an ordinary NS (see, e.g., [23, 24] and references therein). Later the star becomes transparent to neutrinos generated in its interior. It cools down gradually, initially through neutrino emission ($t \leq 10^5$ years) and then through the emission of photons ($t \geq 10^5$ years) [25], and transforms into an ordinary NS. The weak interaction responsible for the emission of these neutrinos eventually drive the stars to the state of $\beta-$equilibrium along with the imposed condition of charge neutrality.

The mass, radius and other characteristics of such a star depend on the equation of state (EOS), which in turn, is determined by the composition of the star [26]. The possible central density of a compact star may be high enough for the usual neutron-proton matter to undergo a phase transition to some exotic forms of strongly interacting matter. Some of the suggested exotic forms of strongly interacting matter are the hyperonic matter, the quark matter, the superconducting quark matter etc. If there is a hadron to quark phase transition inside the NS, then all the characteristics of the NS will depend on the nature of the phase transition [27, 28].

Furthermore, there have been suggestions that the strange quark matter, containing almost equal numbers of u, d and s quarks, may be the ground state of strongly interacting matter (see [29] and references therein). If such a conjecture is true, then there is a possibility of the existence of self-bound pure strange stars as well. In fact, the conversion of NS to strange star may really be a two step process [30]. The first process involves the deconfinement of nuclear to two-flavor quark matter; the second process deals with the conversion of excess down quarks to strange quarks resulting into a $\beta-$equilibrated charge neutral strange quark matter. There are several mechanisms by which the conversion of strange quark may be triggered at the center of the star [31, 32]. The dominant reaction mechanism by which the strange quark production in quark matter occurs [33] is the non-leptonic weak interaction pro-

cess.

$$u_1 + d \leftrightarrow u_2 + s \tag{2.1}$$

Initially when the quark matter is formed, $\mu_d > \mu_s$, and the above reaction converts excess d quarks to s quarks. But in order to produce chemical equilibrium the semileptonic interactions,

$$d(s) \rightarrow u + e^- + \bar{\nu_e} \tag{2.2}$$

$$u + e^- \rightarrow d(s) + \nu_e \tag{2.3}$$

play important role along with the above non-leptonic interactions. These imply the $\beta-$equilibrium condition $\mu_d = \mu_u + \mu_e + \mu_{\bar{\nu}}$; and $\mu_s = \mu_d$.

Actually, the only conserved charges in the system are the baryon number n_B and the electric charge n_Q. Since we are assuming neutrinos to leave the system, lepton number is not conserved [10]. Strange chemical potential μ_S is zero because strangeness is not conserved. So two of the four chemical potentials (μ_u, μ_d, μ_s and μ_e) are independent. In terms of the baryon chemical potential (μ_B), which is equivalent to the quark chemical potential (μ_q=μ_B/3), and the charge chemical potential (μ_Q) these can be expressed as, $\mu_u = \mu_q + \frac{2}{3}\mu_Q$; $\mu_d = \mu_q - \frac{1}{3}\mu_Q$; $\mu_s = \mu_q - \frac{1}{3}\mu_Q$; $\mu_e = -\mu_Q$. These conditions are put as constraints in the description of the thermodynamics of a given system through the NJL and PNJL models which will be discussed in the next section.

2.2.1 NJL Model

Nambu and Jona-Lasinio (NJL) model is one of the widely used effective models that mimics QCD within certain limits [34]. In its original version, the NJL model was a model of *interacting nucleons*. The (approximate) chiral symmetry implies (almost) massless fermions on the Lagrangian level. There was no proper explanation of the large nucleon mass without destroying the symmetry. Nambu and Jona-Lasinio first proposed the idea that the mass gap in the Dirac spectrum of the nucleon can be generated in the same way as energy gap of a superconductor in BCS theory. They introduce the Lagrangian with a point like four-fermi interaction as:

$$\mathcal{L}_{NJL} = \bar{\psi_N}(i\partial\!\!\!/^{\mu} - m + \mu\gamma^0)\psi_N + \frac{G}{2}[(\bar{\psi_N}\psi_N)^2 + (\bar{\psi_N} i\gamma_5 \vec{\tau}\psi_N)^2] \tag{2.4}$$

Here Ψ_N is the nucleon field, m is the small bare mass of the nucleon, τ is a Pauli matrix acting in isospin space, and G a dimensionful coupling constant. The self energy of the nucleons induced by the interaction actually gives rise to a large mass of the nucleons, even if their bare mass is zero (chiral symmetric limit).

Reinterpretation of NJL model as a quark model was done in [35]. After this reinterpretation the nucleon field Ψ_N is replaced by the quark field Ψ in the NJL Lagrangian. The quark self energy is calculated in Hartree or Hartree-Fock approximation, and this gives a constant shift in the quark mass.

$$M = m_0 + 2iG \int \frac{d^4p}{(2\pi)^4} \mathrm{Tr} S(p) \tag{2.5}$$

where, m_0 is the bare quark mass, M is quark constituent mass and $S(p)$ is the dressed quark propagator.

$$S(p) = (\not{p} - M)^{-1} \tag{2.6}$$

Restricting the interaction term in scalar and pseudo scalar-isovector channels only, the NJL Lagrangian in terms of quark field Ψ is now

$$\mathcal{L}_{NJL} = \bar{\psi}(i\partial\!\!\!/^{\mu} - m + \mu\gamma^0)\psi + \frac{G}{2}[(\bar{\psi}\psi)^2 + (\bar{\psi} i\gamma_5 \vec{\tau}\psi)^2] \tag{2.7}$$

Under mean field approximation we get the pion condensate $\langle \bar{\psi} i\gamma_5 \vec{\tau}\psi \rangle = 0$ and the Lagrangian can be rewritten in terms of the chiral condensate $\sigma = \langle \bar{\psi}\psi \rangle$ as;

$$\mathcal{L}_{\mathrm{MF}} = \bar{\psi}(i\partial\!\!\!/ - m_0 + \gamma_0\mu + G\sigma)\psi - \frac{G}{2}\sigma^2 \tag{2.8}$$

where σ is the mean field which is basically the trace of the modified fermionic propagator ($S(p)$) corresponding to the modified quark mass $M = m_0 - G\sigma$ i.e.

$$\sigma = -i \int \frac{d^4p}{(2\pi)^4} \mathrm{Tr} S(p) \tag{2.9}$$

As we see from Eq.(2.5) or Eq.(2.9) the integrals are divergent. When thermodynamic variables are calculated from this model generally a three momentum cut-off Λ is used in most of the cases. Thus, NJL model has three parameters i.e. the bare quark mass m_0, the three momentum cut-off Λ and the coupling constant G which are fixed by fitting the values of pion mass, pion decay constant and the quark condensate.

One of the important aspects of QCD namely the chiral symmetry breaking is successfully realized in this model. The massless Lagrangian of NJL model is chirally symmetric, but depending on the coupling strength, quark mass can be generated dynamically by the formation of non zero chiral condensate. Thus the chiral symmetry is broken i.e. $SU(2)_R \times SU(2)_L \rightarrow SU(2)_V$. However, this model does not describe the confinement property of QCD because of the absence of gluon dynamics.

2.2.2 PNJL Model

The incorporation of effect of confinement in NJL model is done by coupling the model with the Polyakov loop. The Polyakov loop extended Nambu Jona-Lasinio (PNJL) model was first introduced in Ref.[36, 37, 38]. In Refs.[39, 14] the model is extended by the inclusion of the Polyakov loop effective potential [40, 41]. While the NJL part is supposed to give the correct chiral properties, the Polyakov loop part should simulate the deconfinement physics. With the success of the Polyakov loop model, people were encouraged to include the dynamical fermions along with the gauge degrees of freedom inside a single theoretical framework. The PNJL model is the result of this endeavor. The initial motivation for the PNJL model was to understand the coincidence of chiral symmetry restoration and deconfinement transition observed in LQCD simulation (see discussions in Ref.[42]).

The Lagrangian of PNJL model consists of two parts: the conventional NJL part and an effective potential for gluons expressed in terms of the traced Polyakov loop. The ordinary derivative in the NJL Lagrangian is replaced by the covariant derivative incorporating the coupling between the gauge field and the quark fields.

The explicit expression for the Lagrangian density for two flavor quark matter is given by [14]:

$$\mathcal{L}_{PNJL} = \bar{\psi}(i\gamma_\mu D^\mu - \hat{m}_0 + \mu\gamma^0)\psi + \frac{G}{2}[(\bar{\psi}\psi)^2 + (\bar{\psi}i\gamma_5\vec{\tau}\psi)^2] \\ -\mathcal{U}(\Phi, \bar{\Phi}, T) \tag{2.10}$$

where,

$$D^\mu = \partial^\mu - iA^\mu \\ A_\mu = \delta_{\mu 0}A^0 \tag{2.11}$$

A^{μ} is given by $A^{\mu} = gA^{\mu}_{a}\frac{\lambda_a}{2}$ with gauge coupling constant g, A^{μ}_{a} is the SU(3) gauge field and λ_a are the Gell-Mann matrices. $\hat{m_0}$ = current quark matrix whose diagonal components are the up and down quark masses, ψ is the quark field and G is the effective coupling constant of the scalar-pseudo scalar four-point interaction of the quark fields.

The effective potential $\mathcal{U}(\Phi, \bar{\Phi}, T)$ is expressed in terms of the traced Polyakov loop $\Phi = (\mathrm{Tr}_c\, L)/N_c$ and its (charge) conjugate $\bar{\Phi} = (\mathrm{Tr}_c L^{\dagger})/N_c$, where L is a matrix in color space given by, $L(\vec{x}) = \mathcal{P}\exp\left[-i\int_0^{\beta} d\tau\, A_4(\vec{x}, \tau)\right]$, $\beta = 1/T$ is the inverse temperature and $A_4 = A^a_4\lambda_a$, A^a_4 being the temporal component of the Eucledian gluon field . Assuming a constant A^a_4 and the A_i's to be zero for ($i = 1, 2, 3$), Φ and its conjugate $\bar{\Phi}$, are treated as classical field variables in PNJL model. The choice of $\mathcal{U}(\Phi, \bar{\Phi}, T)$ differs among different versions of the model. But, its form is chosen to reproduce the Lattice data.

Following the bosonization procedure the contact interaction term can be written in terms of bosonized σ and $\overrightarrow{\pi}$ fields and an effective Lagrangian can be constructed [14]:

$$\mathcal{L}_{eff} = -\frac{\sigma^2 + \overrightarrow{\pi}^2}{2G} - \mathcal{U}(\Phi, \bar{\Phi}, T) - iTr\ ln\ S^{-1}, \tag{2.12}$$

where S^{-1} is the inverse quark propagator given by,

$$S^{-1} = i\gamma_{\mu}\partial^{\mu} - \gamma_0 A^0 - \hat{M} \tag{2.13}$$

with σ and $\overrightarrow{\pi}$ are the chiral condensate and pion condensate respectively. For two flavor quark matter in isospin symmetric limit ($m_u = m_d$) the chiral condensate of u quark and d quark are same, and we write it as: $\sigma_u = \sigma_d = \sigma$. The constituent quark mass is;

$$\hat{M} = \hat{m_0} - \sigma - i\gamma_5\overrightarrow{\tau}.\overrightarrow{\pi}. \tag{2.14}$$

Under mean field approximation we get the $\overrightarrow{\pi}$ condensate equals to zero and the Lagrangian can be rewritten only in terms of the chiral condensate σ. All the thermodynamic quantities can be calculated from the thermodynamic potential which is obtained from the effective Lagrangian [39, 14]).

Since gluon dynamics in this model is limited to spatially constant temporal background field expressed in terms of Polyakov loop, the model cannot be

applied to high temperature regime where transverse degrees of freedom starts to contribute significantly.

In this particular work we have considered a system of u, d and s quark matter in finite density. When strange quark is included in the model we have to deal with the 2+1 flavor PNJL model Lagrangian. Here, $m_u = m_d \neq m_s$.

The thermodynamic potential of 2+1 flavor PNJL model for non-zero quark chemical potential is [17]

$$\begin{aligned}\Omega = \mathcal{U}'[\Phi, \bar{\Phi}, T] + 2g_S \sum_{f=u,d,s} \sigma_f^2 - \frac{g_D}{2}\sigma_u\sigma_d\sigma_s - 6\sum_{f=u,d,s}\int_0^\Lambda \frac{d^3p}{(2\pi)^3} E_f \Theta(\Lambda - |\vec{p}|) \\ - 2T\sum_{f=u,d,s}\int_0^\infty \frac{d^3p}{(2\pi)^3}\ln\left[1 + 3(\Phi + \bar{\Phi}e^{-\frac{(E_f-\mu_f)}{T}})e^{-\frac{(E_f-\mu_f)}{T}} + e^{-3\frac{(E_f-\mu_f)}{T}}\right] \\ - 2T\sum_{f=u,d,s}\int_0^\infty \frac{d^3p}{(2\pi)^3}\ln\left[1 + 3(\bar{\Phi} + \Phi e^{-\frac{(E_f+\mu_f)}{T}})e^{-\frac{(E_f+\mu_f)}{T}} + e^{-3\frac{(E_f+\mu_f)}{T}}\right] \end{aligned} \tag{2.15}$$

where, $\sigma_f = \langle\bar{\psi}_f\psi_f\rangle$ and $E_f = \sqrt{p^2 + M_f^2}$ with, $M_f = m_f - 2g_S\sigma_f + \frac{g_D}{2}\sigma_{f+1}\sigma_{f+2}$.

$\mathcal{U}'(\Phi, \bar{\Phi}, T)$ is so chosen to have exact $Z(3)$ center symmetry and is given by,

$$\frac{\mathcal{U}'(\Phi, \bar{\Phi})}{T^4} = \frac{\mathcal{U}(\Phi, \bar{\Phi})}{T^4} - \kappa\ln[J(\Phi, \bar{\Phi})], \tag{2.16}$$

where,

$$\frac{\mathcal{U}\left(\Phi, \bar{\Phi}, T\right)}{T^4} = -\frac{b_2\left(T\right)}{2}\bar{\Phi}\Phi - \frac{b_3}{6}\left(\Phi^3 + \bar{\Phi}^3\right) + \frac{b_4}{4}\left(\bar{\Phi}\Phi\right)^2 \tag{2.17}$$

with $b_2\left(T\right) = a_0 + a_1\left(\frac{T_0}{T}\right) + a_2\left(\frac{T_0}{T}\right)^2 + a_3\left(\frac{T_0}{T}\right)^3$, and $J[\Phi, \bar{\Phi}] = (27/24\pi^2)(1 - 6\,\bar{\Phi}\Phi + 4\left(\bar{\Phi}^3 + \Phi^3\right) - 3\left(\bar{\Phi}\Phi\right)^2)$ is the Vandermonde determinant. A fit of the coefficients $a_i,\ b_i$ is performed to reproduce the pure-gauge Lattice data and $T_0 = 270$ MeV is adopted in our work. Finally $\kappa = 0.2$ is used which gives reasonable values for pressure for the temperature range used here at zero baryon density as compared to full Lattice QCD computations. In the present work we have considered a system of u, d, s quarks with electrons. For simplicity, electrons are considered as free non-interacting fermions [10] and the corresponding thermodynamic potential is,

$$\Omega_e = -(\frac{{\mu_e}^4}{12\pi^2} + \frac{{\mu_e}^2T^2}{6} + \frac{7\pi^2T^4}{180}) \tag{2.18}$$

where, μ_e is the electron chemical potential.

2.3 Results and Discussions

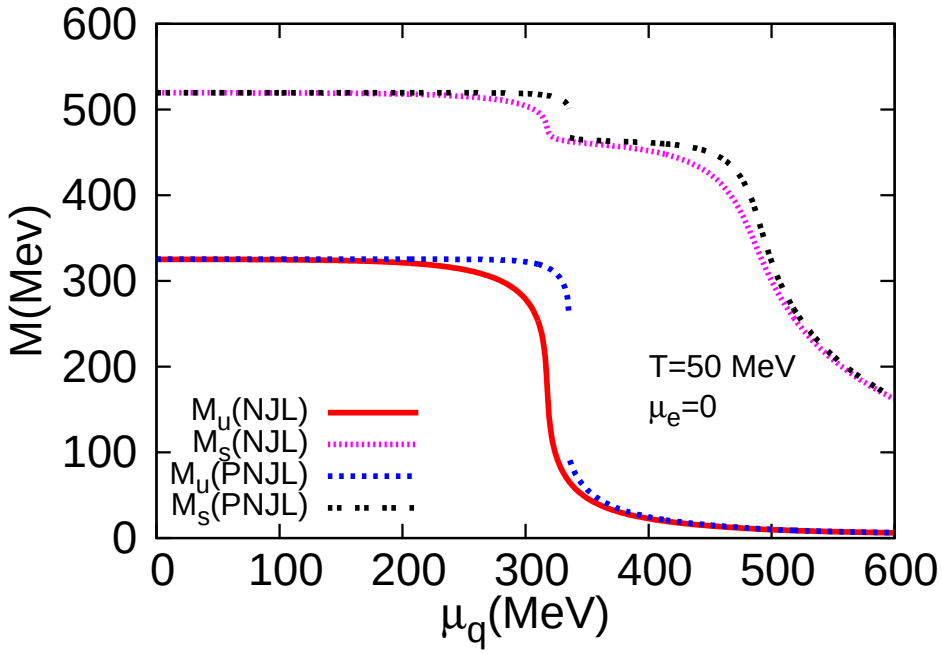

(a)

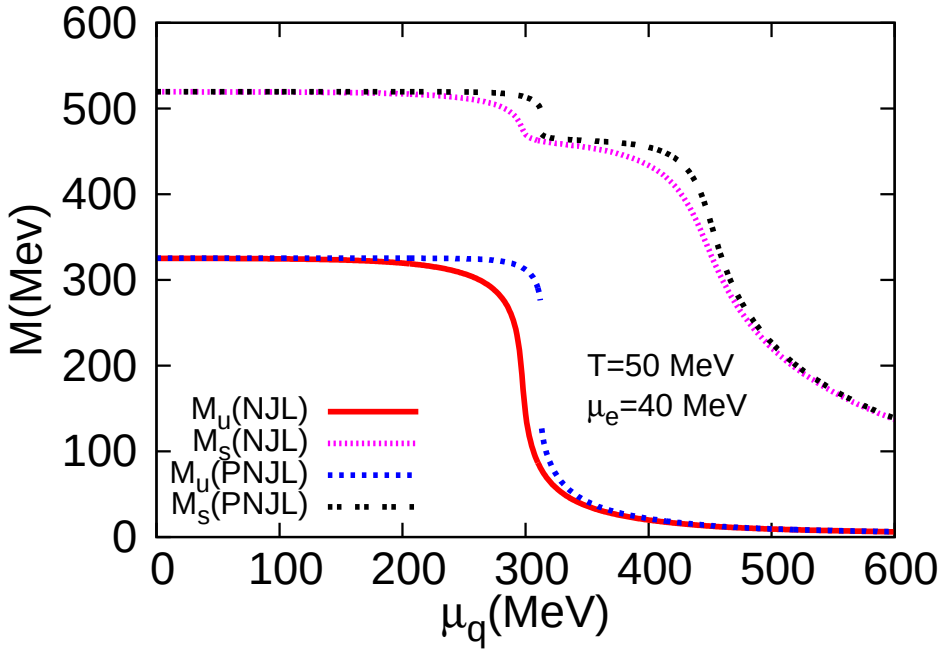

(b)

Figure 2.1: Constituent quark masses as functions of μ_q for (a) $\mu_e = 0$ MeV and (b) $\mu_e = 40$ MeV, at $T = 50$ MeV.

The thermodynamic potential Ω is extremised with respect to the scalar fields under the condition $\mu_d = \mu_u + \mu_e$ and $\mu_s = \mu_d$. The equations of motions for the mean fields σ_u, σ_d, σ_s, Φ and $\bar{\Phi}$ for any given values of temperature T, quark chemical potential μ_q and electron chemical potential μ_e are determined through the coupled equations,

$$\frac{\partial\Omega}{\partial\sigma_u} = 0, \quad \frac{\partial\Omega}{\partial\sigma_d} = 0, \quad \frac{\partial\Omega}{\partial\sigma_s} = 0 \quad \frac{\partial\Omega}{\partial\Phi} = 0, \quad \frac{\partial\Omega}{\partial\bar{\Phi}} = 0. \tag{2.19}$$

In Fig.2.1, we show the typical variation of constituent quark masses as a function of μ_q, for two representative values of electron chemical potential $\mu_e = 0$ MeV and $\mu_e = 40$ MeV, with a fixed temperature $T = 50$ MeV. At this temperature, both m_u and m_s in the PNJL model, show a discontinuous jump at around $\mu_q = 350$ MeV indicating a first order phase transition. The jump in m_s is smaller, and is actually a manifestation of chiral transition in the two flavor sector, arising due to the coupling of the strange condensate to the light flavor condensates. On the other hand in the NJL model the quark masses show a smooth variation at this temperature, indicating a crossover. It is important to note that the constituent mass of the strange quark goes down to the current mass at a larger μ_q in both the models, leading to sort of a second crossover at around $\mu_q = 500$ MeV. This will have important implications for some of the thermodynamic observables as we discuss below.

2.3.1 Phase Diagram

The phase diagrams for NJL and PNJL models are obtained from the behavior of the mean fields, and are shown in Fig. 2.2(a) and Fig. 2.2(b) for $\mu_e = 0$ MeV and $\mu_e = 40$ MeV respectively.

As is evident from the figures, the broad features of the phase diagrams remain same in all cases. The difference between the NJL and PNJL models arise mainly due to the Polyakov loop, whose presence is primarily responsible for raising the transition/crossover temperature in the PNJL model. Thus the CEP for PNJL model occurs at slightly higher T and lower μ_q compared to NJL model. Note that the phase diagram with $\mu_e = 0$ MeV is identical to the case without $\beta-$equilibrium [17]. This is because the minimization conditions (2.19) are independent of the electrons except through the $\beta-$equilibrium conditions. However this is true only so far as the phase diagram is concerned. Various other physical quantities are found to differ even for $\mu_e = 0$ as dis-

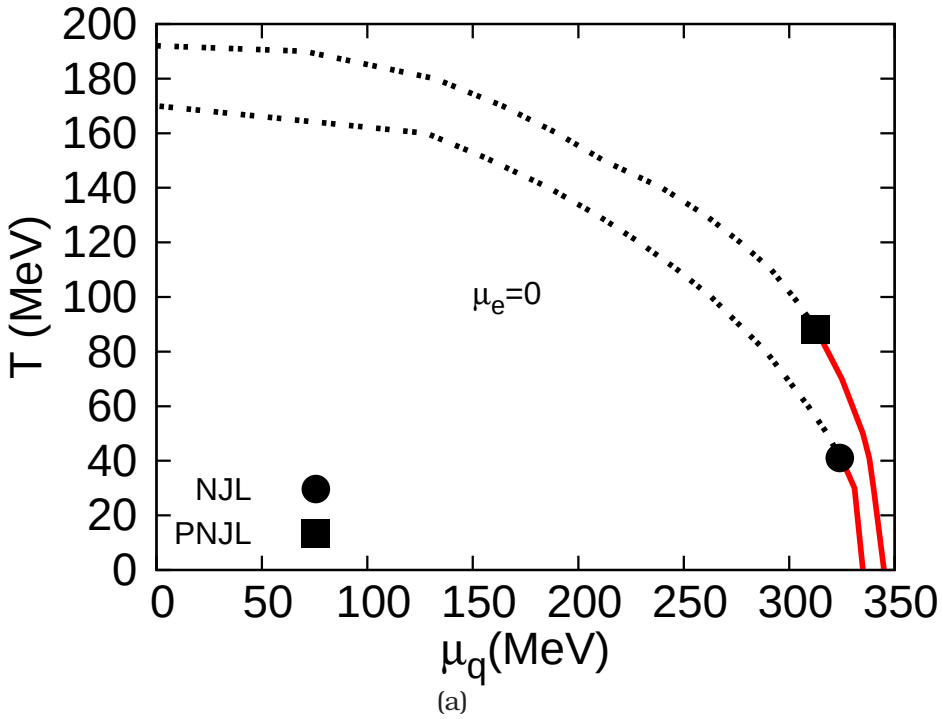

(a)

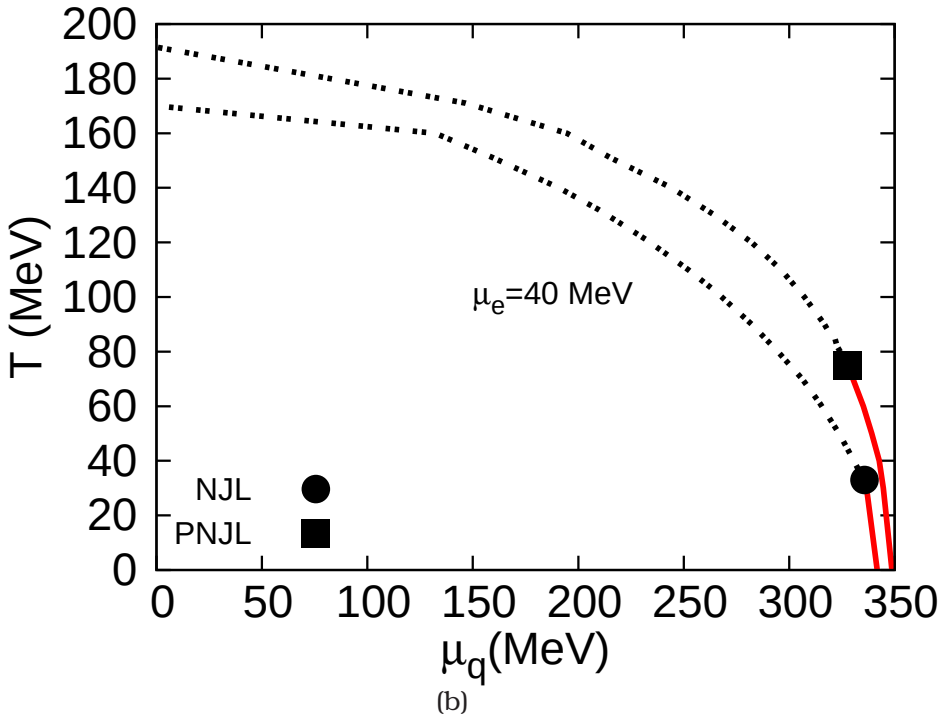

(b)

Figure 2.2: Comparison of phase diagram in NJL and PNJL model at $\beta-$equilibrium for (a) μ_e=0 ; (b) μ_e=40. The solid circle and square represent the CEP for NJL and PNJL model respectively.

cussed below. For non-zero μ_e we find a slight lowering of the temperature for the CEP by about 10 MeV. This is an important quantitative difference between the physics of neutron stars and that of compressed baryonic matter created in the laboratory. In this context we would like to mention that in Ref. [43] QCD phase diagram has been studied both for isospin asymmetric and symmetric situations. The authors considered a two equation of state model where non-linear walecka model was used to describe hadronic sector and (P)NJL model for quark sector. It has been shown in [43] that CEP remain unaffected by the isospin asymmetry.

2.3.2 Equation of State

The system under investigation can be characterized primarily by the behavior of the EOS. Generally for a many body system, increase in pressure at large densities is indicative of a repulsive behavior of the interaction at large densities (large μ_q) or short distances and an attractive nature at larger distances or lower densities [44, 45]. Consequentially the energy density will show similar behavior. The resulting EOS given by the variation of pressure $P = -\Omega$ with energy density $\epsilon = -T^2 \frac{\partial(\Omega/T)}{\partial T}$, is shown in Fig. 2.3(a) at $T = 50$ MeV, for both NJL and PNJL models, for the two representative electron chemical potentials. Here again for the PNJL model there exists a discontinuity due to a first order nature of the transition, whereas for NJL model the EOS is smooth. Beyond this region a smaller steepening in ϵ is visible, that occurs due to second crossover feature noted above as the strange quark condensate starts to melt. A possible implication for this small surge may be that in a strange quark star, at a given central density, the pressure would be somewhat lesser than the situation without this surge.

Generally, the EOS can be used to study the dynamics of neutron star and that of heavy-ion collisions through the respective flow equations. The main differences would be due to the presence of $\beta-$equilibrium and the back reaction of the non-trivial space-time metric on the EOS for neutron stars. Such a comprehensive comparative study will be taken up in a later work.

In Fig. 2.3(b), the variation of the isentropic speed of sound squared $c_s^2 = \partial P/\partial\epsilon$ is plotted against μ_q at $T = 50$ MeV. In the NJL model the c_s^2 starts from a non-zero value, steadily decreases and then shows a sharp fall around the crossover region at $\mu_q \sim 320$ MeV. This is followed by a sharp rise, a dip and then approaches the ideal gas value of $1/3$. In contrast the c_s^2 in the PNJL

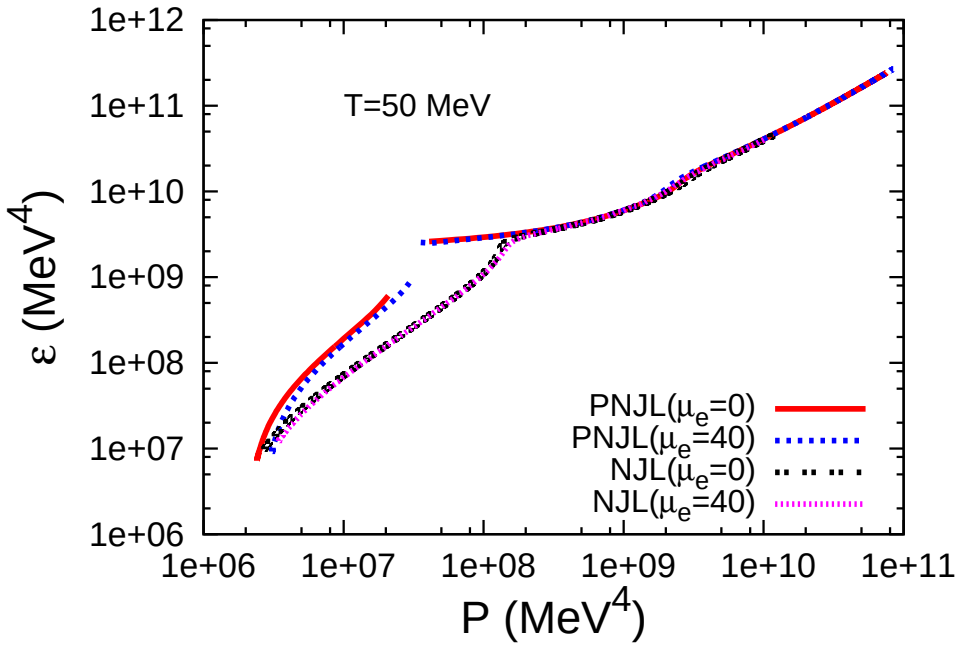

(a)

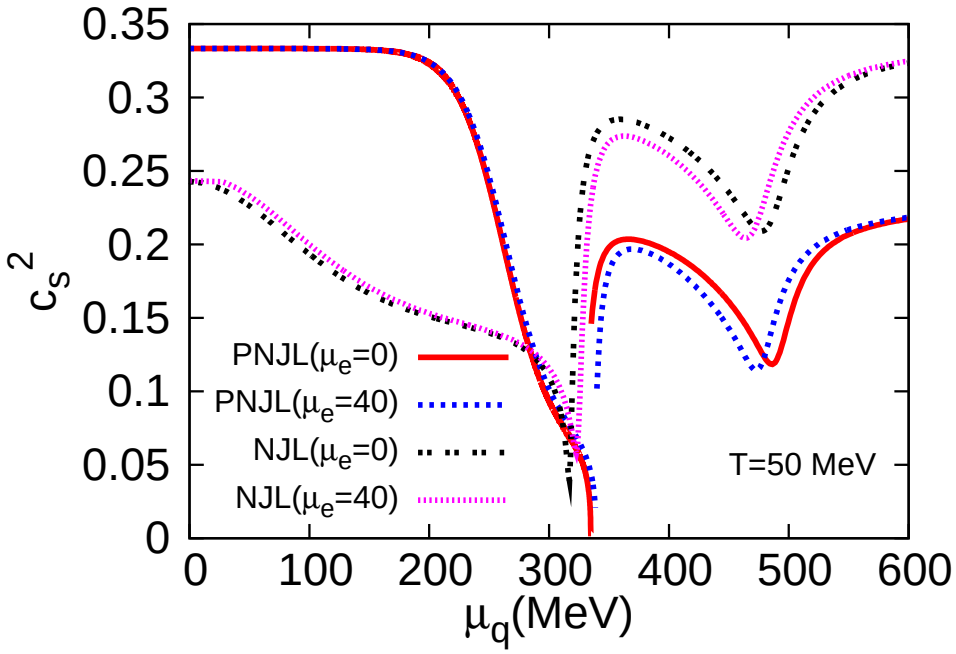

(b)

Figure 2.3: (a) Equation of state and (b) isentropic speed of sound, for NJL and PNJL models at $T = 50$ MeV.

model starting from the ideal gas value remains almost constant up to $\mu_q \sim 200$ MeV and then falls sharply to almost zero. This is followed by a discontinuous

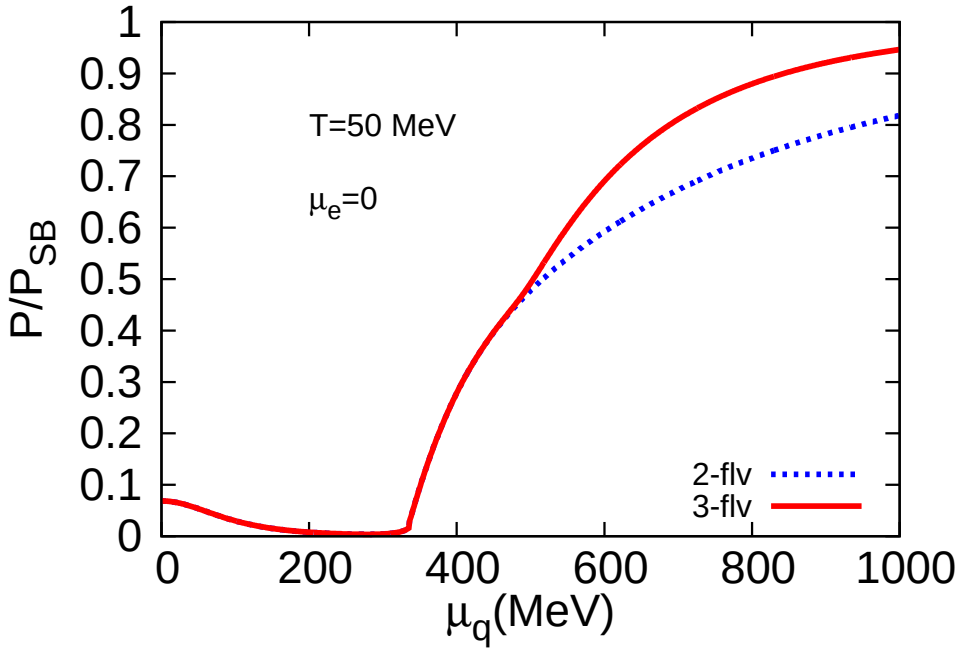

(a)

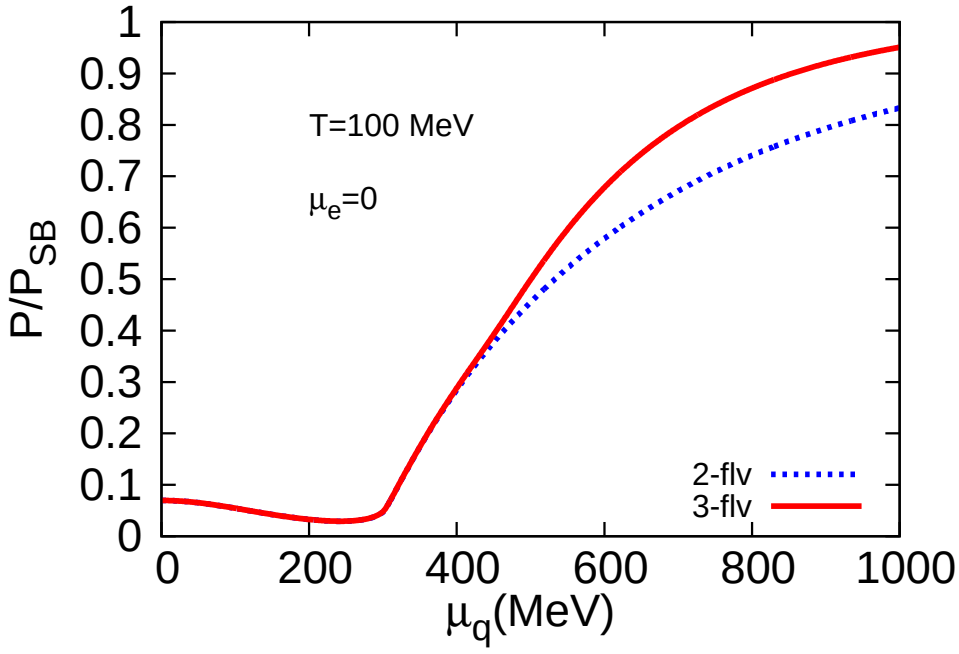

(b)

Figure 2.4: Comparison of pressures quark matter with and without strangeness at $\mu_e = 0$; (a) T=50 MeV and (b) T=100 MeV in PNJL model .

jump, a similar dip at $\mu_q \sim 500$ MeV and a gradual approach to a non-zero value quite different from the ideal gas limit.

The difference at $\mu_q = 0$ MeV occurs specifically due to the Polyakov loop which suppresses any quark-like quasi-particles. As a result the c_s^2 is completely determined by the ideal electron gas. On the other hand those quasi-particles with heavy constituent masses tend to lower the c_s^2 in the NJL model. The difference at the transition region is again mainly due to the discontinuous phase transition in PNJL model which leads to c_s^2 almost going down to zero, and a crossover in the NJL model where c_s^2 is small but non-zero. In [46] it was noted that for two conserved charges, pressure is not constant any more in the mixed phase, rather its variation becomes slower, resulting in a smaller but non-zero speed of sound. In our computation though we do not find c_s^2 exactly equal to zero, but to confirm such an effect we need a full space-time simulation of the mixed phase through the process of bubble nucleation which is beyond the scope of the present work.

In both the models the dip around $\mu_q = 500$ MeV arises due to the behavior of the strange quark condensate as discussed earlier. If it were possible to achieve such extremely high densities in heavy-ion experiments, then such a dip would slow down the flow and would result in a larger fire ball life time. At even higher μ_q the c_s^2 in NJL model approaches the free field limit quite fast but in the PNJL model it still remains quite low due to the non-trivial interaction brought in by the Polyakov loop. It would be interesting to study the implication of slow speed of sound inside the core of a neutron star.

If Witten's conjecture is true, then the free energy should be minimum in a strange quark matter compared to the matter without strangeness. We have checked by comparing the pressures of a 2+1 flavor and 2 flavor quark matter separately for two different temperatures in PNJL model at $\mu_e = 0$ as shown in Fig.2.4. As we see the pressure of 2+1 flavor is larger than that of 2 flavor quark matter. Since pressure is negative of thermodynamic potential (free energy), we can say that 2+1 flavor matter is more stable.

2.3.3 Specific Heat and Compressibility

Specific heat and isothermal compressibility are two most important thermodynamic quantities which show critical behaviors near the phase boundary. They should reflect the large fluctuation near critical point because they are proportional to the fluctuations of the entropy and the density, respectively. Commensurate with the relative stiffening of the equation of state we find that the compressibility $\kappa = \frac{1}{n_q^2}\left(\frac{\partial n_q}{\partial \mu_q}\right)_T$, where n_q is the quark number density, be-

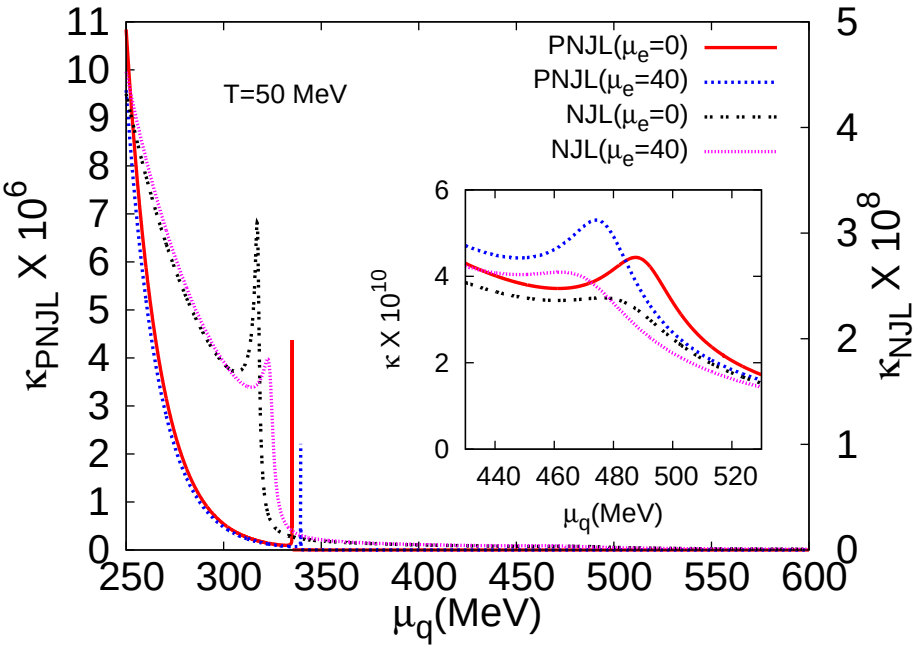

(a)

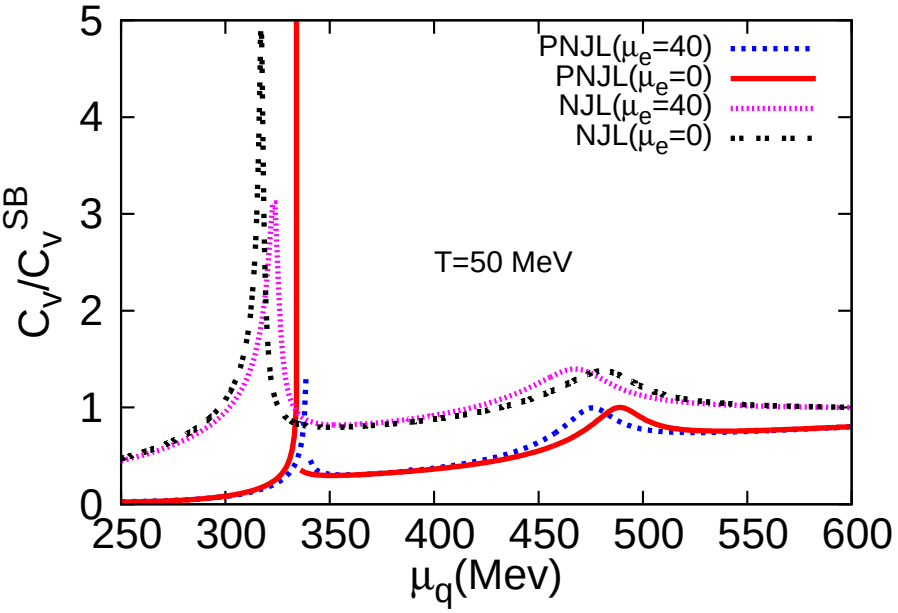

(b)

Figure 2.5: (a) Variation of compressibility κ with μ_q. The peak around $\mu_q = 500$ MeV is shown in the inset where κ represents the compressibility in both NJL and PNJL models. (b) Variation of specific heat scaled by its Stefan Boltzmann value.

haves accordingly. While κ in the NJL model is found to be higher than that of the PNJL model in the hadronic phase, it is just the opposite in the partonic

phase as shown in Fig. 2.5(a). In the NS scenario this would mean that the core of the star would be much softer compared to the crust if described by the PNJL model rather than the NJL model.

The variation of the specific heat $C_V = T\left(\frac{\partial s}{\partial T}\right)_V$, where $s = \left(\frac{\partial P}{\partial T}\right)$ is the entropy density of the system, is shown in Fig. 2.5(b). For a crossover (here in NJL model) the specific heat shows a peak. For a first order transition (here in the PNJL model) the C_V is discontinuous. Also we see that the specific heat in the PNJL model is lower than that in the NJL model for a general variation of μ_q and μ_e. A system described by the PNJL model is thus less susceptible to changing temperature than that described by the NJL model.

The variation of compressibility and specific heat shown here also captures the signature of a phase transition in the PNJL model and a crossover in the NJL model. Both compressibility as well as specific heat are second derivatives of Ω and represent respectively the quark number fluctuations and energy fluctuations [44]. Discontinuity in compressibility as well as specific heat indicates a first order phase transition for the PNJL model. At $\mu_q \sim 500$ MeV, both the models exhibit a small peak due to the onset of melting of the strange quark condensate.

2.3.4 Quark Number Densities and Charge Neutral Contours

We now consider the net charge density given by $n_Q = \frac{2}{3}n_u - \frac{1}{3}n_d - \frac{1}{3}n_s - n_e$, where the number density of individual quarks and electrons are obtained from the relations, $n_u = \frac{\partial\Omega}{\partial\mu_u}$, $n_d = \frac{\partial\Omega}{\partial\mu_d}$, $n_s = \frac{\partial\Omega}{\partial\mu_s}$, and $n_e = \frac{\partial\Omega_e}{\partial\mu_e}$. For $\mu_e = 0$, $n_e = 0$ and $\mu_u = \mu_d = \mu_S$. Since masses of light flavors (u and d) are equal,we have n_u = n_d in the whole chemical potential range. However, n_s is very small at low μ_q because of the large mass of strange quarks. At large μ_q, the number density n_s of strange quarks become almost equal to the light quark number densities as the constituent masses of strange quarks are reduced significantly. So the net charge density n_Q will be close to zero and the system will become charge neutral asymptotically as shown in Fig. 2.6(a). At small μ_q, $n_Q << 1$ as the individual number densities themselves are exceedingly small. In fact this feature continues till the transition region where the light constituent quark masses drop sharply giving rise to non-zero number densities. Therefore n_Q shows a non-monotonic behavior, rising from almost zero it reaches a maxima at certain μ_q determined mainly by the melting of the strange quark condensate and thereafter decreases steadily towards zero.

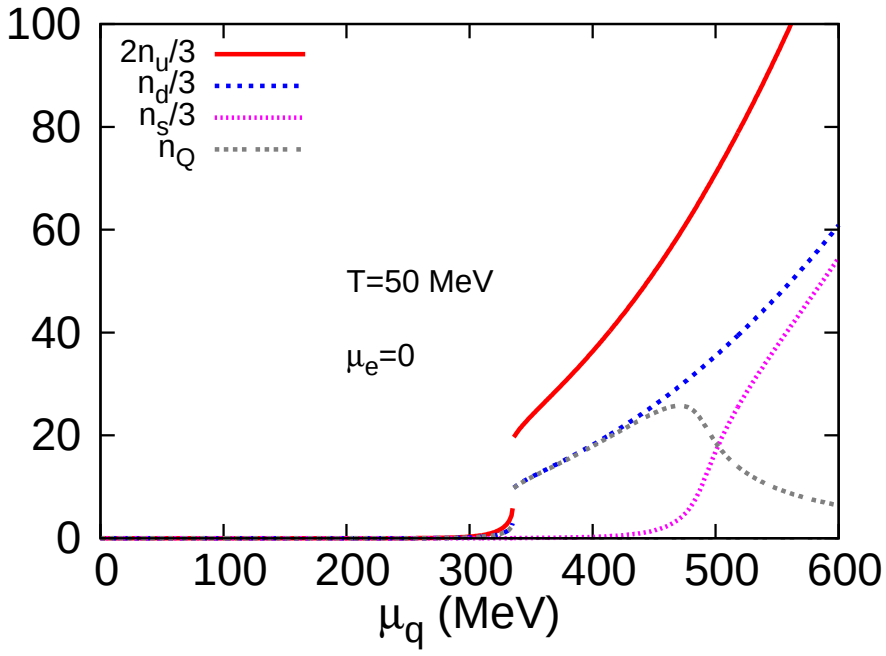

(a)

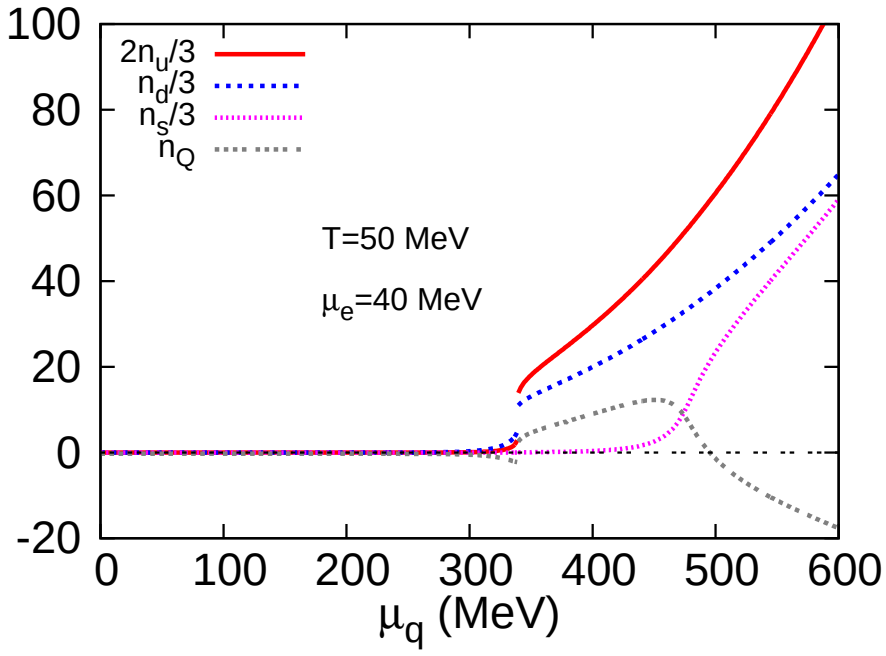

(b)

Figure 2.6: Total charge and quark number densities scaled by T^3 as a function of quark chemical potential in the PNJL model

For non-zero μ_e, even at non-zero moderate values of μ_q one can expect charge neutral configuration. In the present study we have taken a constant

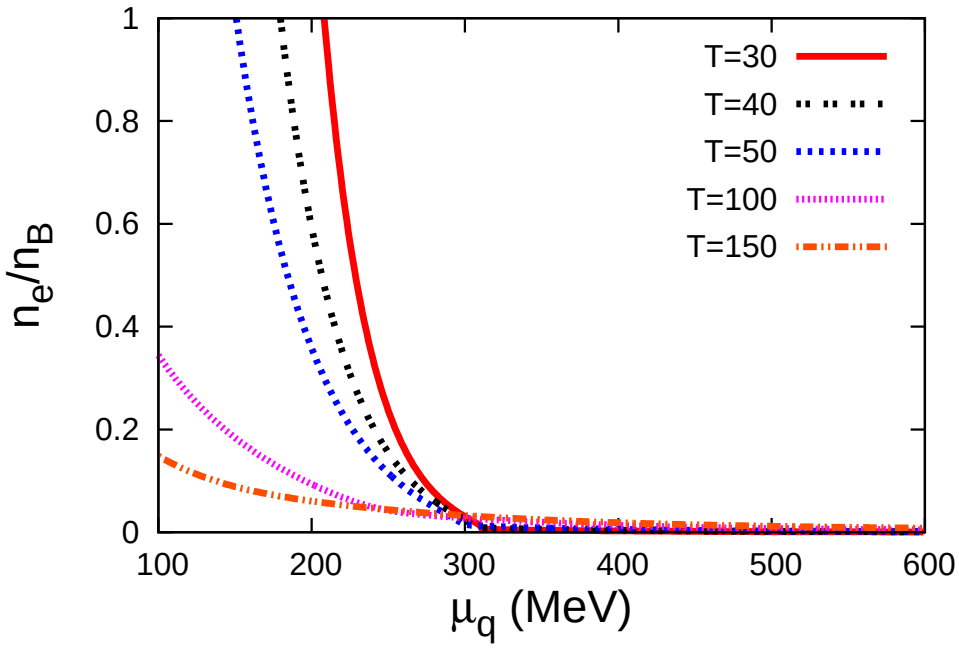

(a)

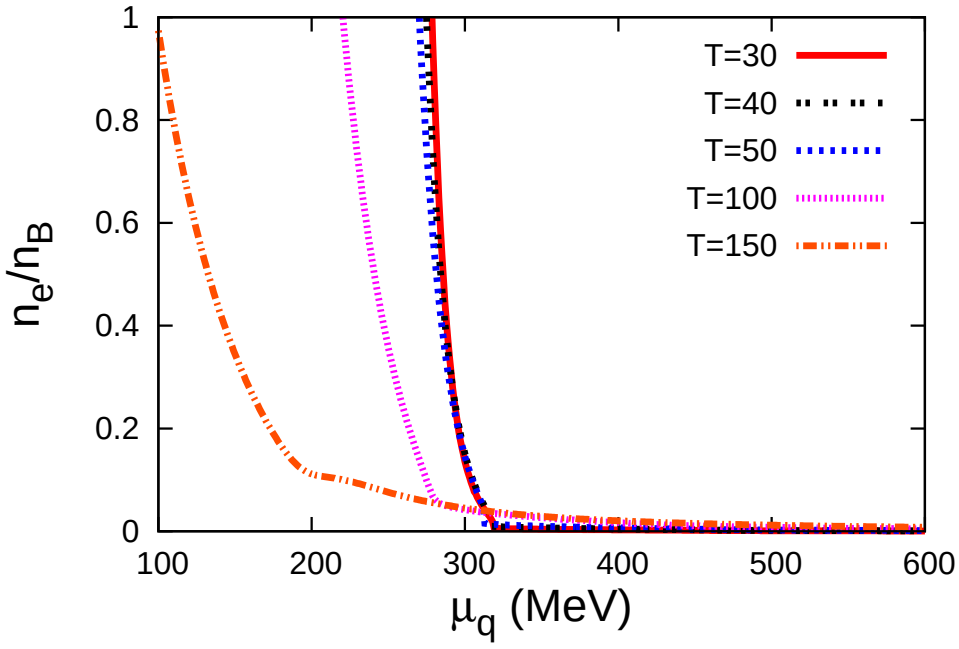

(b)

Figure 2.7: Electron fraction at $\mu_e = 40$ MeV for (a) NJL and (b)PNJL model

value of the electron chemical potential so at a particular temperature the electron number density is fixed and it is negligible compared to the quark number densities at high μ_q. For small μ_q, it is the n_e which dominates and

keeps n_Q negative. As soon as n_u becomes large with increasing μ_q, n_Q goes through zero and becomes positive. Now since μ_s and μ_d are greater than μ_u due to $\beta-$equilibrium, both n_s and n_d start to grow faster with the increase of μ_q. Finally at some μ_q the net charge becomes zero due to the mutual cancellation of n_u, n_d, and n_s, and thereafter it remains negative for higher μ_q as d and s quarks overwhelms the positively charged u quark. So the quarks alone are responsible for the occurance of charge neutrality at high μ_q. The electron fraction ($\frac{n_e}{n_B}$) basically diminishes to zero as one goes to higher chemical potential as shown in Fig.2.7.

The behavior of n_Q is similar for both PNJL and NJL model though the actual values of the various chemical potentials for the charge neutrality conditions vary.

Given that one may be interested in the charge neutral condition *e.g.* in the case of neutron stars, in Fig. 2.8 the charge neutral trajectories for NJL model are compared with those of PNJL model along with the phase diagrams. The trajectories are quite interesting in that they are closed ones pinned on to the μ_q axis. They start off close to $\mu_q = M_{vac}$, the constituent quark mass in the model in vacuum. They make an excursion in the $T - \mu_q$ plane and join back at a higher μ_q. There is a maximum temperature T_Q up to which the trajectory goes. Beyond this temperature no charge neutrality is possible. Below this temperature we have essentially two values of μ_q where charge neutrality occurs. There are significant differences between the contours of NJL and PNJL model in the hadronic phase. However beyond the transition and inside the deconfined region, the differences subside as the Polyakov loop relaxes the confining effect leading to the PNJL model behaving in a similar way to that of the NJL model.

The behavior of the charge neutral contour is highly dependent on μ_e. With increasing μ_e the contour gradually closes in towards the transition line. For a given T there are two μ_q values where charge neutrality is obtained – one on the hadronic side and one on the partonic side. As a result of the closing in of the contour, these two values come closer to the transition line from opposite sides with increasing μ_e. Higher the μ_e closer we are to the transition region. Now suppose we are looking for an isothermal evolution of a system, or the isothermal configuration of a system such as the NS. Given the constraint of charge neutrality we would have a varying μ_e as the density profile changes. Similarly if μ_e is held constant then charge neutrality would not allow the temperature to remain fixed throughout and the evolution would take place

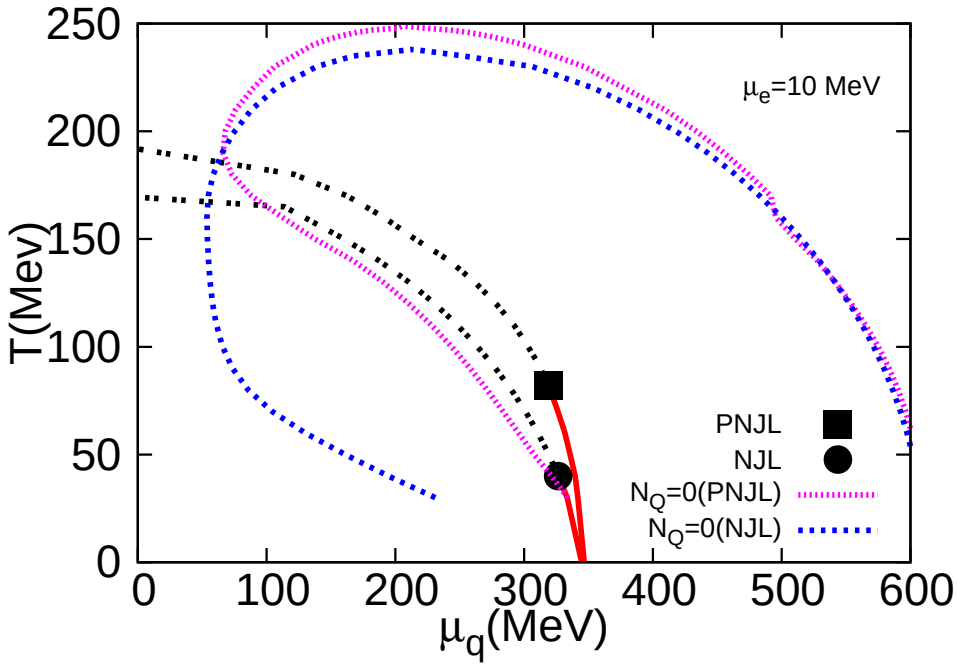

(a)

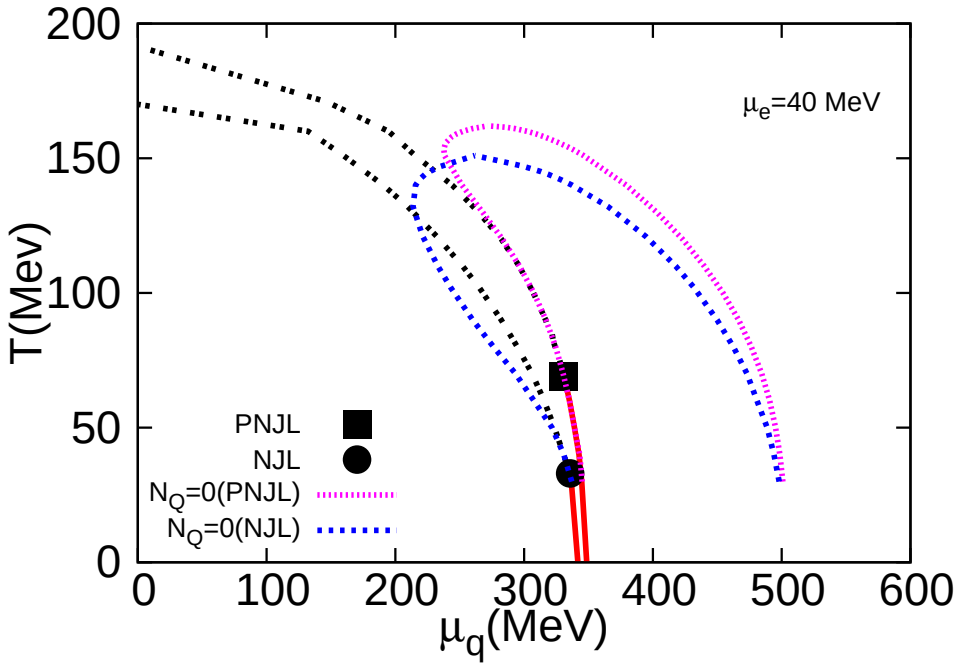

(b)

Figure 2.8: Comparison of charge neutral trajectory in NJL and PNJL model at (a) μ_e=10 ; (b) μ_e=40

along the contours described above. So in general a combination of T and μ_e is expected to maintain charge neutrality in a given system. A practical

picture of NS which has a profile of low density crust to gradual increase in density to have a highly condensed core would be that there is a complex profile for temperature and μ_e inside the NS. In fact if there exist a hadron-parton boundary, it may be either with high temperature or high electron density.

2.3.5 Constant Baryon Number Density ($\frac{n_B}{n_0}$) Contours

To contemplate this scenario in the light of the baryon densities achieved we plot the contours for constant baryon densities, scaled by the normal nuclear matter density ($n_0 = 0.15fm^{-3}$) in Fig. 2.9 for μ_e =40 MeV. The charge neutral trajectories are also plotted along with the phase boundary. Obviously with increasing baryon (quark) chemical potential baryon density would increase. What is interesting is the fact that high densities can also occur for lower chemical potential if the temperature is higher. For both NJL and PNJL model at and above 3 times nuclear matter density the matter seems to be always in the partonic phase. A little below this density matter may be in partonic phase if it is at high temperature otherwise in the hadronic phase at low temperature. Thus the actual trajectory on the phase diagram would determine whether a hadron-parton boundary in the NS is in the mixed phase or in a state of crossover. Within the range of the charge neutral contour we find the baryon density increasing from a very small value to almost 10 times the normal nuclear matter density. If μ_e is increased further the baryon densities would also be much higher for a given μ_q. So if we assume local charge neutrality as well as isothermal profile along a hadron-parton phase boundary, the baryon density close to the phase boundary may be too large. On the other hand for reasonable densities close to the phase boundary it would be impossible to maintain local charge neutrality along an isothermal curve. In that case it may be possible that the charge neutrality condition takes the system around the CEP to hold on to a reasonable density in the phase boundary region. This leads us to speculate that the transition in a NS itself may also be a cross-over, quite unlike the picture in most of the studies of NS.

2.3.6 Contour of Net Strangeness Fraction ($\frac{n_s}{n_B}$)

The net strangeness fraction (n_s/n_B) along with n_B/n_0 is shown in Fig. 2.10. For a given temperature, there is a critical μ_q below which there is no net

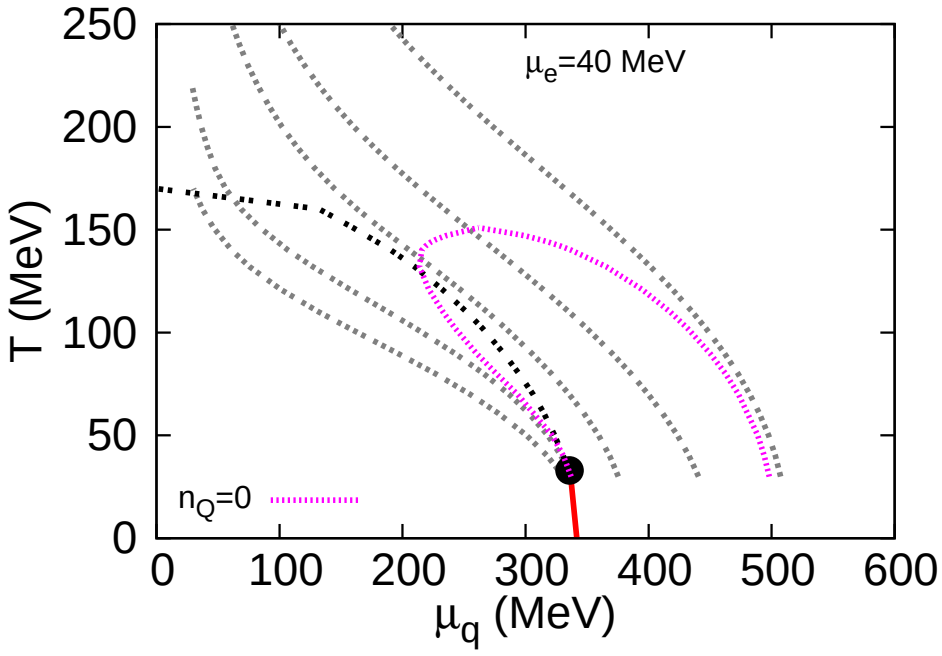

(a)

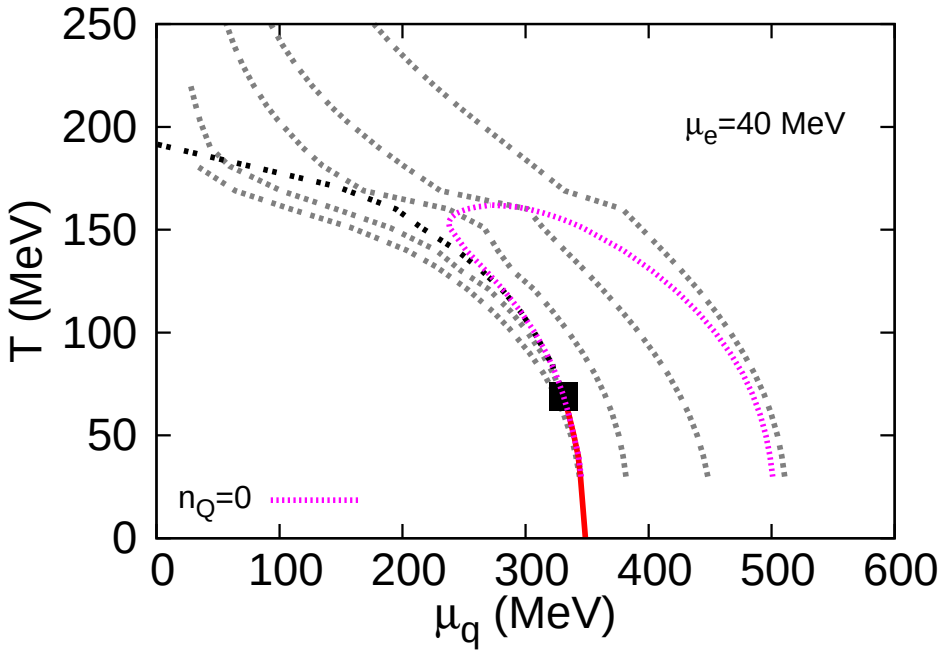

(b)

Figure 2.9: The contour of scaled baryon number density n_B/n_0; (scaled by normal nuclear matter density) along with phase diagram at μ_e=40 for (a) NJL model and (b) for PNJL model; (From left $n_B/n_0 = 0.5,\ 1,\ 3,\ 5,\ 10$ respectively)

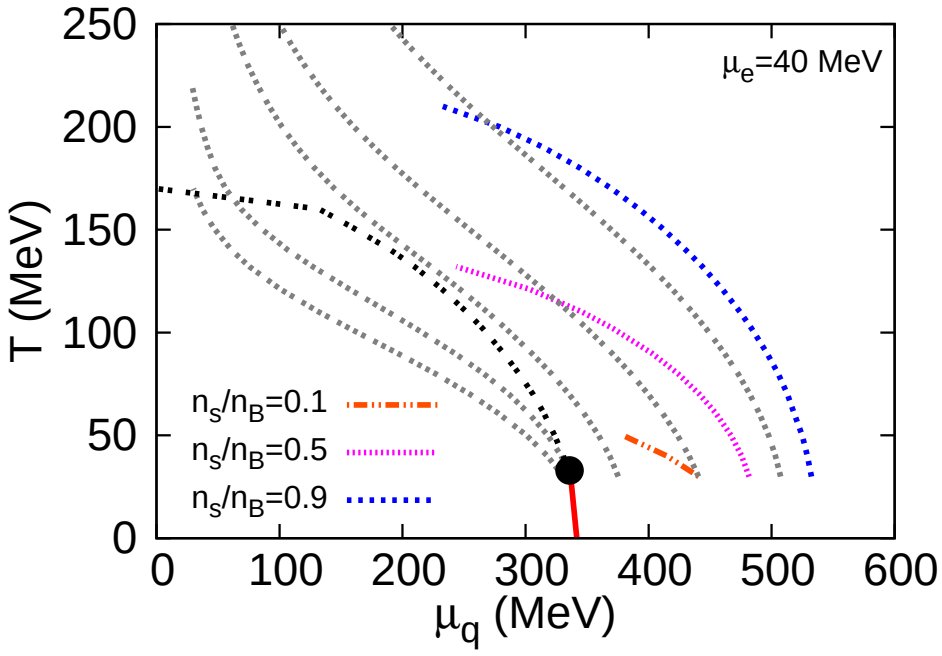

(a)

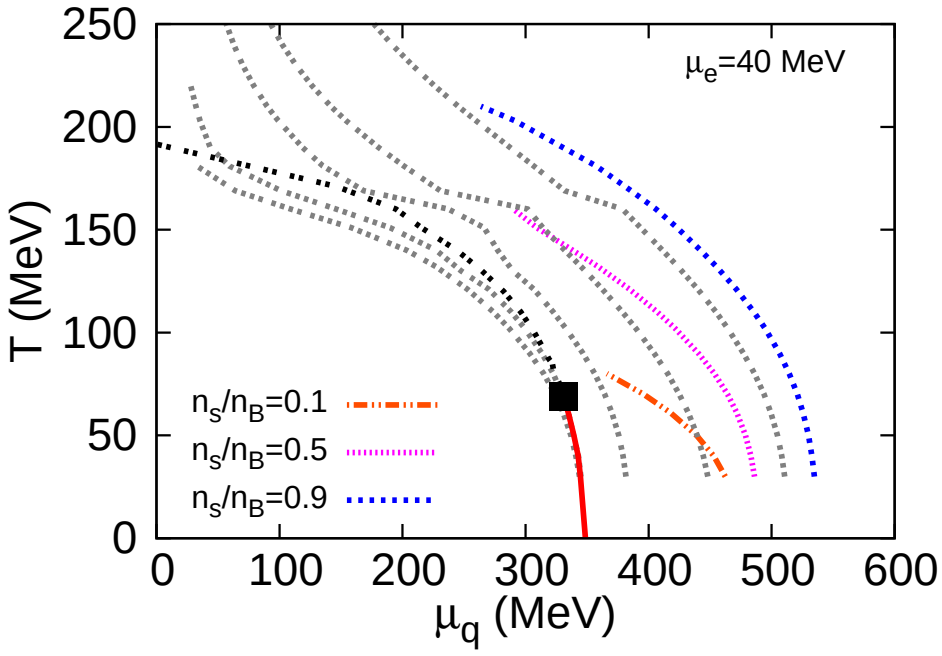

(b)

Figure 2.10: The contour of net strangeness fraction (n_s/n_B) along with n_B/n_0 at μ_e=40 for (a) NJL model and (b) PNJL model; the values of n_B/n_0 are 0.5, 1, 3, 5 and 10 (from left).

strangeness formation. At the critical μ_q a non-zero n_s/n_B occurs depend-

ing on the T. This strangeness fraction continues to appear at lower T for some higher μ_q. So a given strangeness fraction can occur only upto a certain critical temperature. The intersection of lines of constant baryon density and strangeness fraction indicates the possibility of evolution of a system to higher (lower) strangeness fraction with increase (decrease) of T at a constant density. In the range of 5 - 10 times nuclear matter density we see that the strangeness fraction is increasing significantly towards unity indicating a possibility of formation of quark matter with almost equal number of u, d and s quarks. Similar results have also been found in other model studies [8]. Chunks of matter with $n_s/n_B = 1$, called strangelets is expected to be stable (metastable up to weak decay) relative to nuclear matter in vacuum [47]. Investigation of these and various other properties of strange matter would be undertaken in future.

2.3.7 Isentropic Trajectories

Usually the hydrodynamic evolution of a system is expected to follow certain adiabat along which the entropy per baryon number (s/n_B) is a constant quantity. Among the various adiabats the system would choose one given its initial conditions. In the context of NS, a fixed entropy per baryon is expected in a proto-neutron star as well which is very different from a cold neutron star. It is usually hot and rich in leptons *i.e.* electrons and trapped neutrinos. Few seconds after birth, the matter in the core of a hot NS has almost constant lepton fraction (0.3 -0.4) and entropy per baryon (1 - 2, in units of Boltzmann constant) [48, 49]. The question as to whether the later evolution of the NS can be described to be one close to an adiabat is a matter of debate. On the other hand the commonly used approach of an isothermal evolution looks not quite favorable according to the above discussion on charge neutrality condition.

The behavior of s/n_B in a plasma and in a hadron gas was analyzed within the framework of an extended Bag model by [50]. A case study of such adiabats was done in NJL model in [51]. It was found that unlike the prescription of adiabats meeting at the CEP given by [52], they meet close to the critical value of μ_q at $T = 0$ which is incidentally equal to the constituent quark mass M_{vac} in the model in vacuum. It was argued in [51] that as $T \to 0$, $s \to 0$ by the third law of thermodynamics. Hence in order to keep s/n_B constant, n_B should go to zero. This condition is satisfied when $\mu_q = M_{vac}$ of the theory. These authors also found similar results for the linear sigma model. In the

PNJL model the introduction of Polyakov loop produced a slight change in the configuration of the adiabats [53]. The constraint on the strangeness number to be zero also was found not to have a very significant effect [54].

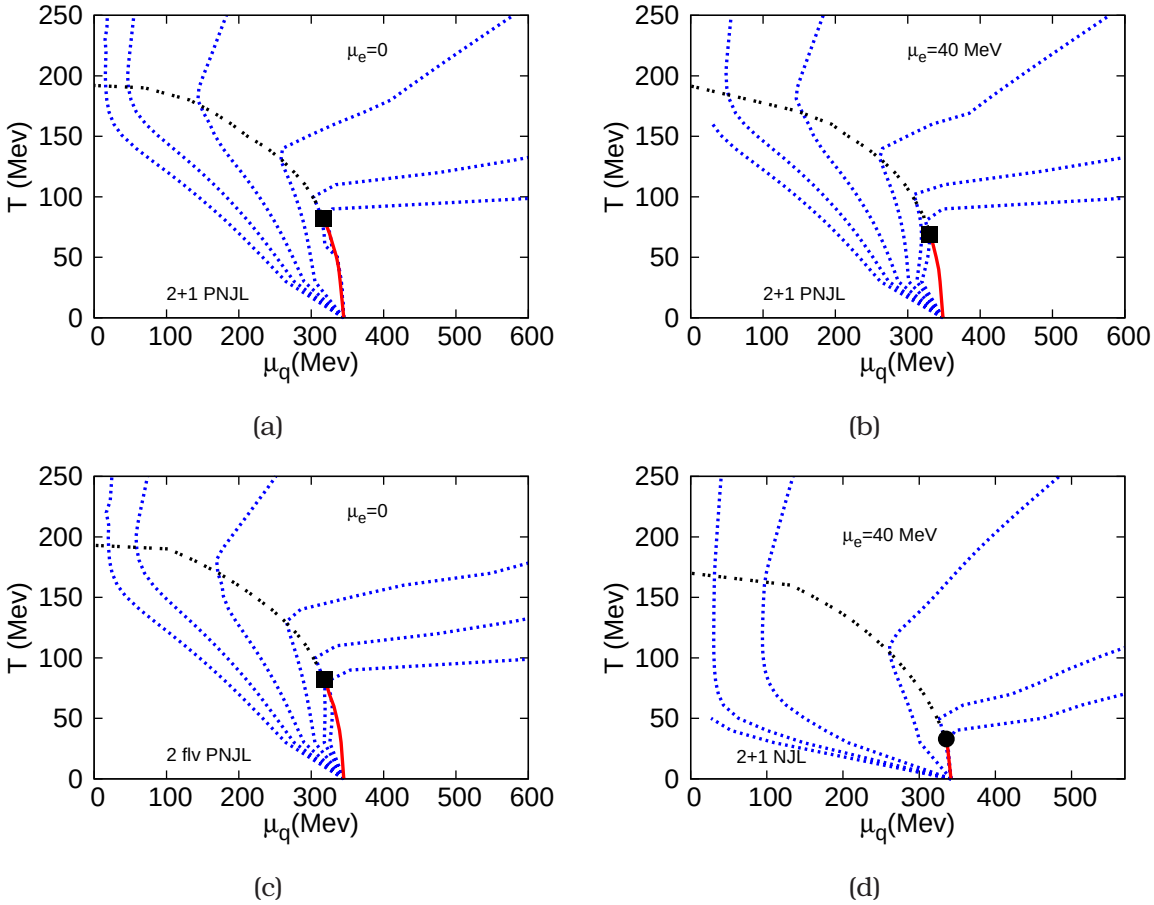

Figure 2.11: The isentropic trajectories along with phase diagram for (a) at μ_e=0, 2+1-flavor PNJL, (b) at μ_e=40, 2+1-flavor PNJL, (c) at μ_e=0, 2-flavor PNJL and (d) at μ_e=40, 2+1-flavor NJL model. s/n_B=300,100,30,10,5,3.5 (from left).

The corresponding picture of isentropic trajectories with the condition of $\beta-$equilibrium is shown in Fig. 2.11. Four cases are depicted here. Fig. 2.11(a) and Fig. 2.11(b) show the cases with 2+1 PNJL model at $\mu_e = 0$ MeV and $\mu_e = 40$ MeV respectively. From these two figures we find that the electron density does not have a significant effect on the isentropic trajectories. This means that the quark degrees of freedom seem to have dominant effect in entropy over the electrons. The case with $n_s = 0$, *i.e.* effectively for a $2-$flavor system is shown in Fig. 2.11(c). In general the situation is similar. For small μ_q there is almost no change in Fig. 2.11(c) and Fig. 2.11(a) as both the cases are identical to 2 flavors. At intermediate values strange quarks start to pop out.

Now the contours in Fig. 2.11(c) appear to be shifted and bent towards higher μ_q. This is because for 2 flavors, a given baryon number density appears at a higher μ_q than that for 2+1 flavors. Hence to get a fixed s/n_B the μ_q required is also higher. At even higher μ_q the thermal effects are negligible and hence s/n_B become almost independent of the degrees of freedom. Thus again the contours become identical.

The results in the NJL model are significantly different from that of the PNJL model as can be seen by comparing the PNJL results with that of the NJL model shown in Fig. 2.11(d). Even for low T and μ_q there is a significant entropy generation as there is no Polyakov loop to subdue the same. Similar differences continue to appear even in the partonic phase.

Considering a system that has been compressed to a few times the nuclear matter density it can try to relax back to lower densities along the adiabats. Interestingly the isentropic trajectories in the high density domain seem to behave as isothermals in the PNJL model. However as soon as the system converts into the hadronic phase, the adiabats drive it to a steep fall in temperature. We would like to mention that for a hadronic proto neutron star with beta-equilibrated nuclear matter with nucleons and leptons in the stellar core, the EOS evaluated in Bruckner−Bethe−Goldstone theory, was found to be similar for both isothermal and isentropic profiles [55].

In Ref.[56] isentropic trajectories were found in PNJL model for two different sets of parameters which were obtained by using the cutoff in the zero temperature integrals only (case I) and in all integrals (Case II). We in the present study followed the first method (case I) for regularisation and our result for PNJL model is quite similar to those studied in [56].

While the possibility that a neutron star can be described using adiabatic conditions is a point to be pondered about, we note here that an excursion of the phase diagram of a $\beta-$equilibrated matter is highly possible even in heavy-ion collisions to some extent. This is because both the isentropic lines as well as the characteristics of the phase boundary are quite similar for a wide variation of μ_e and μ_q. At the same time one should remember that in the laboratory conditions n_s is strictly zero. Anyway if a system is found to have travelled along an adiabat with $s/n_B \simeq 3$ to 4, it has most probably traversed close to the CEP. One can therefore try to correlate different observables like the enhancement of fluctuations of conserved charges and s/n_B to be in the above range to study the approach towards the CEP in heavy-ion collisions.

2.4 Summary

In this chapter we have studied the 2+1 flavor strongly interacting matter under the condition of $\beta-$equilibrium. We have presented a comparative study of NJL versus PNJL model. The phase diagrams in these two models are broadly similar, but quantitatively somewhat different. The presence of the Polyakov loop delays the transition for larger values of temperature for a given quark chemical potential. As a result the CEP in the PNJL model is almost twice as hot as that in the NJL model. We have illustrated characteristics of the phase diagram with the behavior of some thermodynamic quantities like the constituent mass, compressibility, specific heat, speed of sound and the equation of state for $\mu_e = 0$ MeV and $\mu_e = 40$ MeV at T=50 MeV. We found striking differences between the NJL and PNJL model in terms of the softness of the equation of state in the hadronic and partonic phases.

The behavior of electric charge and baryon densities in the two models also differ in the hadronic phases to some extent. The differences become less with increasing electron density. We explained how the charge neutral trajectory is important in deciding the path along which the core of NS can change from hadronic to quark phase. For all values of μ_e we find that the contours are all closed ones and give a restricted range of temperature and densities that are allowed. We speculated a possible scenario in which the quark-hadron transition in a NS would be a crossover. Again the baryon density contours seemed to suggest that if a system has baryon density three times the nuclear matter density it is quite surely in the partonic phase. We also found that the strangeness fraction increases steadily with increasing baryon density implying a possibility of having a strange NS.

The isentropic trajectories were obtained along which a system in hydrodynamic equilibrium is expected to evolve. The adiabats flow down from high temperature and low density towards low temperature and $\mu_q = M_{vac}$, the constituent quark mass in vacuum. The adiabats then steeply rise along the transition line, thereafter goes towards higher densities with almost a constant slope. For small s/n_B ratio the slope is so small that the isentropic trajectories almost become isothermal trajectories as well.

To summarize the scenario inside neutron stars we note that inside a newly born NS the temperature drops very quickly and gives rise to a system of low temperature nucleonic matter which may also be populated by hyperons and strange baryons due to high density near the core. The star is assumed to

be $\beta-$equilibrated and charge neutral. Now it is possible that due to some reason, *e.g.* sudden spin down, this nucleonic matter will start getting converted to predominantly two flavor quark matter within strong interaction time scale. This transition would start at the center and a conversion front moving outward will convert much of the central region of the star. Along the path of the conversion front, each point inside the star may lie on an isentropic trajectory. Gradually this system of predominantly 2 flavor quark matter will get converted to strange quark matter through weak interactions and finally a $\beta-$equilibrated charge neutral strange quark matter will be produced. The strangeness production occurs mainly through non-leptonic decay [33], the system is expected to lie on a constant density line and move towards the point with highest strangeness possible at that density. Finally the semi-leptonic processes will take over and system will then evolve along a $\beta-$equilibrated charge neutral contour.

The natural extension of the work is to obtain the detailed evolution of a family of neutron stars starting with different initial conditions and gravity effects incorporated. We hope to study this in future. It would also be important to consider colored exotic states like diquarks [57] that may arise at high densities.

Bibliography

[1] Berndt Müller, The Physics of Quark Gluon Plasma, Lecture Notes in Physics (Springer Publication) **225**, 1 (1985)

[2] K. Rajagopal and F. Wilczek, At the frontier of particle physics / Handbook of QCD (World Scientific), **3**, 2061 (2001) (arXiv: hep-ph/**0011333**)

[3] D. Blaschke, J. Berdermann, R. Lastowiecki, Prog. Theor. Phys. Suppl. **186**, 81 (2010)

[4] N. K. Glendenning, J. Phys. G**23**, 2013 (1997)

[5] J. Schaffner-Bielich, PoS (CPOD07), 062 (2007) (arXiv:0709.1043)

[6] G. F. Burgio, M. Baldo, P. K. Sahu, A. B. Santra and H.-J.Schulze, Phys. Lett. B**526**, 19 (2002); G. F. Burgio, M. Baldo, P. K. Sahu, and H.-J. Schulze, Phys. Rev. C **66**, 025802 (2002)

[7] M. Alford, M. Brady, M. Paris and S. Reddy, Astrophys. J. **629** 969 (2005)

[8] S. K. Ghosh and P. K. Sahu, Int. J. Mod. Phys. E **2** 575 (1993)

[9] S. K. Ghosh, S. C. Phatak and P. K. Sahu, Z. Phys. A **352** 457 (1995)

[10] M. Buballa, Phys. Rept. **407**, 205 (2005)

[11] M. Baldo, M. Buballa, G. F. Burgio, F. Neumann, M. Oertel and H.-J. Schulze, Phys. Lett. B **562**, 153 (2003) and references therein.

[12] K. Schertler, S. Leupold and J. Schaffner-Bielich, Phys. Rev. C **60**, 025801 (1999)

[13] M. Baldo, G. F. Burgio, P. Castorina, S. Plumari, D. Zappala, Phys. Rev. C **75**, 035804 (2007)

[14] C. Ratti, M. A. Thaler and W. Weise, Phys. Rev. D **73**, 014019 (2006)

[15] S. K. Ghosh, T. K. Mukherjee, M. G. Mustafa and R. Ray, Phys. Rev. D **73**, 114007 (2006)

[16] S. Mukherjee, M. G. Mustafa and R. Ray, Phys. Rev. D **75**, 094015 (2007); S. K. Ghosh, T. K. Mukherjee, M. G. Mustafa and R. Ray, Phys. Rev. D **77**, 094024 (2008)

[17] A. Bhattacharyya, P. Deb, S. K. Ghosh and R. Ray, Phys. Rev. D **82**, 014021 (2010)

[18] A. Bhattacharyya, P. Deb, A. Lahiri and R. Ray, Phys. Rev. D **82**, 114028 (2010); *ibid* D **83**, 014011 (2011)

[19] S. B. Ruster, V. Werth, M. Buballa, I. A. Shovkovy and D. H. Rischke, Phys. Rev. D **72**, 034004 (2005)

[20] M. Hanauske, L. M. Satarov, I. N. Mishustin and H. Stöcker, and W. Greiner, Phys. Rev. D **64**, 043005 (2001)

[21] P. Costa, M. C. Ruivo, Yu. L. Kalinovsky and C. A. de Sousa, Phys. Rev. C **70**, 025204 (2004)

[22] P. Costa, M. C. Ruivo and Yu. L. Kalinovsky, Phys. Lett. B **560**, 171 (2003)

[23] J. A. Pons, J. A. Miralles, M. Prakash and J. M. Lattimer, Astrophys. J. **553**, 382 (2001)

[24] D. G. Yakovlev and C. J. Pethick, Ann. Rev. Astron. Astrophys. **42**, 169 (2004)

[25] D. G. Yakovlev, O. Y. Gnedin, M. E. Gusakov, A. D. Kaminker, K. P. Levenfish and A. Y. Potekhin, Nucl. Phys. A **752**, 590 (2005)

[26] J. M. Lattimer and M. Prakash, Astrophys. J. **550**, 426 (2001)

[27] A. Bhattacharyya, I. N. Mishustin and W. Greiner, J. Phys. G **37**, 025201 (2010)

[28] I. N. Mishustin, M. Hanauske, A. Bhattacharyya, L. M. Satarov, H. Stoecker and W. Greiner, Phys. Lett. B **552**, 1 (2003)

[29] E. Witten, Phys. Rev. D **30**, 272 (1984)

[30] A. Bhattacharyya, S. K. Ghosh, P. Joarder, R. Mallick and S. Raha Phys. Rev. C **74**, 06580 (2006)

[31] C. Alcock, E. Farhi and A. Olinto, Astrophys. J. **310**, 261 (1986)

[32] N. K. Glendenning, S. Pei and F. Weber, Phys. Rev. Lett. **79**, 1603 (1997)

[33] S.K. Ghosh, S.C. Phatak and P.K. Sahu, Nucl. Phys. A **596**, 670 (1996)

[34] Y. Nambu and G. Jona-Lasinio, Phys. Rev. **122**, 345 (1961); Phys. Rev. **124**, 246 (1961)

[35] T. Hatsuda, T. Kunihiro, Phys. Lett. B **145**, 7 (1984)

[36] P. N. Meisinger and M. C. Ogilvie, Phys. Lett. B **379**, 163 (1996); Nucl. Phys. B (Proc. Suppl.) **47**, 519 (1996)

[37] P. N. Meisinger, T. R. Miller and M. C. Ogilvie, Phys. Rev. **65**, 034009 (2002);

[38] P. N. Meisinger, M. C. Ogilvie and T. R. Miller, Phys. Lett. B **585**, 149 (2004);

[39] K. Fukushima, Phys. Lett. B **591** 277 (2004)

[40] R. D. Pisarski, Phys. Rev. D **62** 111501 (2000); "Marseille 2000, Strong and electroweak matter"pg. 107-117 (hep-ph/0101168)

[41] E. Megias, E. Ruiz Arriola, L.L. Salcedo, Phys. Rev. D **69**, 116003 (2004)

[42] S. Digal, E. Laermann, H. Satz, Eur. Phys. C **18**, 583 (2001)

[43] G. Y. Shao *et. al*, Phys. Rev. D **83**, 094033 (2011); *ibid* D **84**, 034028 (2011)

[44] M. Iwasaki, Phys. Rev. D **70**, 114031 (2004).

[45] S. V. Molodtsov and Z. M. Zinovjev, Europhys. Lett. **93**, 11001 (2011).

[46] N. K. Glendenning, Phys. Rev. D **46**, 1274 (1992).

[47] E. Farhi and R. L. Jaffe, Phys. Rev. D **30**, 2379 (1984).

[48] A. Burrows and J. M. Lattimer, Astrophys. J. **307**, 178 (1986).

[49] D. Gondek, P. Haensel and J. L. Zdunik, ASP conference series **138**, 131 (1998).

[50] A. Leonidov, K. Redlich, H. Satz, E. Suhonen and G. Weber, Phys. Rev. D **50**, 4657, (1994).

[51] O. Scavenius, A. Mocsy, I.N. Mishustin and D.H. Rishke, Phys. Rev. C **64**, 045202 (2001).

[52] M. Stephanov, K. Rajagopal, E. Shuryak, Phys. Rev. Lett. **81**, 4816 (1998).

[53] T. Kahara and K. Tuominen, Phys. Rev. D **78**, 034015 (2008).

[54] K. Fukushima, Phys. Rev. D **79**, 074015 (2009).

[55] G.F. Burgio and H.-J. Schulze, Phys. Atom. Nucl. **72** 1197 (2009).

[56] P. Costa, H. Hansen, M. C. Ruivo, and C. A. de Sousa, Phys. Rev. D **81**, 016007 (2010).

[57] N. Bentz, T. Horikawa, N. Ishii, A.W. Thomas, Nucl. Phys. A **720**, 95 (2003); S. Roessner, C. Ratti and W. Weise, Phys. Rev. D **75** 034007 (2007).

CHAPTER 3

1+1 Flavor Quark Matter With Explicit Isospin Symmetry Breaking

3.1 Introduction

In the previous chapter we have discussed the various properties of strongly interacting quark matter at high density region. The study has been done by considering 2+1 flavor quark matter and the masses of u and d quarks were same. Introducing the beta equilibrium condition i.e. $\mu_d = \mu_u + \mu_e$, among the different flavor chemical potentials, we have found that u-d flavor asymmetry arises at non zero electron chemical potential μ_e. Flavor asymmetry can also be generated if the masses of u-d flavor are taken to be different.

In the present chapter we will analyze the properties of two flavor quark matter by considering the flavor asymmetry where the asymmetry comes solely through the assumption of different mass of u and d quarks. Signatures of phases of matter with deconfined color charges is under critical investigation for last few decades, both theoretically and experimentally. Quantum Chromodynamics (QCD), the first principle of strongly interacting matter, has a number of global symmetries associated with it, apart from the local color symmetry. As discussed earlier, for a two flavor system, in the limit of zero quark masses, the QCD Lagrangian obeys the symmetry $SU_L(2) \otimes SU_R(2)$, which can be recast into the form of vector and axial vector symmetry $SU_V(2) \otimes SU_A(2)$. When quarks acquire non-zero masses, the axial symmetry $SU_A(2)$ is explicitly

broken. The QCD Lagrangian is then symmetric under $SU_V(2)$, the isospin symmetry which is a good approximation in nature. Isospin symmetry $SU_V(2)$ is explicitly broken for non-zero mass difference of u and d quarks. At low energies the isospin symmetry breaking (ISB) has relevance in many aspects of hadronic observables [1]. There are some recent work where the isospin-breaking effects play a prominent role. In the invariant mass distribution for $k \to 3\pi$ a pronounced wigner cusp was observed and it was proposed that the cusp was due to the mass difference of charged and neutral pion [2] implying the mass difference of u and d quarks. Apart from the quark mass difference ISB effects may be brought in by electromagnetic contributions as well. Low energy $\pi - \mathrm{K}$ scattering has been studied considering the inclusion of electromagnetic correction into the effective Lagrangian [3]. The isospin symmetry at parton level indicates that $u(d, \bar{u}, \bar{d})$ quark distribution in the proton is equal to the $d(u, \bar{d}, \bar{u})$ quark distribution in the neutron. The flavor asymmetry in the nucleon sea and isospin symmetry breaking between the proton and the neutron can lead to the violation of the Gottfried sum rule reported by the New Muon Collaboration[4].

ISB of valence and sea quark distributions in protons and neutrons has been studied in the chiral quark model [5, 6]. ISB may also have significant effect in the context of existence of CP violating phase [7]. First Lattice QCD (LQCD) investigation of the effect of unequal quark masses was done in Ref. [8] and recently a study has shown the effect of ISB on different hadronic observables like Kaon masses, Kaon decay constant, neutron-proton mass splitting *etc* [9, 10]. Within the framework of chiral perturbation theory the isospin breaking effect in quark condensates has been studied considering $m_u \neq m_d$ and electromagnetic corrections as well, where the authors have given an analysis of quark condensate and scalar susceptibilities [11, 12]. It has been shown that the order parameter for chiral symmetry restoration i.e. $\sigma_u + \sigma_d$ receives a very small changes due to isospin breaking effect. In the context of high energy heavy ion collisions where strongly interacting matter is supposed to exist in a state of thermal and chemical equilibrium, the ISB effects have not been explored much. Fluctuations and correlations of conserved charges are important and sensitive probes for heavy ion physics. Most of the theoretical studies in this respect are in isospin symmetric limit [13, 14, 15, 16, 17, 18, 19, 20, 21, 22, 23, 24, 25, 26, 27]. Now, in experiment the situation is not exactly isospin symmetric, as predicted by Particle Data Group. Whether this asymmetry puts some imprints on the observables or

not, is a matter of crucial investigation, which serves as the motivation for our current study. In this chapter we are going to present first case study of ISB effect on fluctuations and correlations of strongly interacting matter within the framework of the Polyakov loop enhanced Nambu–Jona–Lasinio (PNJL) model.

3.2 Formalism

The PNJL model Lagrangian for two flavors can be written as [28, 29, 30]:

$$\mathcal{L} = \mathcal{L}_0 + \mathcal{L}_1 + \mathcal{L}_2 - \mathcal{U}(\Phi[A], \bar{\Phi}[A], T) \tag{3.1}$$

where,

$$\begin{aligned}
\mathcal{L}_0 &= \bar{\psi}(i\not{D} - \hat{m})\psi \quad , & \text{(3.2a)}\\
\mathcal{L}_1 &= G_1[(\bar{\psi}\psi)^2 + (\bar{\psi}\vec{\tau}\psi)^2 + (\bar{\psi}i\gamma_5\psi)^2 + (\bar{\psi}i\gamma_5\vec{\tau}\psi)^2] \quad , & \text{(3.2b)}\\
\mathcal{L}_2 &= G_2[(\bar{\psi}\psi)^2 - (\bar{\psi}\vec{\tau}\psi)^2 - (\bar{\psi}i\gamma_5\psi)^2 + (\bar{\psi}i\gamma_5\vec{\tau}\psi)^2] \quad . & \text{(3.2c)}
\end{aligned}$$

with $\psi = (u, d)^T$ and $D^\mu = \partial^\mu - ig\mathcal{A}^\mu_a(x)\lambda_a/2$. $\mathcal{A}^\mu_a(x)$ are $SU(3)$ gauge fields and λ_a are Gell-Mann matrices. $\mathcal{L}_2$ represents the t'Hooft determinant term and breaks $U_A(1)$ axial symmetry [31, 32, 33, 34]. The effective Polyakov loop potential is given by;

$$\begin{aligned}
\frac{\mathcal{U}(\Phi, \bar{\Phi}, T)}{T^4} &= -\frac{b_2(T)}{2}\Phi\bar{\Phi} - \frac{b_3}{6}(\Phi^3 + \bar{\Phi}^3) + \frac{b_4}{4}(\bar{\Phi}\Phi)^2, \qquad \text{(3.3)}\\
b_2(T) &= a_0 + a_1(\frac{T_0}{T}) + a_2(\frac{T_0}{T})^2 + a_3(\frac{T_0}{T})^3.
\end{aligned}$$

Φ is Polyakov loop and $\bar{\Phi}$ is its complex conjugate [30]. Values of coefficients $a_0, a_1, a_2, a_3, b_3, b_4$ have been taken from Ref. [35]. For studying isospin asymmetric situation, here we have taken the mass matrix in the PNJL Lagrangian, Eq.3.2, as

$$\begin{aligned}
\hat{m} &\equiv m_1 \mathbb{1}_{2\times2} - m_2\tau_3 \\
&= \begin{pmatrix} m_1 - m_2 & 0 \\ 0 & m_1 + m_2 \end{pmatrix} = \begin{pmatrix} m_u & 0 \\ 0 & m_d \end{pmatrix}.
\end{aligned}$$

where, $\mathbb{1}_{2\times2}$ is the identity matrix in flavor space and τ_3 is the third Pauli matrix. This is in sharp contrast with our previous works [30, 36], where we

took $m_2 = 0$. When $m_u \neq m_d$, it can be shown that the $m_2\tau_3$ term explicitly breaks the isospin symmetry $SU_V(2)$. The thermodynamic potential can be written as:

$$\begin{aligned}\Omega(T,\mu_u,\mu_d) &= \mathcal{U}'\left(\Phi[A],\bar{\Phi}[A],T\right) + + \sum_{f=u,d}\Omega_0(T,\mu_f;m_f) \\ &\quad +2G_1\left(\sigma_u^2+\sigma_d^2\right)+4G_2\sigma_u\sigma_d \end{aligned} \tag{3.4}$$

where the fermionic part of the thermodynamic potential is given by;

$$\begin{aligned}\Omega_0(T,\mu_f;m_f) &= -2N_c\int\frac{d^3p}{(2\pi)^3}E_f\theta(\Lambda^2-\vec{p}^{\,2}) \\ &\quad -2T\int\frac{d^3p}{(2\pi)^3}\ln\left[1+3\Phi e^{-(E_f-\mu_f)/T}+3\bar{\Phi}e^{-2(E_f-\mu_f)/T}+e^{-3(E_f-\mu_f)/T}\right] \\ &\quad -2T\int\frac{d^3p}{(2\pi)^3}\ln\left[1+3\bar{\Phi}e^{-(E_f+\mu_f)/T}+3\Phi e^{-2(E_f+\mu_f)/T}+e^{-3(E_f+\mu_f)/T}\right]\end{aligned}$$

where, the energy E_f and constituent quark mass M_f are given by,

$$E_f = \sqrt{M_f^2+p^2}\ , \tag{3.5}$$

$$M_f = m_f - 4G_1\sigma_f - 4G_2\sigma_{f'}, \tag{3.6}$$

where, $f, f' \in u, d$ and $f \neq f'$. Flavor chemical potentials are given by,

$$\mu_u = \frac{\mu_B}{3}+\frac{\mu_I}{2} \quad \text{and} \quad \mu_d = \frac{\mu_B}{3}-\frac{\mu_I}{2} \tag{3.7}$$

with μ_B and μ_I as the chemical potential corresponding to conserved baryon number (B) and third component of isospin (I_3) respectively. The Polyakov loop potential $\mathcal{U}'$ with the Vandermonde (VdM) term [36] can be expressed as;

$$\mathcal{U}'(\Phi,\bar{\Phi},T)/T^4 = \mathcal{U}(\Phi,\bar{\Phi},T)/T^4 - \kappa\ln[J(\Phi,\bar{\Phi})] \tag{3.8}$$

where the Vandermonde determinant is given by,

$$J[\Phi,\bar{\Phi}] = (27/24\pi^2)(1-6\Phi\bar{\Phi}+4(\Phi^3+\bar{\Phi}^3)-3(\Phi\bar{\Phi})^2)$$

For the present work, we restrict ourselves in the mean field approximation and consider $G_1 = G_2$. It could be easily checked that, under the second constraint, difference between the constituent masses of two flavors is equal to difference in current masses.

3.3 Results

Here we consider the average quark mass $m_1 = (m_u + m_d)/2$ fixed at 0.0055 GeV and study the effect of ISB with three representative values of $m_2 = (m_d - m_u)/2$. The parameter set in the NJL sector has been determined separately for the different values of m_2. The differences in the parameter values were found to be practically insignificant. The bulk thermodynamic properties of the system expressed through pressure, energy density, specific heat, speed of sound etc. did not show significant dependence on m_2. Even the diagonal susceptibilities were almost identical to those at the isospin symmetric limit. However, interesting differences were observed for the off-diagonal susceptibilities in the $B - I$ sector. The fluctuations and correlations of conserved charges and their higher order cumulants are important to study because they provide information about the degrees of freedom of strongly interacting matter. They also help to analyse the existence of critical behavior of the system, if any. In Lattice QCD as well as in PNJL model they are extracted by studying the diagonal and off diagonal susceptibilities, respectively.

3.3.1 Baryon-Isospin Correlators at $\mu_B = 0$

Let us first discuss the $\mu_B = 0$ case. We shall consider $\mu_I = 0$ in this work. It should be noted that even for $\mu_I = 0$, a non-zero m_2 would generate some non-zero isospin number.

In Fig.3.1 the second order off-diagonal susceptibility χ_{11}^{BI}, is plotted against T/T_c for different values of m_2. Here T_c is the crossover temperature obtained from the inflection point of the scalar order parameters - the mean values of chiral condensate and Polyakov Loop [20, 30, 36]. As expected we find $\chi_{11}^{BI} = 0$ for $m_2 = 0$. For non-zero m_2 the non-monotonic behavior observed here can be understood as follows. At low temperatures the fermionic excitations are suppressed due to their large constituent masses as well as the suppression due to the Polyakov loop. On the other hand at high temperatures the mass difference m_2 become insignificant compared to the temperature scale. Therefore only at some intermediate temperatures one can expect a non-zero χ_{11}^{BI}. The peak value appears very close to T_c. The sensitivity of χ_{11}^{BI} on m_2 is clearly visible. An exciting feature observed here is the almost linear scaling of χ_{11}^{BI} with m_2. This is shown in the inset of Fig.3.1.

At the fourth order we have the off-diagonal susceptibilities, χ_{13}^{BI}, χ_{31}^{BI} and χ_{22}^{BI}. For $\mu_B = 0$ the T dependence for the first two quantities and their linear

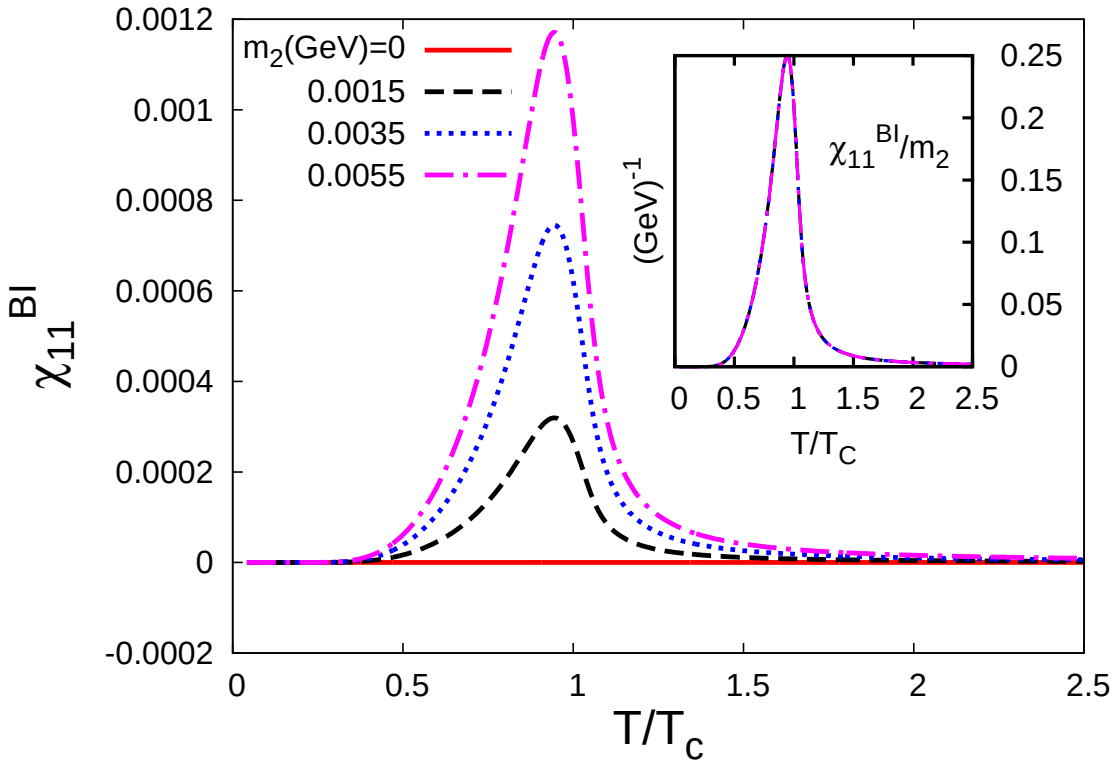

Figure 3.1: Second order off-diagonal susceptibility in $B-I$ sector at $\mu_B = 0$.

scaling with m_2 is shown in Fig.3.2. For χ^{BI}_{22} we found no such scaling behavior and the m_2 dependence was insignificant. Qualitatively one can understand the behavior of χ^{BI}_{13} and χ^{BI}_{31} by noticing that these are correlators between the fluctuations χ^I_2 of isospin and χ^B_2 baryon number respectively, with the $B-I$ correlator χ^{BI}_{11}. In our earlier studies [20, 30, 36] we found that the both the fluctuations increase monotonically with temperature. Here we found in Fig.3.1 above that with increase in T, χ^{BI}_{11} first increases and then decreases with a turning point close to T_c. Thus χ^{BI}_{11} is correlated with χ^I_2 and χ^B_2 below T_c and is anti-correlated above. Therefore one can expect that the correlations given by χ^{BI}_{13} and χ^{BI}_{31} are positive and negative respectively below and above T_c. To understand the presence of m_2 scaling for some correlators and absence in others we first note that the different $B-I$ correlators may be expressed in terms of those in the flavor space. The corresponding relation between the chemical potentials are $\mu_u = \frac{1}{3}\mu_B + \frac{1}{2}\mu_I$ and $\mu_d = \frac{1}{3}\mu_B - \frac{1}{2}\mu_I$. This implies,

$$\chi^{BI}_{11} = \frac{1}{6}(\chi^u_2 - \chi^d_2). \tag{3.9}$$

The flavor diagonal susceptibilities can be expanded in a Taylor series of the

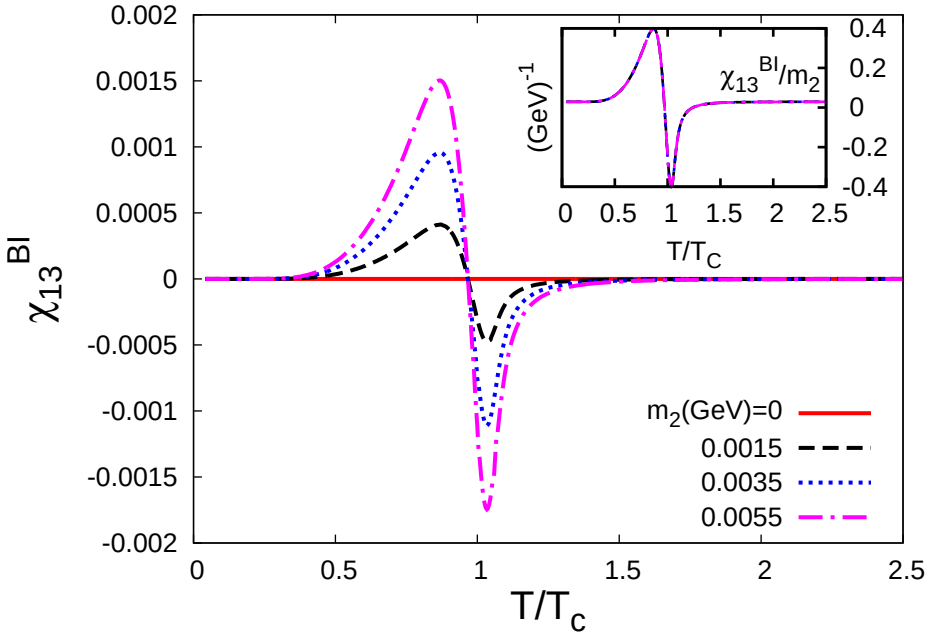

(a)

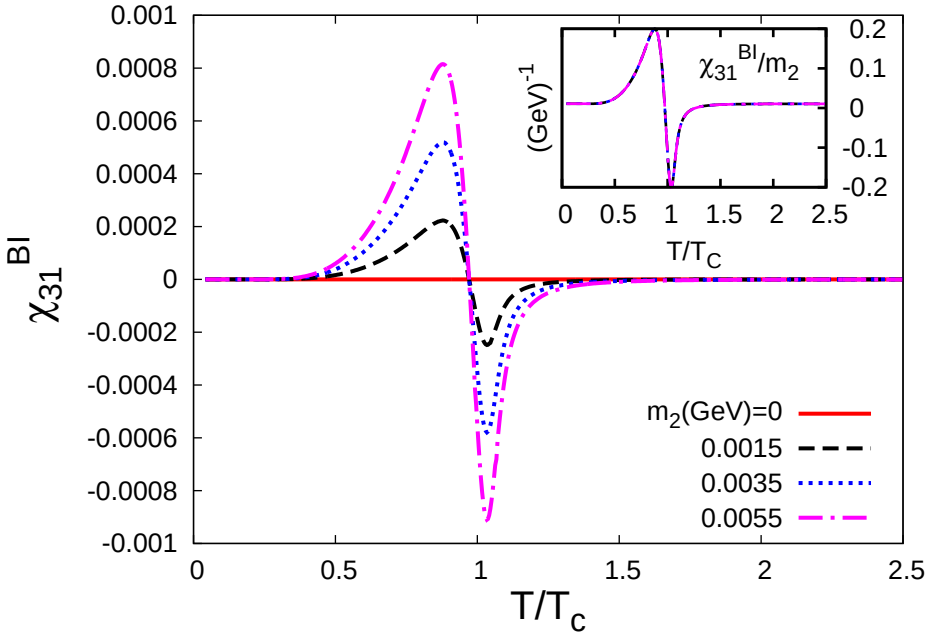

(b)

Figure 3.2: Fourth order off-diagonal susceptibilities.

quark masses around $m_u = m_d = 0$.

$$\chi_2^f(m_u, m_d) = \sum_{n=0}^{\infty} \sum_{i=0}^{n} a_{i,j}^f m_u^i m_d^j \tag{3.10}$$

where, $a^f_{i,j} = \frac{1}{i!j!}\left[\frac{\partial^n \chi^f_2}{\partial m^i_u \partial m^j_d}\right]_{m_u=m_d=0}$ are the Taylor coefficients, with $i+j=n$ and $f \in u,d$. Here $a^u_{0,0}$ and $a^d_{0,0}$ are respectively u and d flavor susceptibilities in the chiral limit; hence they are equal. Moreover, response of χ^u_2 to a change in m_u (m_d) and that of χ^d_2 to a change in m_d (m_u) are identical in the chiral limit. Thus we have $a^u_{i,j} = a^d_{j,i}$, $\forall\ i,j$. Therefore we get,

$$\begin{aligned}&\chi^u_2(n^{th}\text{order}) - \chi^d_2(n^{th}\text{order})\\ &= \sum_{i=0}^{n} \alpha_i m_u^i m_d^i (m_d^{n-2i} - m_u^{n-2i}).\end{aligned} \tag{3.11}$$

where $\alpha_i = a^u_{i,n-i} = a^d_{n-i,i}$. It is clear that for any given n and i, the R.H.S. contains a factor $(m_d - m_u)$. Therefore χ^{BI}_{11} (Eq.3.9) is proportional to m_2 if the higher order terms are sub-dominant. This is what we observed for the range of m_2 considered here. For the higher order correlators one can similarly write,

$$\chi^{BI}_{13} = \frac{1}{24}(\chi^u_4 - \chi^d_4 + 2\chi^{ud}_{13} - 2\chi^{ud}_{31}) \tag{3.12}$$

$$\chi^{BI}_{31} = \frac{1}{54}(\chi^u_4 - \chi^d_4 - 2\chi^{ud}_{13} + 2\chi^{ud}_{31}) \tag{3.13}$$

$$\chi^{BI}_{22} = \frac{1}{36}(\chi^u_4 + \chi^d_4 - 2\chi^{ud}_{22}) \tag{3.14}$$

For all these quantities the first two terms on R.H.S. were found to be dominant. Considering again the Taylor expansion in quark masses, χ^{BI}_{13} and χ^{BI}_{31} were found to be proportional to m_2. No such proportionality was found for χ^{BI}_{22}.

3.3.2 Baryon - Isospin Correlators at finite μ_B

Finally let us discuss χ^{BI}_{11} for non-zero μ_B. In Fig.3.3 we present the results for three different temperatures - one above, one below and one close to the crossover temperature T_c. For large T, μ_B effects are small and χ^{BI}_{11} while remaining positive slowly approaches zero with increasing μ_B. Close to T_c χ^{BI}_{11} changes fast with increase of μ_B and in fact changes sign and then slowly approaches zero. This effect becomes much more prominent at lower temperatures and at the first order phase transition boundary changes sign almost discontinuously. The negativity of the correlator indicates that the isospin number decreases while increasing the baryon chemical potential. This is not expected for an ideal gas of quarks even with non-zero masses. Given $m_2 > 0$, we have $m_u < m_d$ and therefore it is expected that $\chi^{BI}_{11} > 0$. It is thus apparent

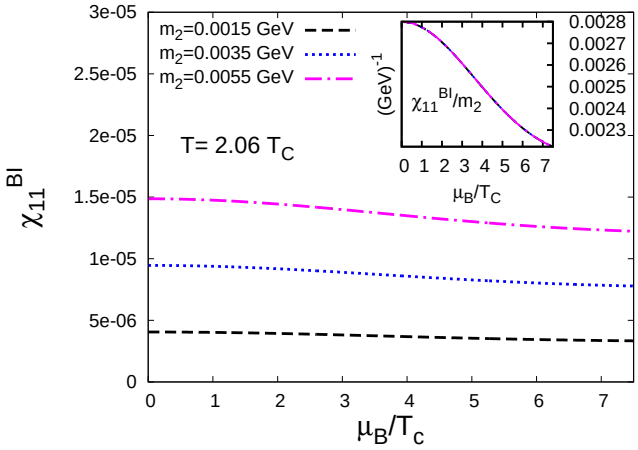

(a)

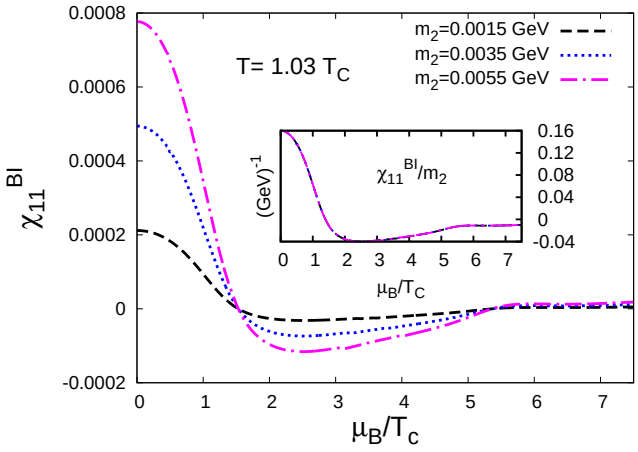

(b)

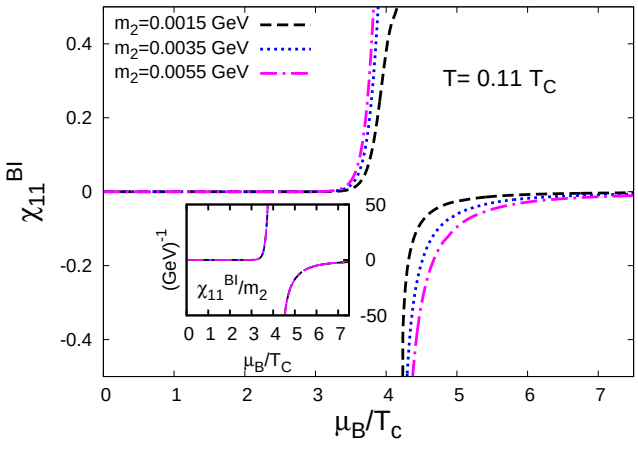

(c)

Figure 3.3: Second order off-diagonal susceptibilities along chemical potential for three different temperatures.

that interactions play a major role in the high density matter. An amazing fact remains that the scaling of the correlators with m_2 survives for all conditions of T and μ_B. This is shown in the insets of Fig.3.3. Now expanding χ_{11}^{BI} in a Taylor series in μ_B about $\mu_B = 0$ we have,

$$\chi_{11}^{BI}(\mu_B) = \chi_{11}^{BI}(0) + \frac{\mu_B^2}{2!}\chi_{31}^{BI}(0) + \frac{\mu_B^4}{4!}\chi_{51}^{BI}(0) + \cdots\cdots\cdots \tag{3.15}$$

In the above series odd order terms vanish identically as χ^{BI} is CP even. Since $\chi_{11}^{BI}(\mu_B)$ on the L.H.S scales with m_2, the same can be expected to hold true individually for all the coefficients on the R.H.S up to any arbitrary order. Incidentally the first two Taylor coefficients have already been shown to respect this scaling in Fig.3.1 and Fig.3.2(b) respectively.

3.3.3 Estimation of u-d Flavor Mass Asymmetry in Heavy-Ion Collision

Correlation between conserved charges, is an experimentally measurable quantity obtained from event-by-event analysis in heavy-ion collisions. The sign change of χ_{11}^{BI} at high μ_B may be an important signature of phase transition in this region. This will of course need fluctuations to freeze out close to the critical value of μ_B. To compare with experiments it is often useful to consider ratios like $\mathrm{R}_2 = \chi_{11}^{BI}/\chi_2^B$ and $\mathrm{R'}_2 = \chi_{11}^{BI}/\chi_2^I$. The temperature variation of these ratios are shown in Fig.3.4(a) and Fig.3.4(b). As we see R_2 decreases monotonically to zero above T_c. On the other hand, $\mathrm{R'}_2$ increases with increase of temperature and then decreases monotonically to zero above T_c like R_2. A systematic study of these ratios can thus indicate how close one could approach the phase boundary in heavy-ion collisions.

Also using the m_2 scaling one can estimate the mass asymmetry of constituent fermions in a physical system as, ${m_2}^{\mathrm{expt}} = \frac{\mathrm{R}_2^{\mathrm{expt}}(T,\mu_B)}{\mathrm{R}_2^{\mathrm{PNJL}}(T,\mu_B)} \times {m_2}^{\mathrm{PNJL}}$. To the best of our knowledge this is the first theoretical formulation that indicates that quark mass asymmetry in thermodynamic equilibrium can be directly measured from heavy-ion experiments. There still remains the question whether the isospin asymmetry brought in through QED effects may disturb the scaling. Another important point to observe is that for fractional baryon number of the constituents $\chi_{13}^{BI} > \chi_{31}^{BI}$, and vice versa for integral baryon number i.e. for protons and neutrons. From Fig.3.2 we see that the former inequality persist well below T_c. This may well be an artifact of PNJL model.

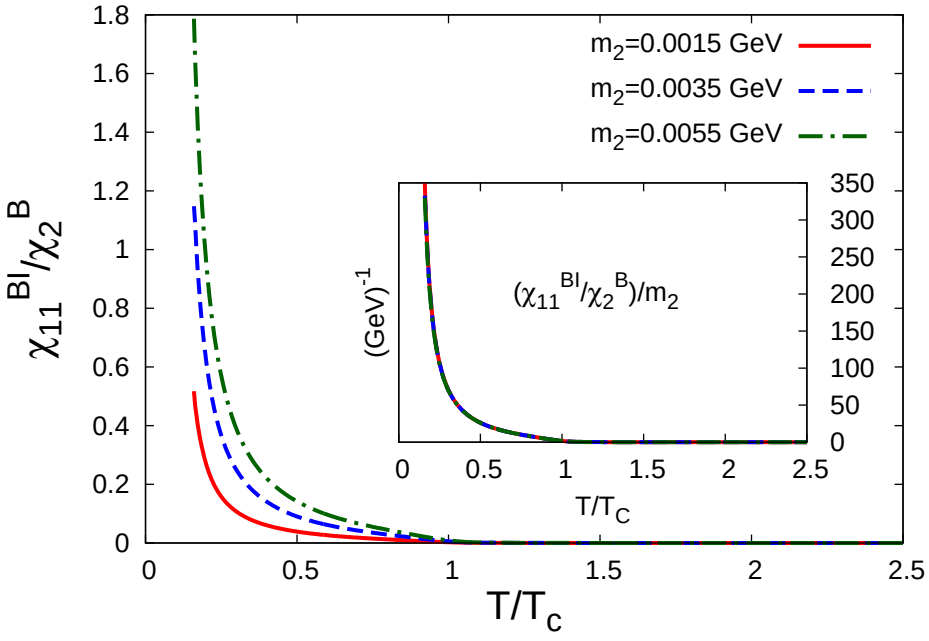

(a)

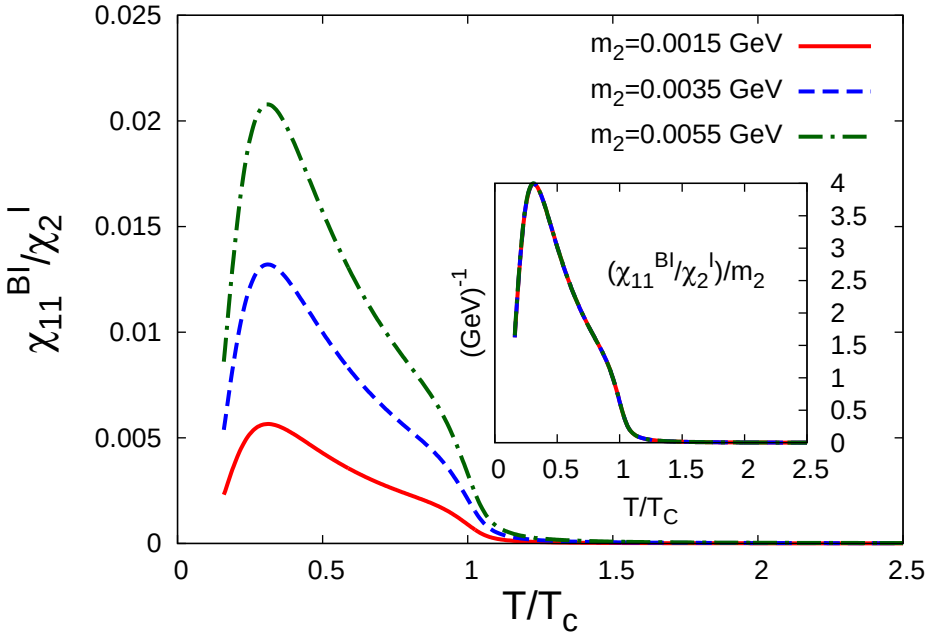

(b)

Figure 3.4: (a) Ratio of B–I correlation to baryon number fluctuation at $\mu_B = 0$. (b) Ratio of B–I correlation to isospin number fluctuation at $\mu_I = 0$.

Thus it would be important to see corresponding results from Lattice QCD. Enhanced statistics of present and future experiments may make it possible to measure this extremely sensitive probe. The direction of the above inequal-

ity would be important in deciding if partonic matter may have been produced in the experiments.

3.4 Summary

The effect of explicit isospin symmetry breaking through the mass term of u and d flavors in the PNJL model Lagrangian has been discussed in this chapter. We have found that the thermodynamic behavior of the system at $\mu_B = 0$ does not exhibit any remarkable changes when the symmetry is broken. We have studied the second and fourth order off diagonal susceptibilities in the B-I sector at finite temperature but zero baryon chemical potential. At finite baryon chemical potential second order off diagonal susceptibilities has also been studied. The isospin chemical potential μ_I was kept at zero for the entire study. These susceptibilities show a critical behavior near T_c, and also depend on the amount of mass asymmetry $m_2 = \frac{(m_u - m_d)}{2}$. We have also found that there is almost linear scaling relation between these susceptibilities with m_2 . We expect that this should help in estimating the actual mass asymmetry in the Heavy Ion Collision.

Bibliography

[1] A. Rusetsky, PoS C **D09**, 071 (2009)

[2] N. Cabibbo, Phys. Rev. Lett. **93**, 121801 (2004)

[3] A. Nehme, P. Talavera, Phys. Rev. D **65**, 054023 (2002)

[4] M. Arneodo *et al.* (New Muon Collaboration), Phys. Rev.D **50**, R1 (1994)

[5] H. Song, X. Zhang, B.-Q. Ma, Phys. Rev. D **82**, 113011 (2010)

[6] B.-Q. Ma, Phys. Lett. B **274**, 111 (1992)

[7] M. Creutz, PoS (LAT2005) **119**, hep-lat/**0508012** (2006)

[8] R. V. Gavai and S. Gupta, Phys. Rev. D **66**, 094510 (2002)

[9] G.M. de Divitiis *et.al* [RM123 collaboration], JHEP **1204**, 124 (2012)

[10] R. Horsley *et.al* [QCDSF-UKQCD Collaboration], Phys. Rev. D **86**, 114511 (2012)

[11] A. G. Nicola, R. T. Andrés, Phys. Rev. D **83**, 076005 (2011)

[12] A. G. Nicola, R. T. Andrés, J. Phys. G:Nucl. Part. Phys.**39** 015004 (2012)

[13] S. Gottlieb, W. Liu, D. Toussaint, R. L. Renken and R. L. Sugar, Phys. Rev. Lett. **59**, 2247 (1987)

[14] R.V. Gavai and S. Gupta, Phys. Rev. D **73**, 014004 (2006).

[15] C. R. Alton *et. al.*, Phys. Rev. D **71**, 054508 (2007)

[16] J. -P. Blaizot, E. Iancu, A. Rebhan, Phys. Lett. B **523** 143 (2001)

[17] P. Chakraborty, M.G. Mustafa, M.H. Thoma, Eur. Phys. J. C **23**, 591 (2002)

[18] P. Chakraborty, M.G. Mustafa, M.H. Thoma, Phys. Rev. D **68**, 085012 (2003)

[19] C. Sasaki, B. Friman, and K. Redlich, Phys. Rev. D **75**, 054026 (2007)

[20] S. K. Ghosh, T. K. Mukherjee, M. G. Mustafa and R. Ray, Phys. Rev. D **73**, 114007 (2006)

[21] C. Ratti, S. Rößner and W. Weise, Phys. Lett. B **649**, 57 (2007)

[22] K. Fukushima, Phys. Rev. D **77**, 114028, (2008).

[23] B.-J. Schaefer and J. Wambach, Phys. Rev. D **75**, 085015 (2007)

[24] A. Bhattacharyya, P. Deb, A. Lahiri, R. Ray, Phys. Rev. D **82**, 114028 (2010)

[25] A. Bhattacharyya, P. Deb, A. Lahiri, R. Ray, Phys. Rev. D **83**, 014011 (2011)

[26] N. Haque, M. G. Mustafa, M. H. Thoma, Phys. Rev. D **84**, 054009 (2010)

[27] S. Chatterjee and K. A. Mohan, Phys. Rev. D **86**, 114021 (2012).

[28] M. Asakawa and K. Yazaki, Nucl. Phys. A **504**, 668 (1989)

[29] M. Frank, M. Buballa and M. Oertel, Phys. Lett. B **562**, 221 (2003)

[30] S. Mukherjee, M. G. Mustafa and R.Ray, Phys. Rev. D **75**, 094015 (2007)

[31] U. Vogl and W. Weise, Prog. Part. Nucl. Phys. **27**, 195 (1991)

[32] S.P. Klevansky, Rev. Mod. Phys. **64**, 649 (1992)

[33] T. Hatsuda and T. Kunihiro, Phys. Rept. **247**, 221 (1994)

[34] M. Buballa, Phys. Rept. **407**, 205 (2005)

[35] C. Ratti, M. A. Thaler and W. Weise, Phys. Rev. D **73**, 014019 (2006)

[36] S.K. Ghosh, T.K. Mukherjee, M.G. Mustafa and R. Ray, Phys. Rev. D **77**, 094024 (2008)

CHAPTER 4

Heavy Lepton Pair production: A Possible QGP Signature

4.1 Introduction

In this chapter we are going to study heavy dilepton pairs namely $\tau^+\tau^-$ created in Pb-Pb collision at LHC energy. As already discussed in chapter 1, the lepton pair mass distribution has been used for the detection of QGP formation as well as to study the in-medium properties of low mass vector mesons [1, 2, 3]. The transverse momentum (p_T) distribution of lepton pairs in various invariant mass ranges has been used to study the radial flow development of the system [4, 5, 6]. The HBT interferometry using dilepton pairs has been proposed to provide information on the time development of collectivity in heavy-ion collisions [7]. The major advantage of looking at $\tau^+\tau^-$ dilepton pair arises due to the mass of the τ ($\sim$ 1.77 GeV). The τ pair mass distribution would then start beyond known contribution of hadronic resonances (ω, ρ and ϕ) which dominates in the respective mass regions in e^+e^- and $\mu^+\mu^-$ sector. This would in turn mean the remaining contribution for τ production are due to thermal sources from partonic medium, pion annihilation in hadronic medium and Drell Yan Mechanism. We think that the results will definitely provide some useful baseline for experimental search and further detailed studies.

4.1.1 Source of τ Lepton Pair in Heavy Ion Collision

The main source of heavy dilepton $\tau^{\pm}$ pair production we have considered in this work is quark and anti-quark annihilation through photon, Z and Higgs bosons intermediated process. The corresponding Feynman diagrams are shown in Fig. 4.1. They all contribute to thermal production of $\tau^{\pm}$ pair in quark gluon plasma.

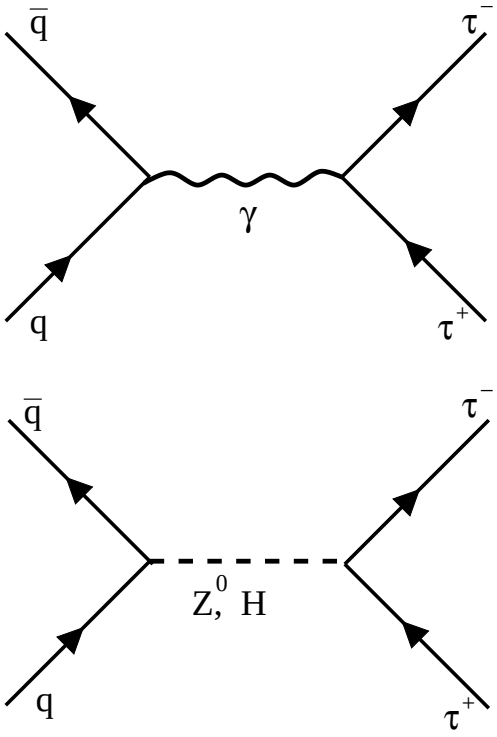

Figure 4.1: Feynman diagrams for heavy dilepton production.

The productions for these processes are evaluated from the matrix elements indicated below. The matrix element for the process $q\bar{q} \xrightarrow{Z} \tau^{+}\tau^{-}$ is given by,

$$M_Z = \frac{g^2}{4cos^2\theta_w}\frac{1}{(q^2 - {m_z}^2)}[v(\bar{p}_2)\Gamma_q u(p_1)][u(\bar{k}_1)\Gamma_\tau v(k_2)] \tag{4.1}$$

where,

$$\Gamma_q = \gamma^\mu({c_V}^q - {c_A}^q\gamma_5)$$

$$\Gamma_\tau = [\gamma_\mu - \frac{q_\mu\gamma_\nu q^\nu}{{m_z}^2}][{c_V}^\tau - {c_A}^\tau\gamma_5]$$

Now, starting from Eq.(4.1) one arrives at

$$M_Z^* = \frac{g^2}{4cos^2\theta_w}\frac{1}{(q^2 - {m_z}^2)}[v(\bar{k}_2)\Gamma'_\tau u(k_1)][u(\bar{p}_1)\Gamma'_q v(p_2)] \tag{4.2}$$

where,

$$\Gamma'_q = ({c_V}^q + {c_A}^q\gamma_5)\gamma^\mu \quad ;\Gamma'_\tau = [{c_V}^\tau + {c_A}^\tau\gamma_5][\gamma_\mu - \frac{q_\mu\gamma_\nu q^\nu}{M_Z^2}] \tag{4.3}$$

Having done the average over initial and sum over final electron spin, we have;

$$|M_Z^2| = [\frac{g^2}{4cos^2\theta_w}\frac{1}{(q^2 - {m_z}^2)}]^2 L_q \cdot L_\tau \tag{4.4}$$

where,

$$L_q = 4({c_A^q}^2+{c_V^q}^2)[p_2^\mu p_1^\nu+p_2^\nu p_1^\mu-(p_2\cdot p_1)g^{\mu\nu}]+4m_q^2({c_A^q}^2-{c_V^q}^2)g^{\mu\nu}-8ic_A^q c_V^q p_{2\alpha}p_{1\beta}\varepsilon^{\nu\alpha\mu\beta} \tag{4.5}$$

and

$$\begin{aligned} L_\tau &= 4({c_A^\tau}^2 + {c_V^\tau}^2)[k_{1\mu}k_{2\nu} + k_{1\nu}k_{2\mu} - (k_1.k_2)g_{\mu\nu}] \\ &\quad -\frac{4}{m_Z^2}({c_A^\tau}^2 + {c_V^\tau}^2)[(k_2.q)k_{1\mu}q_\nu + (k_1.q)q_\nu k_{2\mu} - (k_1.k_2)q_\mu q_\nu] \\ &\quad -8ic_A^\tau c_V^\tau K_1^\alpha k_2^\beta\varepsilon_{\nu\alpha\mu\beta} + 8i\frac{c_A^\tau c_V^\tau}{m_Z^2}q_\nu k_1^\alpha k_2^\beta q^\delta\varepsilon_{\delta\alpha\mu\beta} \\ &\quad -\frac{4}{m_Z^2}({c_A^\tau}^2 + {c_V^\tau}^2)[(k_1.q)q_\mu k_{2\nu} - (k_1.k_2)q_\mu q_\nu + (k_2.q)q_\mu k_{1\nu}] \\ &\quad +\frac{4}{m_Z^4}({c_A^\tau}^2 + {c_V^\tau}^2)[2(k_2.q)(k_1.q) - q^2(k_1.k_2)]q_\mu q_\nu + 8i\frac{c_A^\tau c_V^\tau}{m_Z^2}q_\mu k_1^\alpha k_2^\beta q^\delta\varepsilon_{\nu\alpha\delta\beta} \\ &\quad 4m_\tau^2({c_A^\tau}^2 - {c_V^\tau}^2)g_{\mu\nu} + 8\frac{m_\tau^2}{m_Z^2}({c_V^\tau}^2 - {c_A^\tau}^2)q_\mu q_\nu + 4\frac{m_\tau^2}{m_Z^4}({c_A^\tau}^2 - {c_V^\tau}^2)q^2 q_\mu q_\nu \end{aligned} \tag{4.6}$$

Finally we have,

$$\begin{aligned} |M_Z^2| &= \frac{g^4}{16cos^4\theta_w}\Big[0.5742[(s+t-m_q^2-m_\tau^2)^2 + (m_q^2+m_\tau^2-t)^2 + (s+t-m_q^2-m_\tau^2)^2(1-\frac{s}{2m_Z^2})] \\ &\quad +s(0.858m_q^2 + 1.14m_\tau^2) - 0.59m_q^2m_\tau^2 - 0.0041\frac{sm_q^2m_\tau^2}{m_Z^2} + 0.002\frac{s^2m_q^2m_\tau^2}{m_Z^2}\Big] \end{aligned} \tag{4.7}$$

The matrix element for the photon mediated process is given by:

$$M_\gamma = \frac{e_q e}{q^2}[v(\bar{p_2})\gamma^\mu u(p_1)][u(\bar{k_1})\gamma_\mu v(k_2)] \tag{4.8}$$

e_q is the average charge of quarks, e is the electronic charge.

$$|M_\gamma^2| = \frac{e^2e_q^2}{s^2}\Big[\frac{1}{4}[(m_q^2+m_\tau^2-t)^2 + (s+t-m_q^2-m_\tau^2)^2] + (\frac{s}{2}-m_q^2)m_\tau^2\Big] \tag{4.9}$$

The matrix element of the interference term is $M_Z M_\gamma^* + M_Z^* M_\gamma$. Now,

$$M_Z M_\gamma^* = \frac{g^2 e_q e}{4cos^2\theta_w} \frac{1}{q^2(q^2 - m_z^2)} \mathcal{L}_q \mathcal{L}_\tau \tag{4.10}$$

where,

$$\mathcal{L}_q = 4c_V^q [p_2^\mu p_1^\nu + p_2^\nu p_1^\mu - (p_2.p_1) g^{\mu\nu} - m_q^2 g^{\mu\nu}] + 4ic_A^q p_{2\alpha} p_{1\beta} \varepsilon^{\alpha\mu\beta\nu} \tag{4.11}$$

and

$$\begin{aligned} \mathcal{L}_\tau &= 4c_V^\tau [k_{1\mu} k_{2\nu} + k_{1\nu} k_{2\mu} - (k_1.k_2) g_{\mu\nu} - m_\tau^2 g_{\mu\nu}] \\ &\quad - \frac{4c_V^\tau}{m_Z^2} [(k_1.q) q_\mu k_{2\nu} + (k_2.q) k_{1\nu} q_\mu - (k_1.k_2) q_\mu q_\nu] \\ &\quad + 4ic_A^\tau k_1^\alpha k_2^\beta \varepsilon_{\alpha\mu\beta\nu} + 4\frac{c_V^\tau m_\tau^2}{m_Z^2} q_\mu q_\nu - 4i\frac{c_A^\tau}{m_Z^2} q_\mu q^\delta k_1^\alpha k_2^\beta \varepsilon_{\alpha\delta\beta\nu} \end{aligned} \tag{4.12}$$

Similarly, we have

$$M_Z^* M_\gamma = \frac{g^2 e_q e}{4cos^2\theta_w} \frac{1}{q^2(q^2 - m_z^2)} \mathcal{L}'_q \mathcal{L}'_\tau \tag{4.13}$$

where,

$$\mathcal{L}'_q = 4c_V^q [p_1^\mu p_2^\nu + p_1^\nu p_2^\mu - (p_2.p_1) g^{\mu\nu} - m_q^2 g^{\mu\nu}] + 4ic_A^q p_{1\alpha} p_{2\beta} \varepsilon^{\alpha\mu\beta\nu} \tag{4.14}$$

and

$$\begin{aligned} \mathcal{L}'_\tau &= 4c_V^\tau [k_{2\mu} k_{1\nu} + k_{2\nu} k_{1\mu} - (k_1.k_2) g_{\mu\nu} - m_\tau^2 g_{\mu\nu}] \\ &\quad - \frac{4c_V^\tau}{m_Z^2} [(k_1.q) q_\mu k_{2\nu} + (k_2.q) k_{1\nu} q_\mu - (k_1.k_2) q_\mu q_\nu] \\ &\quad + 4ic_A^\tau k_2^\alpha k_1^\beta \varepsilon_{\alpha\mu\beta\nu} + 4\frac{c_V^\tau m_\tau^2}{m_Z^2} q_\mu q_\nu - 4i\frac{c_A^\tau}{m_Z^2} q_\mu q^\delta k_2^\alpha k_1^\beta \varepsilon_{\alpha\delta\beta\nu} \end{aligned} \tag{4.15}$$

Putting the values of the parameters, finally we have

$$\begin{aligned} M_Z M_\gamma^* + M_Z^* M_\gamma &= \frac{g^2 e_q e}{4cos^2\theta_w} \frac{1}{s(s - m_z^2)} \Big[(m_q^2 + m_\tau^2 - t)^2 - 0.0912(s + t - m_q^2 - m_\tau^2)^2 \\ &\quad - 12(s + t - m_q^2 - m_\tau^2)^2 (4 - \frac{s}{m_Z^2}) + 0.0912\frac{s^3}{m_Z^2} - 0.1824\frac{m_\tau^2}{m_Z^2} s^2 \\ &\quad + 0.5472\frac{m_q^2 m_\tau^2}{m_z^2} s + 0.1824 m_q^2 s - 1.09 m_q^2 m_\tau^2 \Big] \end{aligned} \tag{4.16}$$

Finally, the matrix element for the Higgs mediated process is:

$$M_H = \frac{m_q m_\tau}{v^2(s - m_H^2)} [v(\bar{p}_2) u(p_1)] [u(\bar{k}_1) v(k_2)] \tag{4.17}$$

Proceeding in a similar fashion like the above we find;

$$|M_H^2| = \frac{m_q^2 m_\tau^2}{vev(s-m_H^2)^2}[2m_q^2 - \frac{s}{2}][2m_\tau^2 - \frac{s}{2}] \tag{4.18}$$

In the above expressions (p_1, p_2) and (k_1, k_2) are initial state and final state momenta respectively. m_q, m_τ, m_Z, m_H, are the masses of quarks, τ leptons, Z boson and Higgs respectively. The total production cross section (σ_q) of $\tau^+\tau^-$ is obtained by taking a coherent sum of the matrix elements given in Eqs. 4.7, 4.9, 4.16 and 4.18 with the following values of various parameters: m_Z=91 GeV, M_τ=1.78 GeV, m_H=120 GeV, $sin\theta_w$=0.234 C_A^q=0.5, C_V^q=0.19, C_A^τ=-0.5, C_V^τ=-0.03 and Higgs vev=246 GeV.

4.2 τ Lepton From Drell-Yan Process

Dilepton production in Drell-Yan mechanism was discussed in detail in chapter 1. The total production cross-section σ_q is folded by the parton distribution functions to obtained the τ lepton pair yield in p-p collisions. In the present work CTEQ5M PDF [8] have been taken to obtain this. The DY production of τ lepton in Pb-Pb collision is;

$$\frac{dN}{dM^2dy} = \frac{N_{coll}(b)}{\sigma_{\rm in}^{pp}} \times \frac{d\sigma^{pp}}{dM^2dy}$$

where, $N_{coll}(b)$ is the number of binary nucleon nucleon collisions an impact parameter b calculated using Glauber model and σ_{in} is the inelastic cross section for p-p interaction. We have taken $\sigma_{in} = 60$ mb and $b = 3.6$ fm corresponding to $0-5\%$ centrality at $\sqrt{s_{NN}} = 5.5$ TeV. The shadowing of parton distribution functions has been taken from [9].

4.3 Space-Time Evolution Of τ Lepton Pairs

The space time evolution of the system formed in Pb+Pb collisions at $\sqrt{s_{\rm NN}}$ = 5.5 TeV has been studied by using ideal relativistic hydrodynamics [10] with longitudinal boost invariance [11] and cylindrical symmetry. We assume that the system reaches equilibration at a time τ_i = 0.08 fm/c after the collision. The initial temperature, T_i is taken to be 700 MeV and is calculated assuming the hadronic multiplicity (dN/dy) to be of the order of 2100 [12]. We use

the equation of state (EOS) obtained from the Lattice QCD calculations by the MILC collaboration [13] for the partonic phase. For the hadronic phase EOS all the resonances with mass 2.5 GeV have been considered [14]. The transition temperature (T_c) between hadronic phase and partonic phase is taken to be 175 MeV [15]. We consider kinetic freeze out temperature, T_f = 120 MeV.

At multi-TeV energies there could be another contribution to heavy dilepton production by fusion of two gluons. As discussed in Ref [16] the gluon fusion process is via a virtual quark loop and an intermediate Z or Higgs boson. This process was found to be dominant for mass of lepton pair greater than the mass of W boson. Our results are concentrated in the mass range of 4 to 20 GeV, where the contribution from such process is found to be orders of magnitude smaller compared to the rest of the sources of $\tau^{\pm}$ pair production.

4.4 Results

The yield ($\frac{dN}{dMdy}$) for τ dilepton pair as a function of $\tau^+\tau^-$ pair invariant mass for Pb+Pb collisions at $\sqrt{s_{\rm NN}}$ = 5.5 TeV is shown in figure 4.2(a). The contributions from Drell Yan (DY, dashed line) and thermal partonic medium (QGP, solid line) are shown. The Drell Yan contribution is higher than the thermal contribution for all the mass range studied. The difference seems to increase with increase in $\tau^+\tau^-$ pair mass.

Figure 4.2(b) shows the ratio $\frac{dN^{PbPb}}{dMdy}$ / $[N_{coll}\frac{dN^{pp}}{dMdy}]$. Where $\frac{dN^{PbPb}}{dMdy}$ is the sum of all the the contributions shown in Figure 4.2(a) from Pb+Pb collisions. The $[N_{coll}\frac{dN^{pp}}{dMdy}]$, is the number of binary collisions scaled contribution from DY process. This contribution can be estimated from the measurement in p+p collisions at the same energy ($\sqrt{s}$ = 5.5 TeV). If there is no QGP formation then the ratio should always be equal to unity indicating the fact that the dilepton yield in the nucleus-nucleus collision is the collection of individual nucleon-nucleon collision only. However, we observe that the ratio is above unity for the mass range of 4 to 6 GeV. Starting with a value of 1.4 at mass of 4 GeV it decreases towards unity beyond mass of 6 GeV. This indicates that one should be able to extract a clear information of thermal contribution from partonic source at LHC energies using heavy dilepton pair measurement within the mass window of 4 to 6 GeV.

In this first such case study, we have not discussed the transverse momentum distribution of $\tau^+\tau^-$ pair, these studies are planned to be presented in our future work. For this theoretical estimate, we have not discuss here

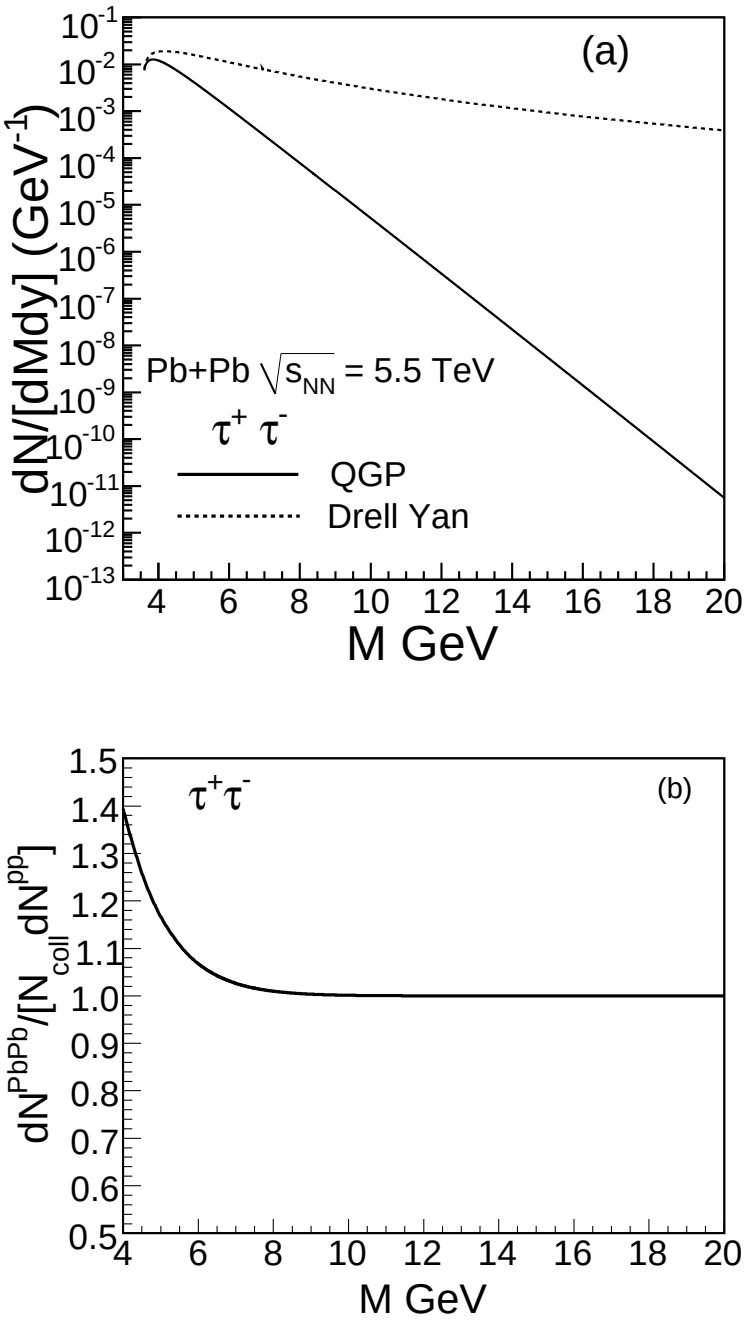

Figure 4.2: (a) τ lepton pair yields as a function of invariant mass of the pair is displayed for Pb+Pb collisions at $\sqrt{s_{\rm NN}}$ = 5.5 TeV. Solid line indicates the spectra from quark gluon plasma and the dashed line stands for contribution from DY process. In (b) the ratio $\frac{dN^{PbPb}}{dMdy}$ / $[N_{coll}\frac{dN^{pp}}{dMdy}]$ is shown, here $\frac{dN^{PbPb}}{dMdy}$ is the sum of the contribution shown in (a), $\frac{dN^{pp}}{dMdy}]$ is the DY contribution from pp collision, and N_{coll} =1369.477 for Pb+Pb collisions at $\sqrt{s_{\rm NN}}$ = 5.5 TeV.

the details about the experimental measurements of heavy dilepton pairs. For more details we refer the readers to [17]. Further the excellent knowledge of τ decay modes and detection from low energy experiments [18] make the heavy dilepton pair production measurements feasible at LHC.

4.5 Summary

A first case study of τ dilepton pair production at LHC energy has been carried out in the present chapter. We have considered Pb+Pb collisions at midrapidity for $\sqrt{s_{\rm NN}}$ = 5.5 TeV. The LHC energy is a factor 27 more compared to RHIC, so we expect that this energy should allow a significant production of τ leptons. The main motivation of considering the τ lepton is its mass. Because of heavy mass the tau lepton yield is expected not to suffer from the huge background production. The main sources for τ pair production considered here by quark and anti-quark annihilation mediated through photon, Z and Higgs boson. The contribution from gluon fusion process via virtual quark loop and intermediate Z and Higgs boson is found to be negligible small in the mass range of our calculations (4 to 20 GeV). The contribution from pion annihilation process is few orders of magnitude small compared to both thermal and Drell Yan contributions. The Drell Yan contribution is found to be higher than the thermal contribution from partonic sources for the entire mass range studied. The non-thermal contributions could be measured experimentally through p+p collisions, then the ratio of yields from nucleus-nucleus collisions to the yields for the binary collision scaled p+p collisions is found to be above unity for the mass range of 4-6 GeV. This indicates the window in mass region for τ dilepton pair where the thermal production can be studied at LHC energy using heavy dilepton pairs as an observable. However, the identification of the τ in the experiments is very crucial in the sense that after formation it decays immediately before reaching at the detectors. The τ is the only lepton heavy enough to decay into hadrons. The τ lepton branching fraction for decays into one or more hadrons is about 65%, and about 35% for decays into muons or electrons [19]. Leptonic decay consists of an electron or muon and a pair of neutrinos whereas the hadronic decay consists of one or three charged particles. Kinematics of QCD jets are similar to that of hadronically decaying tau leptons. Hadronic τ decays are difficult to identify in hadron collisions due to the overwhelming QCD background. τ leptons are considered to be a signature in several discovery channels related to the

Standard Model Higgs boson at low masses, the MSSM Higgs boson or Supersymmetry (SUSY). Hence experimental plans exist at LHC to reconstruct them in one-prong (one charged pion) and three-prong (three charged pions) decay topologies. The lifetime of the τ lepton ($c\tau$ = 87.11μm) in principle allows for the reconstruction of its decay vertex in the case of three-prong decays. The flight path in the detector increases with the Lorentz boost of the τ lepton, but at the same time the angular separation of the decay products decreases. A resulting transverse impact parameter of the τ decay products can be used to distinguish them from objects originating from the production vertex. In fact experiments at LHC claim the the overall efficiency for reconstructing good quality tracks from τ lepton hadronic decays is of the order of 82% [17].

Bibliography

[1] J. Alam, S. Sarkar, P. Roy, T. Hatsuda, B. Sinha, Ann. Phys. **286**, 159 (2000)

[2] R. Rapp, J. Wambach, Adv. Nucl. Phys.**25**, 1 (2000)

[3] G.E. Brown, M. Rho, Phys. Rep. **269**, 333 (1996).

[4] P. Mohanty, J.K. Nayak, J. Alam, S.K. Das, Phys. Rev. C **82**, 034901 (2010)

[5] J.K. Nayak, J. Alam, Phys. Rev. C **80**, 064906 (2009)

[6] J. Deng, Q. Wang, N. Xu, P. Zhuang, Phys. Lett. B **701**, 581 (2011)

[7] P. Mohanty, J. Alam, B. Mohanty, Phys. Rev. C **84** 024903 (2011)

[8] H. L. Lai, J. Huston, S. Kuhlmann, J. Morfin, F. Olness, J. F. Owens, J. Pumplin and W. K. Tung, Eur. Phys. J. C **12**, 375 (2000).

[9] K.J. Eskola, V.J. Kolhinen and P.V. Ruuskanen, Nucl.Phys. B **535**, 351 (1998).

[10] H. von Gersdorff, M. Kataja, L.D. McLerran, P.V. Ruuskanen, Phys. Rev. D **34**, 794 (1986)

[11] J.D. Bjorken, Phys. Rev. D **27**, 140 (1983)

[12] N. Armesto, N. Armesto, N. Borghini, S. Jeon, U.A. Wiedemann *et al.*, J. Phys. G: Nucl. Part. Phys.**35**, 054001 (2008)

[13] C. Bernard et al., Phys. Rev. D **75**, 094505 (2007)

[14] B. Mohanty and J. Alam, Phys. Rev. C **68**, 064903 (2003)

[15] Y. Aoki, Z. Fodor, S. D. Katz and K. K. Szab, Phys. Lett. B **643**, 46 (2006)

[16] S. S. D. Willenbrock and D. A. Dicus, Phys. Lett. B **156**, 429 (1985)

[17] R. Adolphi et al., CMS Collaboration, JINST **3**, S08004 (2008); G. Aad et al., ATLAS Collaboration, JINST **3**, S08003 (2008); arXiv:0901.0512; K. Aamodt et al., ALICE Collaboration, JINST **3**, S08002 (2008)

[18] S. Schael *et al.*, Phys. Rept.**421**, 191 (2005); T. E. Coan *et al.*, Phys. Rev. Lett., **92**, 232001 (2004); T. E. Browder *et al.*, Phys. Rev.D **61**, 052004 (2000)

[19] C. Amsler *et al.*, Phys. Lett. B **667**, 1 (2008)

Conclusion and Outlook

The main goal of the thesis is the description of the behavior of strongly interacting matter via QCD inspired models under extreme conditions of temperature and/or density. We know in the low energy regime the strongly interacting matter is governed by hadronic degrees of freedom in which constituent quarks and gluons remain confined. Now if we increase the temperature and/or density, the hadronic system undergoes a phase transition where deconfined quarks and gluons are the main degrees of freedom. We have studied the strongly interacting matter using phenomenological models namely NJL and PNJL model both at finite temperature and density. The main drawback of NJL model is the absence of confinement property, which is further improved by the inclusion of Polyakov loop part in the Lagrangian. The advantage of these phenomenological models is that, compared to Lattice calculations they are not only cost effective but time saving too.

In chapter 2 we have investigated the Equation of state (EoS) and various thermodynamic properties i.e. specific heat, speed of sound, compressibility etc. of strongly interacting matter at high density. This type of matter is expected to exist in the core of massive astrophysical objects like neutron star. In fact it has been shown that inside the neutron stars, when the matter density exceeds about 5 times normal nuclear matter density the onset of hadron quark phase transition occurs. Initially hadrons convert to two flavor quark matter. However, two flavor quark matter is unstable. It was conjectured by Witten that strange quark matter is the stable ground state of strongly interacting matter. The unstable two flavor matter is eventually converted to stable strange quark matter. So we have considered 2+1 flavor quark matter system in our analysis. Since beta equilibrium and charge neutrality are two basic requirement for the matter inside neutron stars, we have performed our analysis considering beta equilibrium between the three quark chemical

potentials namely μ_u, μ_d and μ_s. Apart from the 2+1 flavor quark system we have considered free electrons with three different electron chemical potentials 0, 10 and 40 MeV. We have not imposed charge neutrality along with beta equilibrium, rather found charge neutral contours for the different electron chemical potentials. The whole study has been done using both NJL and PNJL model, and the results are compared. The QCD phase diagram for the beta equilibrated asymmetric matter was obtained using these models. We have also obtained the contours of constant baryon number density, constant strangeness fraction and constant entropy per baryons. The possible explanations of the behavior of such contours were described in the context of neutron star.

However, actually description of quark matter in neutron star scenario demands the consideration of diquark condensates at high density. Although at this moment we have not included this in our model, we plan to explore the neutron star evolution by incorporating diquark condensates.

The whole study in chapter 2 has been done keeping in mind that the u-d flavor asymmetry comes due to the difference in corresponding chemical potentials. For μ_e equals to zero, the matter is isospin symmetric. There is no significant qualitative difference in the behavior of the thermodynamic variables or phase diagrams when we move to isospin symmetric to asymmetric phase.

We decided to study the isospin asymmetry considering another possibility of isospin breaking i.e unequal masses for u and d flavors. Since the mass difference is very small, mass of u and d quark is considered to be same in all practical purposes. However, they are not equal in true sense. So in chapter 3 we have studied 1+1 flavor quark matter with $m_u \neq m_d$. Here we consider the average quark mass $m_1 = (m_u + m_d)/2$ fixed at 0.0055 GeV and study the effect of ISB with three representative values of $m_2 = (m_d - m_u)/2$. But it should be clarified properly that in this study the isospin chemical potential is strictly kept at zero, that means $\mu_u = \mu_d$ for this case. The asymmetry is entirely due to mass difference unlike the study in previous chapter. We have found that thermodynamic properties, i.e. pressure, energy density, specific heat, entropy do not show any significant changes. The striking results were found for the second and fourth order off diagonal susceptibilities in Baryon-Isospin sectors both in finite temperature and finite chemical potential directions. They show a critical behavior near T_c. They are not only sensitive with different values of m_2, but show almost a linear scaling with m_2. These findings help us to es-

timate the value of m_2 experimentally because the off diagonal susceptibilies give the correlation between the conserved charges that are experimentally measurable. It is worth to mention here that the diagonal susceptibilities do not show any dependences on m_2 unlike the off diagonal susceptibilities. The natural extension of this work is to explore all the quantities in 1+1+1 flavor case, which we plan to do in future.

The detailed understanding of the hadron–quark phase transition and the thermodynamics of quark gluon plasma, both at finite temperature and density, are of particular interest in the studies of relativistic heavy ion collisions. There are lots of theoretical studies where the existence of quark gluon plasma is suggested. In chapter 2 and 3 we have also shown the critical behavior of some thermodynamic quantities and correlations between conserved charges and pointed out that some of them are experimentally measurable, hence can be treated as QGP signatures also.

Production of photons and dileptons are longstanding classic probes for QGP formation as already mentioned in somewhat detail in chapter 1. So finally in chapter 4 we decided to explore dilepton production but with heavier mass ($\tau^+\tau^-$), which is relevant because of the availability of corresponding energy range at LHC. Another reason of considering this, is due to the heavy mass of the τ lepton, its production will not be affected by the overwhelming background production. Comparing the thermally generated τ with that produced in initial hard process (Drell-Yan), we have found that in the invariant mass window of 4 to 6 GeV, τ lepton can be treated as an excellent signature for the formation of quark gluon plasma.

For the first such case study we have considered tree level Feynmann diagrams. We plan to study the next to leading order diagrams and discuss the transverse momentum distribution of $\tau^+\tau^-$ pairs. As heavy quark production will be substantial at RHIC and LHC energies, τ production from heavy flavor decay is another important issue to be considered in future.

List of Publications

1. A General Relativistic study of the neutrino path and calculation of minimum photosphere for different stars, with Ritam Mallick; *Physical Review D* **79**, 023001, 2009.

2. Heavy lepton pair production in nucleus-nucleus collisions at LHC energy : A Case study, With Jan-e Alam, Bedangadas Mohanty, Sanjay K. Ghosh & Rajarshi Ray; *Nuclear Physics A* **889**, 1, 2012.

3. Study of Beta Equilibrated 2+1 Flavor Quark Matter in PNJL Model, With Abhijit Bhattacharyya, Sanjay K. Ghosh, & Rajarshi Ray; *Physical Review D* **86**, 096006, 2012.

4. Isospin symmetry breaking and baryon-isospin correlations from Polyakov-Nambu-Jona-Lasinio model, With Abhijit Bhattacharyya, Sanjay K. Ghosh, Anirban Lahiri, Sibaji Raha & Rajarshi Ray; *arXiv:1212.6134 [hep-ph]*.

Conference Proceedings

Heavy dilepton in nucleus-nucleus collisions at LHC energy, With Jan-e Alam, Bedangadas Mohanty, Sanjay K. Ghosh & Rajarshi Ray; *Will be published by Narosa*.